



UNIVERSITÀ
DI PAVIA



UNIVERSITY OF PAVIA
FACULTY OF ENGINEERING

UNIVERSITY SCHOOL OF ADVANCED
STUDIES - IUSS PAVIA

**On the impacts of structure-to-structure damage correlation for
regional seismic risk assessment**

A Thesis Submitted in Partial Fulfilment of the Requirements
for the Degree of Master of Science (Laurea Magistrale) in

Civil Engineering for the Mitigation of Risk from Natural Hazards

by

Tomas Mejia Saldarriaga

Supervisor: Prof. Gerard O'Reilly

September, 2024

ABSTRACT

One of the main challenges in implementing the performance-based earthquake engineering framework and computing risk and associated consequences on a regional scale is incorporating the structure-to-structure damage correlation in the analysis. This study investigates the impact of considering such correlation through a case study involving the assessment of mid-rise concrete frame buildings in the province of Caserta in Southern Italy. An analytical method is proposed to estimate the correlation, using the results of Incremental Dynamic Analysis (IDA) on equivalent Single-Degree-of-Freedom (SDOF) oscillators. This approach is applicable to various earthquake scenarios and is less computationally demanding than using the results of Multiple-Stripe Analysis (MSA) on full 3D models of the buildings, which were also considered as the benchmark case. The study compares the results of both approaches, finding that while the proposed method tends to overestimate the correlation, it still yields more accurate damage estimates than cases where this correlation is neglected entirely. Additionally, the study confirms that including the damage correlation in the analysis significantly impacts the probability distribution of the number of damaged buildings, particularly by increasing the risk of large-scale damage. Incorporating this aspect in the analysis can lead to more accurate damage and loss estimates, allowing to plan improved strategies for risk preparedness and mitigation.

ACKNOWLEDGEMENTS

I would like to thank all the people who contributed directly and indirectly to the development of this work. To Professor O'Reilly, for always showing interest and being available to help; your suggestions played a crucial role in making this thesis something I can truly be proud of. Thanks to Davit and Volkan, who helped me without having to do so. Without their contribution, it would have surely taken me twice as long to finish this work.

I would also like to thank everyone who made the experience of studying this master's degree and living in Pavia much more enjoyable. To Daniela L., for supporting me in this adventure even before it started; thank you for making me feel accompanied despite being more than 9,000 km away. To David and Andrea, for making me feel like family even when we didn't know each other for that long; to María, for supporting me and giving me company so I wouldn't get bored; and to Daniela P. and Daniela Q., for letting me vent my frustrations at the moments I needed it the most. Thanks also to all my friends in Colombia, who always believed in my abilities and supported me in this adventure from afar.

Finally, thanks to the most important people in my life, my family. Gracias a mis abuelos: Antonio, Alicia, Hernando y Gloria; a mis padres: Juan David y Marcela; y a mis hermanas: Sofía y María Antonia. Gracias por ser mi motor, por confiar siempre en mis capacidades y por hacerme la persona que soy hoy en día. Con ustedes comparto el mérito de todos y cada uno de mis logros. Los amo inmensamente y nunca podré describir con palabras lo mucho que agradezco tenerlos en mi vida.

TABLE OF CONTENTS

ABSTRACT	iii
ACKNOWLEDGEMENTS.....	v
TABLE OF CONTENTS.....	vii
LIST OF FIGURESix
LIST OF TABLES.....	xiii
1. INTRODUCTION	15
2. CASE STUDY: REGIONAL SEISMIC RISK ASSESSMENT OF MID-RISE CONCRETE FRAMES BUILDINGS.....	19
2.1 GENERAL DESCRIPTION.....	19
2.2 EXPOSURE MODEL.....	20
2.2.1 Exposure for the Caserta Province	21
2.2.2 Spatial disaggregation of exposure model	23
2.3 MODELLING OF BUILDINGS	24
2.3.1 Structural characterization	26
2.3.2 Portfolio of buildings	30
2.3.3 Structural Model.....	37
2.3.4 Geographical location	40
3. HAZARD ANALYSIS AND GROUND MOTION SELECTION	41
3.1 SELECTION OF INTENSITY MEASURE	41
3.1.1 Average spectral acceleration	42
3.1.2 Selection of period range for Case Study.....	43
3.2 PROBABILISTIC SEISMIC HAZARD ANALYSIS	44
3.3 RECORD SELECTION	46
4. BUILDING RESPONSE AND DAMAGE QUANTIFICATION	49

4.1 FRAGILITY CURVES.....	49
4.2 BUILDING RESPONSE ESTIMATION	51
4.2.1 IDA vs MSA	51
4.2.2 MSA on Case Study	53
4.3 STATISTICAL FITTING OF FRAGILITY CURVES	54
4.3.1 Maximum Likelihood Method	54
4.3.2 Fragility estimation on Case Study.....	55
5. DETERMINATION OF STRUCTURE-TO-STRUCTURE DAMAGE CORRELATION ..	61
5.1 OVERVIEW	61
5.2 ANALYTICAL DERIVATION OF STRUCTURE-TO-STRUCTURE CORRELATION	63
5.2.1 Correlation between Bernoulli trials.....	63
5.2.2 Determination of joint probability distribution	64
5.2.3 Equivalent SDOF nonlinear oscillators	66
5.3 STRUCTURE-TO-STRUCTURE DAMAGE CORRELATION ON CASE STUDY	68
5.3.1 Linearization of Pushover Curve	69
5.3.2 IDA on equivalent SDOF oscillators	72
5.3.3 Calculation of correlation matrix	77
6. CASE STUDY EVALUATION.....	93
6.1 CONSTANT SHAKING SCENARIOS.....	95
6.1.1 Scenario 1: Exceeding a PIDR of 1% at an AvgSa of 0.268g.....	96
6.1.2 Scenario 2: Exceeding a PIDR of 8% at an AvgSa of 0.746g	100
6.2 EARTHQUAKE RUPTURE SCENARIO	104
6.2.1 Scenario 3: Definition of earthquake rupture.....	105
6.2.2 Intensity Measure Modelling	106
6.2.3 Calculation of structure-to-structure damage correlation.....	109
6.2.4 Estimation of number of damaged buildings.....	109
7. SUMMARY AND CONCLUSIONS	115
REFERENCES	117
APPENDIX A. RECORD SELECTION	123
APPENDIX B. RESULTS OF MSA FOR ALL BUILDINGS	143
APPENDIX C. RESULTS OF IDA FOR ALL BUILDINGS	165

LIST OF FIGURES

Figure 1 Location of Studied Municipalities.....	20
Figure 2 Geographical location of assets	24
Figure 3 Percentage of midrise buildings by number of stories.....	27
Figure 4 Percentage of buildings by slab type	28
Figure 5 Percentage of beam type for slab Type 3	29
Figure 6 Percentage of building by construction quality.....	30
Figure 7 Layouts B01 (left) and B02 (right)	31
Figure 8 Building Layout B03.....	31
Figure 9 Building Layout B04 (left) and B04b (right).....	31
Figure 10 Building Layout B05.....	32
Figure 11 Building Layout B06 (left) and B07 (right).....	32
Figure 12 Building Layout B08 (left) and B09 (right).....	32
Figure 13 Building Layout (B10)	33
Figure 14 Pushover Curves of Building 1	39
Figure 15 Pushover Curves of Building 11	39
Figure 16 Pushover Curves of Building 42.....	39
Figure 17 Geographical Location of Buildings	40
Figure 18 Hazard Curve	45
Figure 19 Example of response spectra of selected ground motions with CS as target spectra for Sa(2.6s) in log scale (a) and linear scale (b)(Adapted from Lin et al., 2013)	46
Figure 20 Target Spectrum vs Spectra of Selected Records for Return Period of 22 years.....	47
Figure 21 Example of Fragility Curves.....	50
Figure 22 Visual representation of IDA and MSA	53
Figure 23 Example of MSA results.....	54
Figure 24 Estimation of probability of collapse at every IM level.....	56

Figure 25 Collapse Fragility Fitting for Building 10.....	57
Figure 26 Collapse Fragility of Buildings by Class	59
Figure 27 Estimation of joined probability distribution from MSA results.....	65
Figure 28 Estimation of joined probability distribution from IDA results	66
Figure 29 Linearization methods according to ATC-19.....	67
Figure 30 Type of Linearization of Pushover Curve	69
Figure 31 Linearization of Pushover for Direction x of Building 11	70
Figure 32 Linearization of Pushover for Direction x of Building 1.....	71
Figure 33 Linearization of Pushover for Direction y of Building 1.....	71
Figure 34 Example of IDA results	76
Figure 35 Correlation Matrix estimated from MSA Exceeding a drift of 1.0%. AvgSa=0.268 g ..	78
Figure 36 Correlation Matrix estimated from IDA Exceeding a drift of 1.0%. AvgSa=0.268 g ..	78
Figure 37 Correlation Matrix estimated from MSA Exceeding a drift of 1.0%. AvgSa=0.383 g ..	79
Figure 38 Correlation Matrix estimated from IDA Exceeding a drift of 1.0%. AvgSa=0.383 g ..	79
Figure 39 Correlation between Building 1 and Building 2 for a drift limit of 1.0%	80
Figure 40 Correlation between Building 1 and Building 8 for a drift limit of 1.0%	81
Figure 41 Correlation between Building 1 and Building 21 for a drift limit of 1.0%	81
Figure 42 Correlation between Building 1 and Building 35 for a drift limit of 1.0%	82
Figure 43 Correlation between Building 1 and Building 60 for a drift limit of 1.0%	82
Figure 44 Marginal and Joint Probabilities for Building 1 and Building 60.....	84
Figure 45 Correlation Matrix estimated from MSA Exceeding a drift of 8.0%. AvgSa=0.746 g ..	85
Figure 46 Correlation Matrix estimated from IDA Exceeding a drift of 8.0%. AvgSa=0.746 g ..	85
Figure 47 Correlation Matrix estimated from MSA Exceeding a drift of 8.0%. AvgSa=0.945 g ..	86
Figure 48 Correlation Matrix estimated from IDA Exceeding a drift of 8.0%. AvgSa=0.945 g ..	86
Figure 49 Correlation between Building 1 and Building 2. Drift limit of 8.0%	87
Figure 50 Correlation between Building 1 and Building 8. Drift limit of 8.0%	88
Figure 51 Correlation between Building 1 and Building 21. Drift limit of 8.0%	88
Figure 52 Correlation between Building 1 and Building 35. Drift limit of 8.0%	89
Figure 53 Correlation between Building 1 and Building 60. Drift limit of 8.0%	89
Figure 54 Marginal and Joint Probabilities for IDA on Building 1 and Building 60.....	90
Figure 55 Monte Carlo Simulation of Damage.....	96

Figure 56 Histogram damaged buildings for Case 1.1.....	97
Figure 57 Histogram Damaged Buildings for Case 1.2.....	97
Figure 58 Histogram Damaged Buildings for Case 1.3.....	98
Figure 59 Comparison of Probability of Exceeding a Given Number of Damaged Building for Scenario 1	99
Figure 60 Histogram damaged buildings Case 2.1	101
Figure 61 Histogram Damaged Buildings Case 2.2	102
Figure 62 Histogram Damaged Buildings Case 2.3	102
Figure 63 Comparison of Probability of Exceeding a Given Number of Damaged Building Scenario 2	103
Figure 64 Disaggregation for return period of 475 years.....	105
Figure 65 Considered Earthquake Rupture for Scenario 3.....	106
Figure 66 Modelled AvgSa with and without spatial correlation for one realization.....	108
Figure 67 Correlation matrix calculated for one of the realizations	109
Figure 68 Histogram damaged buildings Case 3.1	110
Figure 69 Histogram damaged buildings Case 3.2	110
Figure 70 Histogram damaged buildings Case 3.3	111
Figure 71 Histogram damaged buildings Case 3.4	111
Figure 72 Comparison of Probability of Exceeding a Given Number of Damaged Building Scenario 3	112

LIST OF TABLES

Table 1 Attributes of GEM Taxonomy in Exposure Model.....	21
Table 2 Inventory of buildings with selected taxonomies on studied municipalities.....	22
Table 3 Input information to simulate portfolio of buildings.....	25
Table 4 Number of buildings by taxonomy and number of stories	28
Table 5 Summary of characteristics of simulated portfolio of Buildings.....	34
Table 6 Fundamental Period of Buildings in Both Directions.....	38
Table 7 Number of buildings by taxonomy in simulated portfolio.....	43
Table 8 AvgSa for different return periods.....	45
Table 9 Definition of damage states	56
Table 10 Parameters of fitted lognormal distribution to fragility curves.....	58
Table 11 Parameters of equivalent SDOF oscillator in direction 1	72
Table 12 Parameters of equivalent SDOF oscillator in direction 2	74
Table 13 Considered Scenarios for Damage Estimation	94
Table 14 Probability of Exceeding a Given Number of Buildings for Scenario 1	100
Table 15 Probability of Exceeding a Given Number of Buildings Scenario 2.....	104
Table 16 Probability of Exceeding a Given Number of Buildings Scenario 3.....	113

1. INTRODUCTION

The quantification of seismic risk has gained a particular interest of practitioners and researchers in the field of earthquake engineering in recent few decades. This was the objective of the Pacific Earthquake Engineering Research Center (PEER) when developing the performance-based earthquake engineering framework (PBEE), originally defined in the SEAOC's Vision 2000, and later refined in the FEMA P-58 report (ATC, 2018). PBEE has subsequently become the primary methodology for assessing the seismic risk of individual structures worldwide.

The PBEE framework accounts for variability and uncertainty across its different modules: earthquake hazard, building response, damage assessment and loss assessment (ATC, 2018). In the earthquake hazard module, a probabilistic approach is used to estimate a chosen ground motion intensity measure (IM) that conditions the structural response of the building at its location, such as the peak ground acceleration or the spectral acceleration for the fundamental period of the structure. The output of this module is a hazard curve, which provides the mean annual rate of exceedance for various IM values.

In the building response module, the probability distributions of response parameters of the structure, known as engineering demand parameters (EDP), are estimated at different levels of the chosen IM. Commonly used EDPs include the peak interstory drift ratio and peak floor acceleration, which generally condition the seismic behaviour of structural and non-structural components. The response of the building is quantified by different methodologies based on the realization of nonlinear time history analyses, like the incremental dynamic analysis (IDA) (Vamvatsikos & Cornell, 2002) or the multiple stripe analysis (MSA) (Jalayer & Cornell, 2009).

In the damage module, the probabilities of observing a given damage state (DS) are estimated by considering the behaviour of the different building components at a given EDP, commonly referred to as fragility curves. Finally, losses are estimated according to the damage in function of what is called a decision variable (DV), that are usually economic losses, downtime or casualties (ATC, 2018). These four modules are integrated within the PEER PBEE equation, which is based on the total probability theorem and used to estimate the mean annual frequency of exceedance for a given DV:

$$\lambda(DV) = \int_{DM} \int_{EDP} \int_{IM} G(DV|DS)dG(DS|EDP)dG(DS|EDP)|d\lambda(IM)| \quad (1)$$

where $\lambda(\bullet)$ is the mean annual frequency of exceedance of the random variable and $G(\bullet)$ and $dG(\bullet)$ are respectively the complementary cumulative distribution of a random variable and its derivative. Finding an analytical solution to the equation can be challenging when the problem is complex; therefore, Monte Carlo Simulation is commonly employed as the method to solve the problem.

Although the PBEE methodology was originally developed for individual buildings, from a societal perspective it is fundamental to consider the concept of performance in a regional level (Heresi & Miranda, 2023), to estimate the impacts of seismic events on all individuals and take decisions accordingly. Consequently, modifications must be made to the framework in order to accurately model the uncertainties and correlations between variables when quantifying the risk on multiple buildings. This led to the formalization of the regional performance-based earthquake engineering (RPBEE) framework, described by Heresi & Miranda (2023).

Some of the necessary adjustments, for instance, are related with the way the hazard module is handled. At a regional scale, hazard is not considered as a scalar, but as a vector that represents the selected IM's value at the locations of the different buildings. Since a probabilistic approach is used, IMs are typically considered as random variables characterized by a multivariate lognormal distribution, with mean values and standard deviations modelled by ground motion models (GMMs), and a corresponding correlation matrix, generally referred to as spatial correlation. The need of considering a spatial correlation and its effects has been thoroughly studied in the past, leading to the development of several mathematical models to estimate it (i.e, Bodenmann et al., 2023; Esposito & Iervolino, 2011; Jalayer & Cornell, 2009).

Regarding the building response module, a common approach when working at a regional level is grouping the structures with similar characteristics and expected similar behaviours into the so-called taxonomies. This relates directly with the way in which damage is considered at a regional scale, where the focus is on the global performance of buildings rather than the sum of the individual components. Global DSs, such as light damage, moderate damage, or collapse are considered, with fragility curves being derived for each of them for a given taxonomies. Different efforts and methodologies have been developed to do so, with notable results being obtained by the Global Earthquake Model organization (GEM), which created a catalogue of fragility curves for taxonomies commonly observed worldwide (Martins & Silva, 2021).

The use of the same fragility curve on the buildings within a taxonomy translates in the fact that they will have the same percentage probability of experiencing a given DS for a given value of the selected IM. Put another way, it may be viewed as the percentage of buildings of the taxonomy that have exceeded a given DS. While this is useful on a broader picture, it requires further consideration in a given earthquake scenario event to estimate further consequences (e.g., downtime, indirect losses etc.). For example, a single building of a taxonomy during a single earthquake event can either be damaged to a level DS or not, not a only certain percentage of it. Hence, Monte Carlo simulation from the taxonomy fragility function is utilised to simulate a set of buildings that have exceeded DS, and set of buildings that have not, where the overall percentage of this exceedance is the same as the percentage of the fragility function value at that IM level.

It is reasonable to consider, then, that structures built in the same region within the same time period were likely designed and constructed by the same professionals with common practices, resulting in them having either similar strengths or deficiencies (Heresi & Miranda, 2022). Therefore, if an earthquake causes one building to experience higher damage levels than expected, the same thing will occur to structures with similar enough characteristics. This is why in regional seismic risk assessment it is crucial to consider a structure-to-structure damage correlation, which represent the phenomenon previously described. This type of correlation is generally either neglected by risk modelers or handled in a very simplified way, yet it significantly affects the quantification of large-consequence risks (Heresi & Miranda, 2022).

This thesis uses a case study application in the province of Caserta in Southern Italy to demonstrate the effects of including structure-to-structure damage correlation in a regional seismic risk assessment. Different approaches were examined to select a method for calculating the correlation, addressing the limitations of the method, and underscoring the importance of carefully estimating the correlation value used in the assessment.

2. CASE STUDY: REGIONAL SEISMIC RISK ASSESSMENT OF MID-RISE CONCRETE FRAMES BUILDINGS

2.1 GENERAL DESCRIPTION

For the case study it was decided to perform a regional seismic risk assessment of a set of mid-rise residential concrete frame structures. The Built Environment Data's Design service (<https://design.bultenvdata.eu/>) designed to simulate a portfolio of buildings was employed for the analysis. This simulator utilizes Monte Carlo simulation to estimate various structural characteristics for each building, based on the expected proportions of those characteristics within the studied region. Then, each building is designed according to the equivalent lateral force method, using a specified lateral force coefficient (β) and seismic design code category, following the nomenclature used by Crowley et al. (2021), according to European design standards. The building simulator provides an OpenSees model of each building, allowing nonlinear time history analyses to be performed on all the buildings of the region.

To ensure the simulated buildings reflect realistic conditions, their characteristics and locations were chosen to emulate a real-world scenario. A study conducted by Corlito and De Matteis (2019) offers a detailed structural characterization of reinforced concrete buildings in the Caserta province in Italy, giving the data required to generate the portfolio of buildings with the tool previously mentioned. This study, which analysed eight municipalities within the province, included detailed data on the proportions of buildings with specific structural characteristics such as the number of stories, type of slab, and the conservation state of structural elements.

Given that the eight municipalities had varying levels of seismic hazard, for this case study it was decided to focus only on the three of them that had a similar level of seismic hazard, with them being classified as high hazard according to the Italian Seismic Code. The selected municipalities were: Castello del Matese, Gioia Sannitica, and Piedimonte Matese. Figure 1 shows the location of the Caserta Province in Italy, as well as the selected municipalities. The number of buildings included in the analysis, along with their geographical locations, was determined from an actual exposure model of the considered municipalities, which is described next.

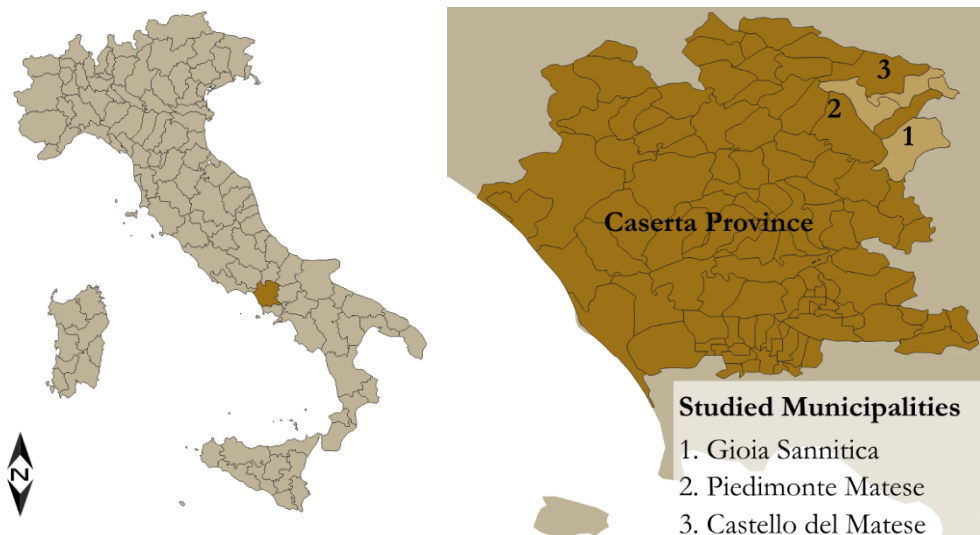


Figure 1 Location of Studied Municipalities

A probabilistic seismic hazard analysis was performed in the region in order to obtain specific data for the seismic risk assessment, as shown in Chapter 3 of this study. Additionally, the fragilities of the buildings were estimated analytically from nonlinear time history analyses performed on the OpenSees models generated with the simulator, as presented in Chapter 4. Different methodologies were then employed to analytically estimate the structure-to-structure damage correlation, allowing the study to verify the effects of incorporating this value into the analysis, and the impacts of adopting different methodologies.

2.2 EXPOSURE MODEL

Exposure is one of the main components of any type of risk. From a seismic risk perspective, significant losses in a seismically active zone are unlikely to occur if there are no buildings or assets located in the area. This is why, one of the main efforts of seismic risk modellers is developing models that represent in the best possible way the exposure information of the region that is being studied. This exposure models contain an inventory of the assets exposed to the earthquake hazard, as well as their geographical location and information about different attributes that condition the vulnerability of the structure, such as use, structural system, material, height and age (Atilla Ansal, 2014). Buildings are then classified into different categories, known as taxonomies, based on these characteristics so that buildings within the same taxonomy share similar vulnerabilities.

2.2.1 Exposure for the Caserta Province

The exposure model used for the current case study is the one considered for the European Seismic Risk Model (ESMR20). This model in particular (Crowley et al., 2021) was developed as part of the SERA project for 44 European countries, using publicly available information. It divides the buildings into residential, commercial and industrial use, and categorizes them according to the GEM Building Taxonomy v3.1. This corresponds to a code with information regarding different attributes of the building. The attributes that are specifically used by the European Exposure Model, and their coding are shown on Table 1.

Table 1 Attributes of GEM Taxonomy in Exposure Model

Attribute	ID
Material type	CR (Reinforced Concrete), S (Steel), MUR (Unreinforced Masonry), MCF (Confined Masonry), MR (Reinforced Masonry), etc.
Type of lateral load resisting system	LN (No lateral load resisting system), LFM (Moment Frame), LFINF (Infilled Frame), LWAL (Wall), etc.
Seismic Code Level	CDN (No Code), CDL (Low Code), CDM (Moderate Code), CDH (High Code)
Lateral Force Coefficient	LFC:n (n is the lateral force coefficient in percentage)
Number of stories	H:n (the exact number of stories is n), HBET:a-b (the range of number of stories is between a and b)

The attribute of seismic code level, as explained by Crowley et al. (2021) represents the characteristics of the seismic design of the building. If that attribute has CDN as an ID, the building was designed using the allowable stress method, with very low material strengths and focusing mostly on gravitational loads. For buildings designed with low codes (CDL), seismic actions were considered in the form a lateral force coefficient, referred to β by the authors and LFC by the GEM Taxonomy. This coefficient, which is a proportion of the

building's weight applied horizontally, was assumed to have a reasonable value depending on the level of knowledge at the time of the design of the building. CDL design considers material-specific standards and allowable stress design. On Moderate Codes (CDM), the seismic load is still considered with a lateral force factor but includes concepts of ultimate capacity design and details to improve ductility. Finally, High Code Class (CDH) include the current standards of seismic design, considering capacity design and local ductility measures.

For this case study, only residential mid-rise concrete frame buildings were analysed. All code levels and values of the lateral force coefficient (LFC) present in the area were considered. With this characteristic only three taxonomies are found in the region:

- CR/LFINF+CDL+LFC:0.0/HBET:4-: Low code reinforced concrete infilled frames with more than four stories designed for a load factor of 0%).
- CR/LFINF+CDL+LFC:7.0/HBET:4-: Low code reinforced concrete infilled frames with more than four stories designed for a load factor of 7.0%.
- CR/LFINF+CDM+LFC:7.0/HBET:4-: Moderate code reinforced concrete infilled frames with more than four stories designed for a load factor of 7.0%).

The inventory of this taxonomies of buildings on the studied municipalities are shown in Table 2, where it can be seen that the majority of the buildings belong to the CR/LFINF+CDL+LFC:0.0/HBET:4- taxonomy, indicating that most of the buildings are low code reinforced concrete infilled frames with more than four stories without seismic design provisions.

Table 2 Inventory of buildings with selected taxonomies on studied municipalities

Taxonomy	Number	Municipality	Lon	Lat
CR/LFINF+CDL+LFC:0.0/HBET:4-	7	Castello del Matese	14.3791	41.3728
CR/LFINF+CDL+LFC:7.0/HBET:4-	7	Castello del Matese	14.3791	41.3728
CR/LFINF+CDM+LFC:7.0/HBET:4-	3	Castello del Matese	14.3791	41.3728
CR/LFINF+CDL+LFC:7.0/HBET:4-	1	Gioia Sannitica	14.4221	41.2968
CR/LFINF+CDM+LFC:7.0/HBET:4-	1	Gioia Sannitica	14.4221	41.2968

CR/LFINF+CDL+LFC:0.0/HBET:4-	34	Piedimonte Matese	14.3701	41.3496
CR/LFINF+CDL+LFC:7.0/HBET:4-	7	Piedimonte Matese	14.3701	41.3496
CR/LFINF+CDM+LFC:7.0/HBET:4-	2	Piedimonte Matese	14.3701	41.3496

2.2.2 Spatial disaggregation of exposure model

It can be seen that in the exposure model, all buildings in the same municipality are lumped at a single point inside its boundaries. However, for an accurate regional seismic risk assessment, it would ideally be necessary to have the exact coordinates of each building in the region, to appropriately model the expected ground motion intensity for each location. Since this detailed information is not available for this case, it is necessary to spatially distribute the assets across the region using approximate methods.

In this case study, the buildings were disaggregated according to the population distribution within the region. This approach utilized Python scripts developed by GEM, which are available in the Spatial Disaggregation repository on GitHub (<https://github.com/GEMScienceTools/spatial-disaggregation>) (GEM, 2021). The data on the distribution of the population used for the analysis was obtained from the WorldPop data of Italy for the year 2020, with a resolution of 100m (WorldPop, 2018). The geographical boundaries of the municipalities were obtained from the Italian National Institute of Statistics (ISTAT) website. The resulting distribution of the assets is shown in Figure 2.

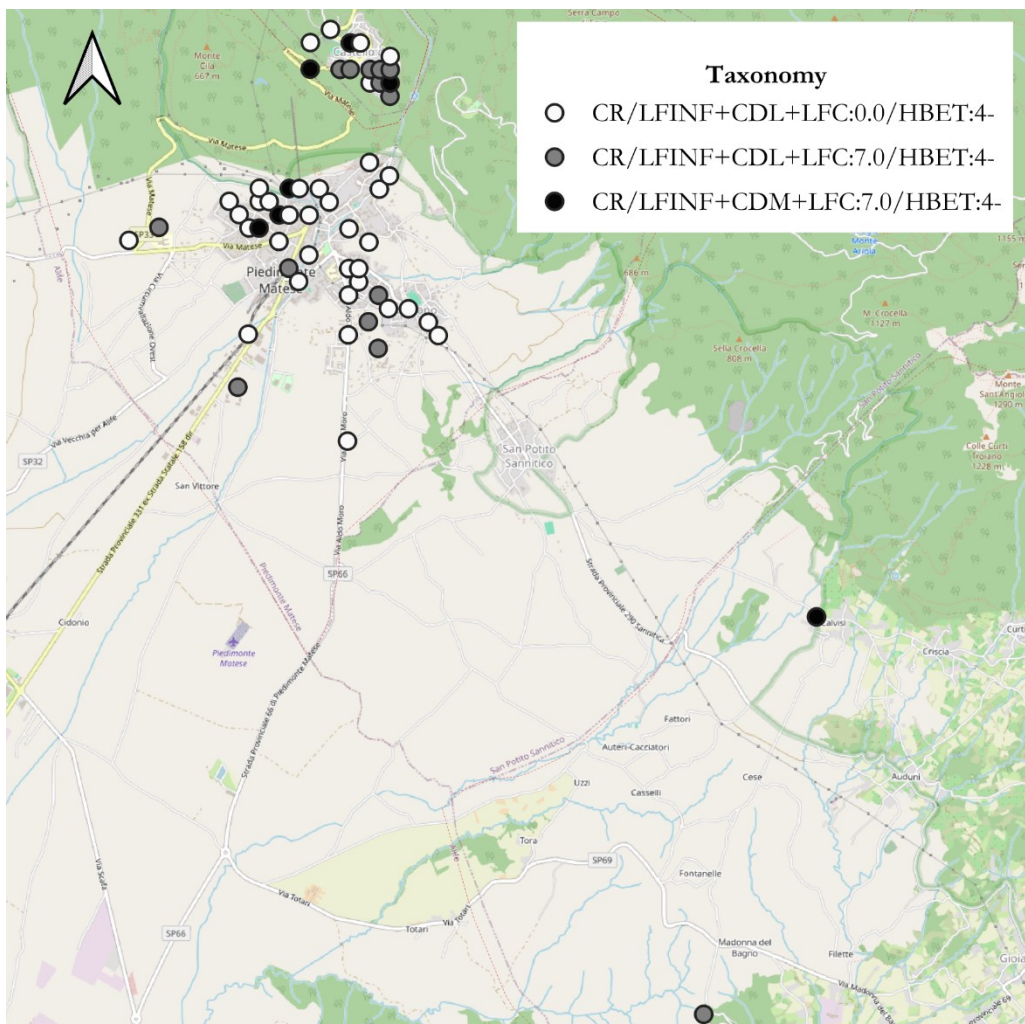


Figure 2 Geographical location of assets

2.3 MODELLING OF BUILDINGS

As previously mentioned, a structural model was generated for each of the buildings belonging to the selected taxonomies in the study region using a building generator tool. The tool simulates a portfolio of buildings using Monte Carlo Simulation, with the known probability of observing certain structural characteristics in the region for which the buildings are being generated. Other structural characteristics like the planar configuration, column spacing, height of each of the story and the strength of the materials are also sampled using Monte Carlo simulation on reasonable values observed in Europe.

The following structural characteristics are required as input to simulate the portfolio of buildings:

Table 3 Input information to simulate portfolio of buildings

Structural Characteristic	Input information
Type of slab. There are two possible types of slabs: solid slabs and composite slabs. Solid slabs are classified into two types: Type 1 if they are bidirectional, and Type 2 otherwise. Composite slabs, which include ceramic blocks and reinforced concrete (RC) joists, are classified as Type 3 regardless of the direction of loading. The direction of loading is determined by the ratio between the building's length (L) and width (W). Type 3 slabs can be constructed with either wide beams or emergent beams.	PSS1: ratio of buildings with a solid slab in the case in which $L/W < 2$ resulting in slab Type 1. PSS2: ratio of buildings with a solid slab in the case in which $L/W \geq 2$ resulting in slab Type 2. PWBA: ratio of buildings with wide beams for slab Type 3.
Geometry of Columns: Buildings can have either square or rectangular columns.	PSquared: ratio of buildings with square columns.
Quality of Building. Represent the quality of the construction of the building. There are three possible quality levels: low, moderate and high.	PQLow: ratio of buildings with low quality of construction. PQModer: ratio of buildings with moderate quality of construction. PQHigh: ratio of buildings with high quality of construction.
Design Class. Level of the code for which the building was designed according to the nomenclature in the GEM Taxonomy. Choose between one of the options.	CDN: No Code. CDL: Low Code. CDM: Moderate Code. CDH: High Code.

Lateral force coefficient. Indicate the value of the lateral force coefficient to design the building according to the GEM Taxonomy.	Beta: Lateral Force Coefficient.
Section of elements. Geometrical dimensions of beams and columns. The dimensions that are not input are calculated to satisfy the demands on the elements.	Bcolfix: fixed width of the column. Bbeamfix: fixed width of the beam.
Thickness of stairs. Initial estimated thickness of the slab of the stairs.	Hstairs: thickness of stairs.
Weight of infills. Load corresponding to infill weight.	Ppinfills: load corresponding to infill weight
Number of stories.	N: number of stories.

To accurately model the buildings, it is essential to have reliable data on these structural characteristics, requiring the realization of a structural characterization of the buildings located in the area.

2.3.1 Structural characterization

The structural characterization of all the assets required to simulate the portfolio of buildings was obtained from different sources. The design class and lateral force coefficient information are provided directly in the building taxonomies within the exposure model. Other information, such as the section of elements, stair thickness, and infill weight, can be estimated from commonly used engineering values for these parameters in the area.

The remaining information, such as type of slab, quality of buildings, and number of stories, was obtained from a structural characterization of reinforced concrete buildings in the region developed by Corlito and De Matteis (2019). This characterization was carried out using the CARTIS form, a tool created under the ReLUIS project, which assesses the typological and structural features of buildings. Specifically, the study by Corlito and De Matteis (2019) collected data on key structural attributes that were later analysed to classify the buildings into distinct vulnerability categories, reflecting their susceptibility to suffer damage from seismic events.

The study was performed on eight municipalities of the province, including the ones selected for the case study, and carries out a characterization of all concrete structures observed in the region, including all types of uses, structural systems and number of stories. Consequently, it is assumed that the information regarding the proportion of buildings with certain characteristics can be applied to the selected building taxonomies in the three municipalities analysed in this study.

Regarding the number of stories, the exposure model indicates that the buildings in question have at least four stories, but the exact number is uncertain. For that, Corlito and De Matteis (2019) found that out of all the concrete buildings in the studied municipalities 2% had four stories, 8% had five stories, and no buildings had more than five. Since the total percentage of buildings with either four or five stories is 10%, we can infer that 20% of midrise buildings have four stories and 80% have five stories.

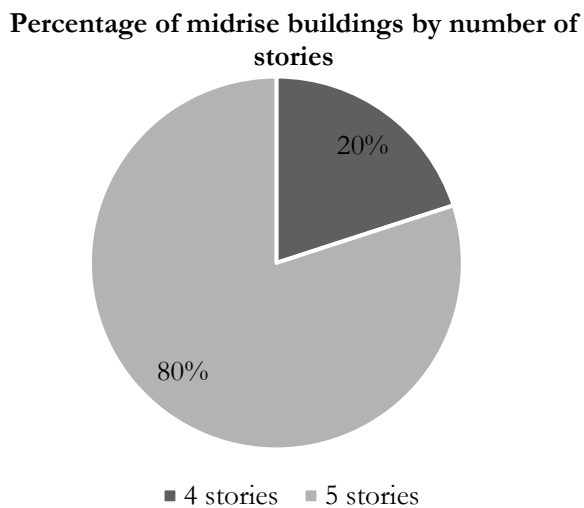


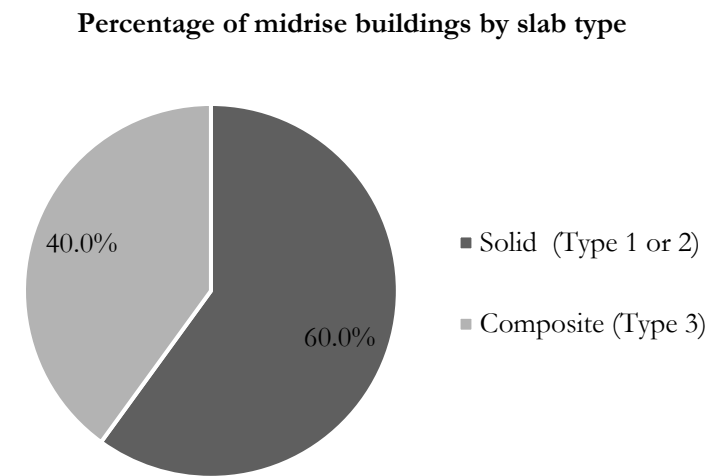
Figure 3 Percentage of midrise buildings by number of stories

The number of buildings in the inventory Table 2 was multiplied by this proportion in order to determine the number of buildings in each taxonomy with both 4 and 5 stories. To simplify the nomenclature from now on, each combination of taxonomy and number of stories is defined as a “Class”, as shown in Table 4.

Table 4 Number of buildings by taxonomy and number of stories

Taxonomy	Number of stories	Number of buildings	Class
CR/LFINF+CDL+LFC:0.0/HBET:4-	4	8	1
CR/LFINF+CDL+LFC:0.0/HBET:4-	5	33	2
CR/LFINF+CDL+LFC:7.0/HBET:4-	4	3	3
CR/LFINF+CDL+LFC:7.0/HBET:4-	5	12	4
CR/LFINF+CDM+LFC:7.0/HBET:4-	4	1	5
CR/LFINF+CDM+LFC:7.0/HBET:4-	5	5	6

From the qualification according to structural system performed by Corlito and De Matteis (2019), it can be noted that 90% of the reinforced concrete buildings correspond to all types of frames. Out of all the buildings 12% have wide beams, and 20% have emergent beams, that are both possible options of Type 3 slabs. So considering only the frames, 12% of the 90% of buildings (13.3%) have Type 3 slabs with wide beams and 20% of 90% (26.6%) have Type 3 slabs with emergent beams. Adding up both values we have that 40% of concrete frame buildings in the region have a slab Type 3. The proportion of buildings with a solid slab is then 60%. Following then the nomenclature presented in Table 3 both PSS1 and PSS2 are 0.6.

**Figure 4 Percentage of buildings by slab type**

For Type 3 slabs, which include composite slabs with ceramic blocks and RC joists, are distributed in the following way according to their characteristics:

- **Wide Beams:** Out of all slab types, 13.3% are made with wide beams. So, wide beams make up 33.3% of the Type 3 slabs.
- **Emergent Beams:** Out of all slab types, 26.7% use emergent beams. This means that emergent beams account for 66.7% of Type 3 slabs.

This means that following the nomenclature presented in Table 3 PWBA is equal to 0.333, which is depicted below.

Percentage of beam type for slab Type 3

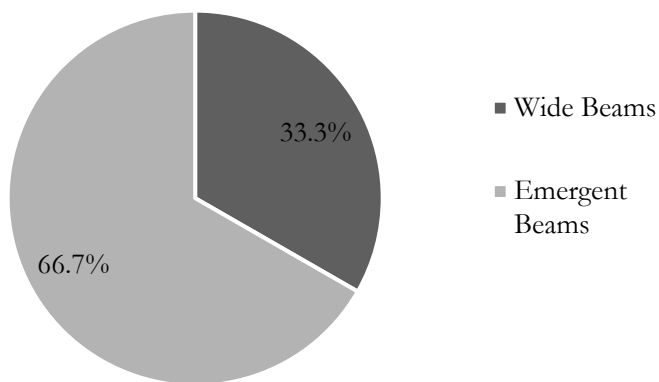


Figure 5 Percentage of beam type for slab Type 3

The value of the quality of the construction is associated with the parameter conservation of horizontal structure estimated by Corlito and De Matteis (2019). The authors defined three classes for this parameter: Class 1 represents the highest vulnerability and was associated with low construction quality, while Class 3 represents the lowest vulnerability and was associated with high construction quality. Class 2, then, was associated with moderate construction quality. The proportions for each of these classes are shown in Figure 6.

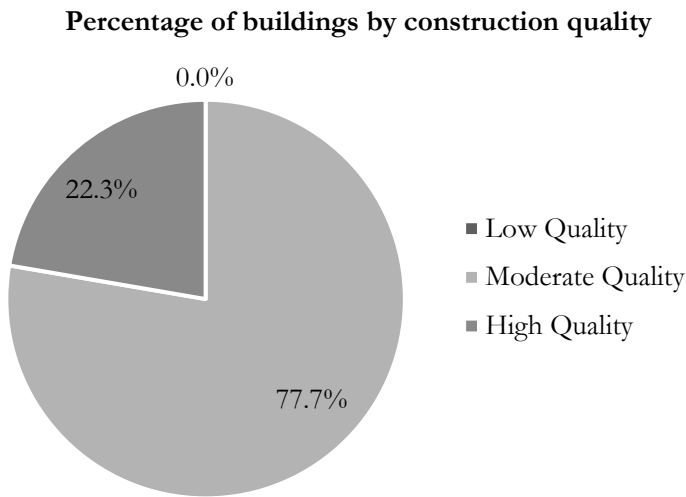


Figure 6 Percentage of building by construction quality

This means that following the nomenclature presented in Table 3, $PQLow=0$, $PQModer=0.777$ and $PQHigh=0.223$.

2.3.2 Portfolio of buildings

The buildings shown in Table 4, with the corresponding design class and lateral force factor associated with each taxonomy were generated using the building simulator considering the proportion of the characteristics shown in Figure 4, Figure 5 and Figure 6. The values of the fixed dimensions of the columns were assumed to be 0.30m which is the common practice in the area. The load of the infills was considered to be 8 kN/m applied directly on the beams. The thickness of the stairs is taken as 0.15m.

The simulator of the portfolio considers the possibility of having a different height of the first story ($H1$) comparing to the one of the other stories ($H2$). Regarding the planar geometry of the buildings, there are 11 possible layouts, which are assigned randomly to each of the buildings. The possible layouts are shown in Figure 7 through Figure 13.

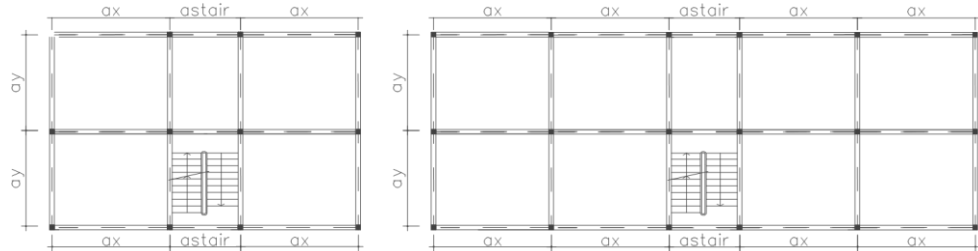


Figure 7 Layouts B01 (left) and B02 (right)

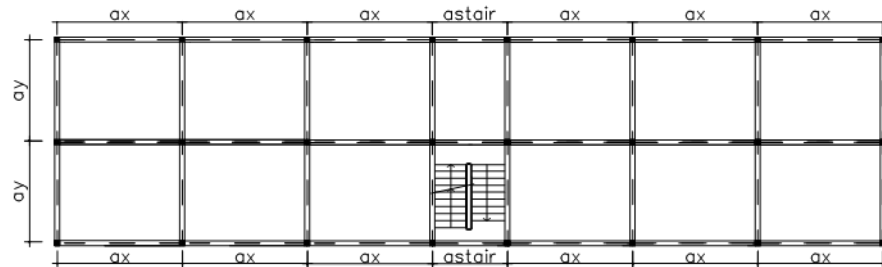


Figure 8 Building Layout B03

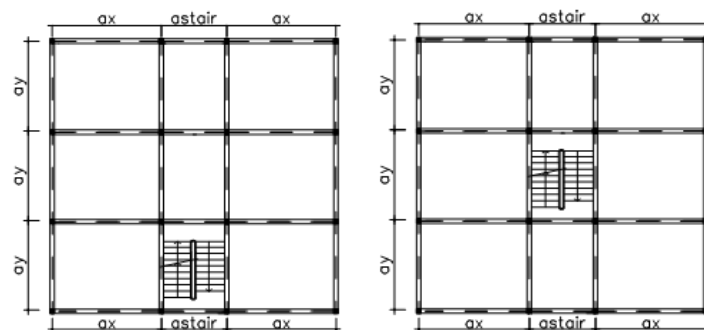


Figure 9 Building Layout B04 (left) and B04b (right)

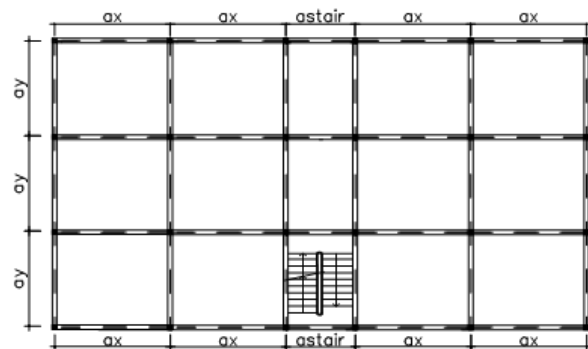


Figure 10 Building Layout B05

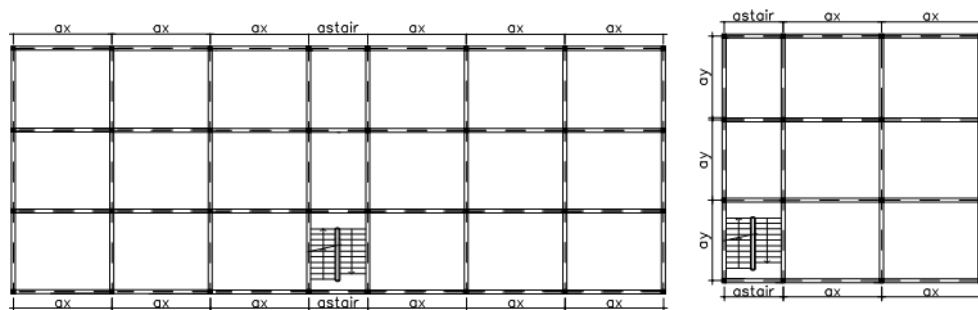


Figure 11 Building Layout B06 (left) and B07 (right)

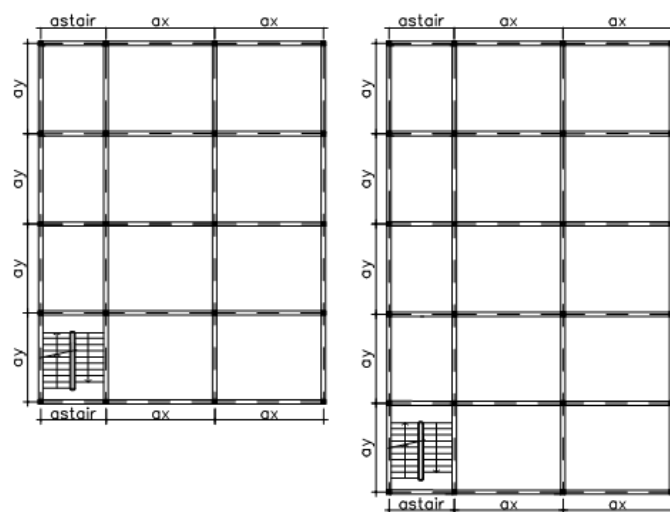


Figure 12 Building Layout B08 (left) and B09 (right)

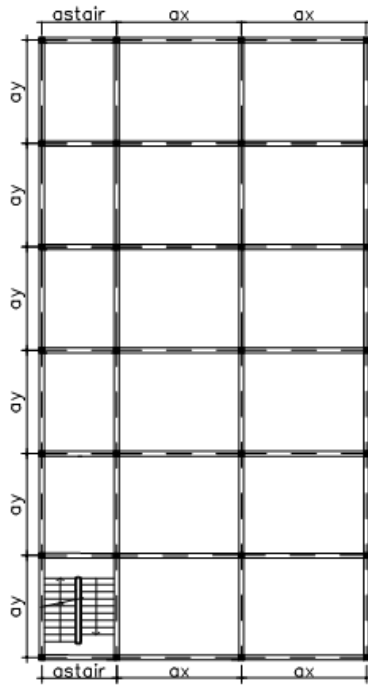


Figure 13 Building Layout (B10)

The actual portfolio of buildings used for the analysis is shown in Table 5. The “Class” value represents each combination of the observed taxonomies and the possible number of stories, as mentioned in Table 4. The geometrical dimensions (astair, ax, and ay) indicate the distances between columns, following the nomenclature used in Figure 7 through Figure 13. The value of H1 and H2 are the height of the first story and the remaining stories respectively. The variable “slab type” corresponds to the nomenclature indicated in Table 3, which also apply to the variable quality type. Finally, f_{ck} and f_{syk} correspond to the characteristic compressive strength of the concrete and characteristic yield strength of the reinforcement steel respectively.

Table 5 Summary of characteristics of simulated portfolio of Buildings

Building	Class	Layout	astair (m)	ax (m)	ay (m)	H1 (m)	H2- (m)	Slab Type	Slab Orient	Beam Type	Quality	f_{ck} (MPa)	f_{syk} (MPa)
1	1	B04	2.9	4.9	4.5	3.6	3	1	x-y	Emergent	Moderate	19	400
2	1	B03	2.85	3.95	4.85	2.8	2.8	1	x-y	Emergent	Moderate	14	500
3	1	B03	3.1	4.5	5.2	3.15	2.85	1	x-y	Emergent	High	19	240
4	1	B05	3.1	4.55	4.95	3	2.5	3	y	Emergent	Moderate	14	400
5	1	B08	3	4.25	5.15	2.75	2.75	1	x-y	Emergent	Moderate	19	400
6	1	B02	2.8	5.65	4.05	3.35	2.8	1	x-y	Emergent	Moderate	19	400
7	1	B02	2.9	4.8	4.25	3.25	3.25	3	x	Emergent	Moderate	25	400
8	1	B04	2.95	4.45	4.4	3.85	2.95	1	x-y	Emergent	Moderate	19	400
9	2	B02	2.9	4.3	4.95	3.4	2.85	3	y	Emergent	High	19	400
10	2	B07	2.85	4.5	5.25	3.35	3.05	1	x-y	Emergent	Moderate	14	400
11	2	B08	3.1	3.55	5.8	3.35	2.8	3	y	Emergent	Moderate	19	400
12	2	B08	3.1	4.2	4.9	2.95	2.95	3	y	Wide	Moderate	25	400
13	2	B10	3	4.35	5	3	3	1	x-y	Emergent	Moderate	14	400
14	2	B03	2.8	7	3.75	2.85	2.85	3	x	Emergent	Moderate	14	400
15	2	B01	2.9	5.1	4.3	3.5	2.9	3	x	Wide	Moderate	25	240
16	2	B02	2.95	5.8	4.25	3.05	3.05	3	x	Emergent	Moderate	19	400
17	2	B04	3	3.85	5.9	3.7	2.85	1	x-y	Emergent	Moderate	25	400
18	2	B06	2.85	5.05	4.95	2.9	2.65	1	x-y	Emergent	Moderate	25	400
19	2	B03	2.95	5.5	4.05	3	3	1	x-y	Emergent	Moderate	14	240
20	2	B02	2.95	4.4	5	3.75	2.9	1	x-y	Emergent	Moderate	14	400
21	2	B04	2.9	5.85	3.7	3.65	2.8	1	x-y	Emergent	High	19	500

22	2	B09	3.1	4.6	5	3.65	3.05	1	x-y	Emergent	Moderate	14	400
23	2	B04	3	6.65	3.55	3.85	2.95	3	x	Emergent	Moderate	14	400
24	2	B06	2.95	3.95	5.45	3.2	3.2	1	x-y	Emergent	High	14	240
25	2	B10	3	3.9	5.25	3.5	2.9	1	x-y	Emergent	Moderate	19	400
26	2	B04b	2.85	3.8	5.75	3.35	2.8	1	x-y	Emergent	Moderate	14	500
27	2	B09	3.15	5.8	4.2	3.4	2.85	3	x	Emergent	Moderate	25	240
28	2	B08	3.05	5	4.5	3.4	2.85	1	x-y	Emergent	Moderate	25	400
29	2	B01	3.05	3.65	5.85	3.1	3.1	3	y	Emergent	Moderate	14	400
30	2	B06	2.95	6.65	3.85	2.55	2.55	1	x-y	Emergent	High	14	240
31	2	B03	2.85	4.9	4.6	3.1	3.1	1	x-y	Emergent	Moderate	25	240
32	2	B04b	2.85	4	5.35	3.55	2.95	3	y	Emergent	High	14	500
33	2	B05	2.9	5.1	4.8	2.9	2.9	3	x	Wide	Moderate	14	400
34	2	B09	2.9	4.25	5.55	2.65	2.65	3	y	Emergent	Moderate	19	400
35	2	B07	2.85	7	3.6	2.75	2.75	1	x-y	Emergent	Moderate	19	400
36	2	B06	3	6.2	3.9	2.85	2.85	3	x	Emergent	Moderate	19	400
37	2	B04b	3.1	5.05	4.4	2.65	2.65	3	x	Emergent	Moderate	19	240
38	2	B10	2.85	7.5	3.5	3.6	3	2	x	Emergent	Moderate	14	240
39	2	B10	2.85	4.45	4.8	2.5	2.5	3	y	Emergent	Moderate	14	400
40	2	B10	2.95	3.75	5.4	2.95	2.95	3	y	Emergent	Moderate	19	400
41	2	B02	3.1	3.75	5.85	2.8	2.8	1	x-y	Emergent	Moderate	25	240
42	3	B02	2.9	5.65	3.9	2.8	2.8	3	x	Emergent	High	19	400
43	3	B04b	2.85	4.7	4.55	3	3	3	x	Wide	Moderate	14	240
44	3	B04b	3.1	3.65	5.75	2.9	2.9	3	y	Emergent	High	14	400
45	4	B04	2.9	4.55	4.4	2.8	2.8	1	x-y	Emergent	Moderate	19	240

46	4	B04b	2.85	4.25	4.55	3.05	3.05	3	y	wide	Moderate	25	400
47	4	B01	3.1	5.65	3.95	3.15	2.85	1	x-y	Emergent	Moderate	14	240
48	4	B04	3.1	4.8	4.3	3.2	3.2	1	x-y	Emergent	High	14	400
49	4	B04	3	4.45	4.55	3.8	2.7	1	x-y	Emergent	Moderate	25	400
50	4	B10	2.8	4.8	4.55	3.25	2.7	3	x	Wide	Moderate	25	400
51	4	B06	2.9	3.7	5.8	2.9	2.65	1	x-y	Emergent	High	19	400
52	4	B08	2.95	6.45	3.65	4.2	3.05	3	x	Emergent	Moderate	14	400
53	4	B02	3	5.45	3.9	2.9	2.9	3	x	Emergent	Moderate	25	400
54	4	B06	2.85	5.3	4.15	2.6	2.6	3	x	Emergent	Moderate	19	400
55	4	B07	2.95	4.6	4.95	3.2	3.2	1	x-y	Emergent	High	25	500
56	5	B08	2.9	3.7	6.9	2.85	2.85	1	x-y	Emergent	Moderate	20	400
57	6	B09	2.9	4.15	5.4	2.8	2.8	1	x-y	Emergent	High	20	500
58	6	B07	2.85	4.45	5.6	2.7	2.7	1	x-y	Emergent	Moderate	16	500
59	6	B07	3.1	4.9	4.75	3.25	2.7	3	x	Emergent	Moderate	20	500
60	6	B04b	3.1	3.95	5.8	2.9	2.9	1	x-y	Emergent	High	16	400
61	6	B02	3	4.5	5.15	3	3	3	y	Emergent	Moderate	25	400
62	6	B01	2.8	4.55	4.45	2.65	2.65	1	x-y	Emergent	Moderate	20	400

2.3.3 Structural Model

Each building in the portfolio was designed using the equivalent lateral force method to determine the reinforcement required to resist both vertical and lateral loads. This design information was then used to create an OpenSeesPy model for nonlinear time history analysis. The model captures the structure's nonlinear behaviour by considering geometric nonlinearity (i.e., P-Delta effects) and employing a lumped plasticity approach to simulate plastic hinge formation in structural elements. Vertical loads were assigned based on the slab weight, which depended on its characteristics, and the weight of the infills as previously defined.

In terms of the model's characteristics, both columns and beams were modelled as elastic elements, while zero-length elements were introduced between nodes to simulate localized nonlinear behaviour where plastic hinges form. These zero-length elements were defined using hysteretic materials to capture the expected nonlinear response at these locations, allowing for the simulation of plastic deformations and energy dissipation during seismic events. The buildings were modelled as bare frames, excluding the lateral strength contribution from the infills, which would have been expected based on the exposure model.

A modal analysis was performed to the buildings to have a general idea of their dynamic characteristics. The results are shown on Table 6.

Table 6 Fundamental Period of Buildings in Both Directions

Building	Period X [s]	Period Y [s]	Building	Period X [s]	Period Y [s]
Building 1	0.994	1.076	Building 32	1.297	0.814
Building 2	0.844	0.815	Building 33	0.698	0.748
Building 3	0.909	0.888	Building 34	1.068	0.724
Building 4	0.868	0.671	Building 35	0.713	1.192
Building 5	0.915	0.850	Building 36	0.764	1.308
Building 6	0.846	1.137	Building 37	0.773	1.130
Building 7	0.945	1.277	Building 38	0.634	1.234
Building 8	1.112	1.196	Building 39	0.951	0.624
Building 9	1.136	0.940	Building 40	1.205	0.881
Building 10	0.985	1.027	Building 41	1.122	1.067
Building 11	1.172	0.944	Building 42	0.700	0.930
Building 12	1.430	1.101	Building 43	0.759	0.943
Building 13	1.022	0.938	Building 44	0.832	0.732
Building 14	0.619	1.219	Building 45	0.928	0.981
Building 15	1.095	1.661	Building 46	1.319	1.318
Building 16	0.839	1.439	Building 47	0.858	0.929
Building 17	1.381	1.278	Building 48	0.905	0.948
Building 18	1.097	1.191	Building 49	1.249	1.323
Building 19	0.826	1.173	Building 50	1.026	1.275
Building 20	1.074	1.022	Building 51	0.924	0.852
Building 21	0.952	1.264	Building 52	0.784	1.007
Building 22	1.004	1.033	Building 53	1.009	1.258
Building 23	0.848	1.300	Building 54	0.753	1.061
Building 24	1.180	0.903	Building 55	1.228	1.305
Building 25	1.276	1.114	Building 56	0.801	0.732
Building 26	1.160	0.926	Building 57	0.993	0.962
Building 27	1.014	1.529	Building 58	0.883	0.902
Building 28	1.210	1.431	Building 59	0.933	1.201
Building 29	1.276	0.868	Building 60	0.817	0.786
Building 30	0.602	0.935	Building 61	1.104	0.989
Building 31	1.192	1.469	Building 62	0.882	0.976

The pushover curve of some of the buildings on both directions are the following.

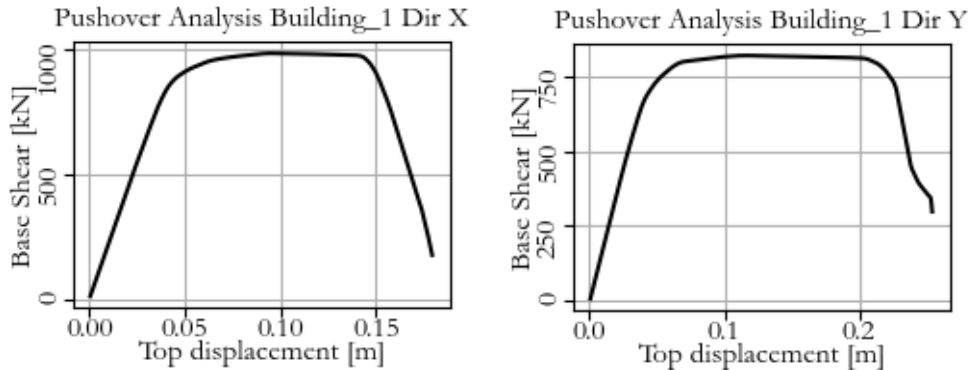


Figure 14 Pushover Curves of Building 1

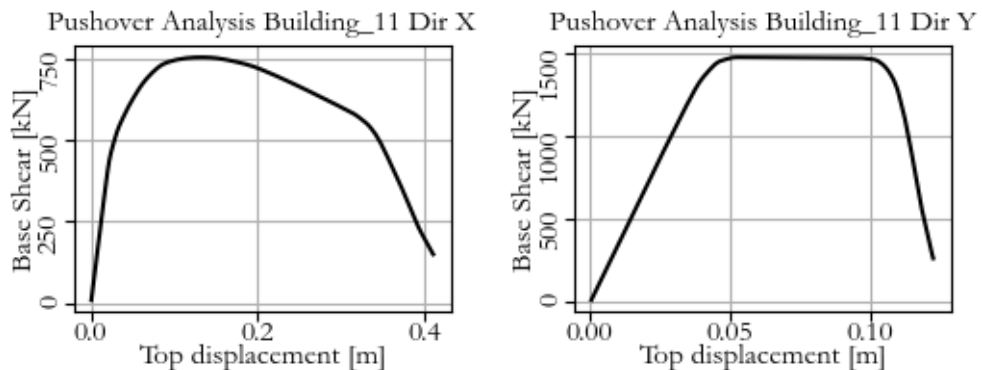


Figure 15 Pushover Curves of Building 11

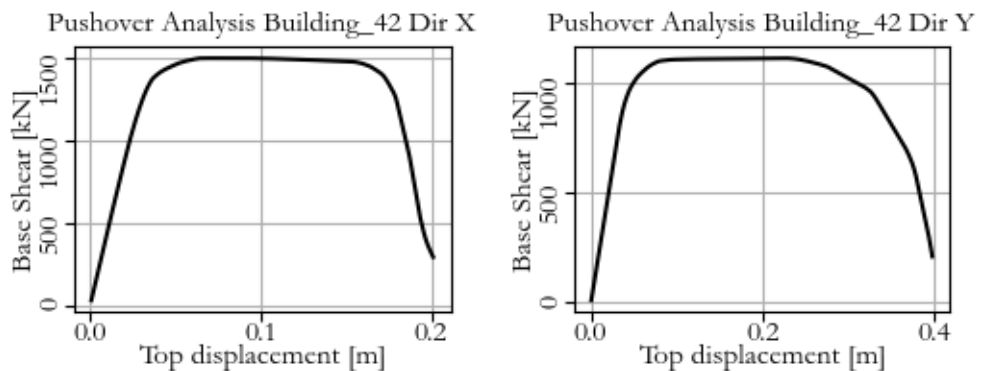


Figure 16 Pushover Curves of Building 42

2.3.4 Geographical location

To conclude the process of generating the portfolio of buildings, each of the assets must be geographically distributed in the area. This process was done assigning randomly a building, out of the ones presented on Table 5, to each of the locations in the previously spatially disaggregated exposure model shown in Figure 2, matching the taxonomy type. The final distribution is presented on Figure 17, in which the location of the buildings in the municipalities of Castello del Matese and Piedimonte Matese are shown on the left figure and the ones in the municipality of Gioia Sannitica are shown on the right figure.

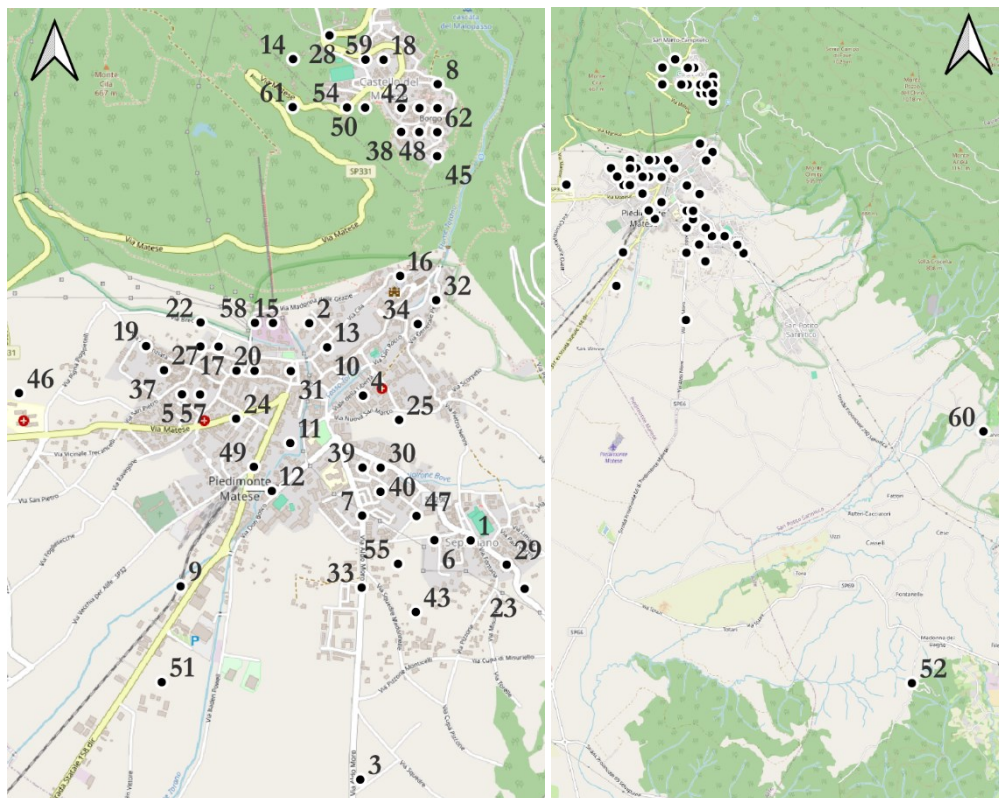


Figure 17 Geographical Location of Buildings

3. HAZARD ANALYSIS AND GROUND MOTION SELECTION

In this section, the process of quantifying the seismic hazard is presented, which is one of the main components of the seismic risk assessment framework. This plays a fundamental role in quantifying seismic risk, as it characterizes the probabilistic nature of earthquake ground motion intensities at the site of interest. Focusing on the methodology given by the PBEE framework, the scope is estimating the levels of ground motion intensity measures (IMs) that best characterise the structural response of buildings from a probabilistic point of view.

The primary objective is to develop a hazard curve, which provides the mean annual rate of exceedance for a selected IM value, such as peak ground acceleration or spectral acceleration. The first step, however, must be selecting which IM is going to be used in the analysis, choosing one that is appropriate for the specific case that is being studied. The curve is generated using probabilistic seismic hazard analysis (PSHA), a methodology that integrates seismic source characterization, ground motion model (GMMs), and site-specific conditions to estimate the likelihood of observing different levels of ground shaking at the location of interest.

Given the regional scale of the case study, it was not deemed necessary to account for spatial variations in ground motion and their correlations across multiple building sites, although further analysis could include these aspects. This would introduce additional complexity, as the hazard is no longer a scalar value but a vector that captures the spatial distribution of IMs across the region.

3.1 SELECTION OF INTENSITY MEASURE

The main purpose of the intensity measure (IM) in performance based seismic engineering is serving as a useful link between the ground motion hazard at a particular site and the response of a given structure (Eads et al., 2015). The response of the structure is represented by the so-called engineering demand parameters (EDP), variables that relate with damage of the building, such as the peak interstory drift ratio or peak floor acceleration. The IM, then, is a variable that quantifies the intensity of ground motion and can be dependent either from the ground motion characteristics alone (e.g., peak ground acceleration) or from a combination of ground motion and structural properties (e.g.,

spectral acceleration at the structure's fundamental period, $S_a(T_1)$). It becomes fundamental then to select an IM that can appropriately relate with the expected response of the building.

Several studies have been conducted in the last years to quantify the accuracy of various IMs for the assessment of different type of structures, focusing generally on the concepts of efficiency and sufficiency. Efficiency refers to the ability of an IM to minimize the variability in the EDPs obtained from nonlinear time history analyses, thereby reducing the number of records required to achieve precise results. Sufficiency, on the other hand, relates to the independence of the resulting EDPs from the magnitude and source-to-site distance of the records used in the analysis (Luco & Cornell, 2007). One IM that has gained widespread use in recent years for the assessment of buildings is the average spectral acceleration.

3.1.1 Average spectral acceleration

The performance of the average spectral acceleration over a range of periods (AvgSa) as an intensity measure for estimating structural collapse was studied by Eads et al. (2015). When assessing an individual building, the use of this IM is justified, as it accounts for changes in the structure's period due to stiffness degradation under nonlinear conditions, an aspect not captured by the commonly used spectral acceleration at the fundamental period ($S_a(T_1)$). This is why, when compared to $S_a(T_1)$, AvgSa proved to be a better predictor of the response of the structure, considering criteria like the efficiency and sufficiency of both IMs (Eads et al., 2015). Other studies that looked at AvgSa as an IM for risk assessment were developed by Aristedidou & O'Reilly (2024), Kohrangi et al. (2018), Nafeh & O'Reilly (2024), O'Reilly (2021) and Vamvatsikos & Cornell (2005).

One of the issues regarding the use of AvgSa as IM is the limited availability of hazard curves in common databases as a function of this parameter when compared to $S_a(T_1)$. However, if a PSHA is being particularly developed for the study, AvgSa can be easily estimated using existing GMMs for different periods, considering the correlation between those variables (Eads et al., 2015). There are two different approaches than can be used then to estimate hazard in terms of AvgSa: using GMMs developed specifically for this IM (i.e., Aristedidou et al., 2024; Dávalos & Miranda, 2021) or compute it indirectly with the methodology derived by Kohrangi et al. (2017).

Beyond the benefits of using AvgSa for individual structures, its application in this study is particularly convenient. Since a regional assessment of different structures is being performed, choosing only one period to use as fundamental period for $S_a(T_1)$ could be problematic. AvgSa, on the other hand, allows for the selection of a range of periods that captures not only the variations in the period of each structure but also the variability across

all the structures considered. This approach has been similarly applied in studies by O'Reilly (2021b) and O'Reilly et al. (2018). The period range for the analysis must be selected carefully so it represents the characteristics of the buildings that are being used.

3.1.2 Selection of period range for Case Study

In the current case study, 62 midrise concrete frame buildings are being considered for the analysis, as shown in Table 5. The period range of these structures in both main directions varies between 0.65s for Building 38 on direction y, and 1.66s for Building 15 on direction x, as it can be observed in Table 6. The geometric mean of the periods of all buildings in all directions is 1.01s. Even though the period range could have been selected according to this data, it was decided to use another simulated portfolio of buildings instead, that included also concrete frame buildings with 1, 2 and 3 stories. This allows to use this analysis in other possible future applications of the work, in which other taxonomies are also included.

In this extended portfolio of 150 buildings, the number of structures included on each taxonomy was proportional to the total number of structures within that taxonomy in the three selected municipalities, according to the European Exposure Model V1.0 (H. Crowley et al., 2021). The characteristics of the buildings are the same for which the 62 midrise buildings were generated, as shown in Section 262.3.1 of this study. The total proportion and number in the simulated portfolio are shown in Table 7.

Table 7 Number of buildings by taxonomy in simulated portfolio

Taxonomy	Total Number	Proportion	Number in simulated portfolio
CR/LFINF+CDL+LFC:0.0/H:1	10	1.44%	2
CR/LFINF+CDL+LFC:0.0/H:2	275	39.57%	59
CR/LFINF+CDL+LFC:0.0/H:3	131	18.85%	28
CR/LFINF+CDL+LFC:0.0/HBET:4-	41	5.90%	9
CR/LFINF+CDL+LFC:7.0/H:1	10	1.44%	2
CR/LFINF+CDL+LFC:7.0/H:2	64	9.21%	14
CR/LFINF+CDL+LFC:7.0/H:3	20	2.88%	4
CR/LFINF+CDL+LFC:7.0/HBET:4-	14	2.01%	3
CR/LFINF+CDM+LFC:7.0/H:1	13	1.87%	3
CR/LFINF+CDM+LFC:7.0/H:2	64	9.21%	14
CR/LFINF+CDM+LFC:7.0/H:3	46	6.62%	10
CR/LFINF+CDM+LFC:7.0/HBET:4-	7	1.01%	2

It was guaranteed that this portfolio included the buildings from the original midrise portfolio with the most extreme periods, as well as other randomly selected buildings. For this new portfolio, the smaller period in any direction is 0.20 s, and the larger period is 1.66s. The mean of the geometric mean of the period on both directions of the building is 0.605s. Following the recommended period range by (Eads et al., 2015), the lower bound should be estimated as 0.2 times the fundamental period of the structure and the upper bound as 3 times the fundamental period of the structure. For this case, the boundaries were estimated with the mean period of all buildings of 0.605s, resulting in a lower bound of 0.12s and an upper bound of 1.82s.

3.2 PROBABILISTIC SEISMIC HAZARD ANALYSIS

The probabilistic seismic hazard analysis (PSHA) developed for the Case Study was performed using the OpenQuake engine (Paganini et al., 2014), an advanced tool developed by the Global Earthquake Model (GEM) Foundation. The PSHA quantifies the likelihood of various levels of earthquake-induced ground shaking at a site over a specific period. OpenQuake, integrates seismic source models, ground motion models, and site-specific parameters to generate hazard curves and maps. This analysis provides a full understanding of the seismic hazard at the study site, forming a foundation for the risk assessment that was performed afterwards.

A source model in PSHA represents the spatial distribution and characteristics of seismic sources that can generate events. These models typically include fault lines, seismic zones, or areas of smeared seismicity, each defined by parameters such as location, geometry, magnitude recurrence, and rupture mechanisms. For this study the source model developed in the frame of the 2013 European Seismic Hazard Model (ESHM13) was used (D. Giardini et al., 2013). It includes three approaches to consider earthquake activity: a classic area source model, a model that combines fully parameterised faults with background seismicity zones, and a smoothed seismicity model.

A Ground Motion Model (GMM) is a mathematical model used in PSHA to estimate the expected level of ground shaking at a site, given an earthquake of a specific magnitude, distance, and other relevant parameters. GMMs incorporate empirical data from past earthquakes and consider factors such as the type of seismic wave, site conditions, and the nature of the fault rupture. Usually, to consider epistemic uncertainty, a logic tree is created using more than one GMM, however, since this is an academic study only the model proposed by Boore et al. (2014) was used. Since there is no information regarding the site conditions in the area, a firm soil with $V_{s,30}=480$ m/s was assumed in the analysis.

The hazard information was used in the following sections to select records to perform nonlinear time history analyses on the buildings, as part of the building response and

damage estimation modules. Considering that the 62 buildings are distributed across the area, the ideal scenario would involve obtaining a hazard curve for each specific site where they are located. To maintain a consistent set of records on all buildings, which was a requirement of the type of analysis that was performed, the hazard curve was estimated for the average coordinates of all buildings instead. This point has a latitude of 41.355 and a longitude of 14.374. As previously stated, the selected IM is the spectral acceleration for a period range of 0.12s-1.82s, estimated as the spectral ordinate for periods (0.12s, 0.22s, 0.32s,, 1.82s). The hazard curve at the site is shown below.

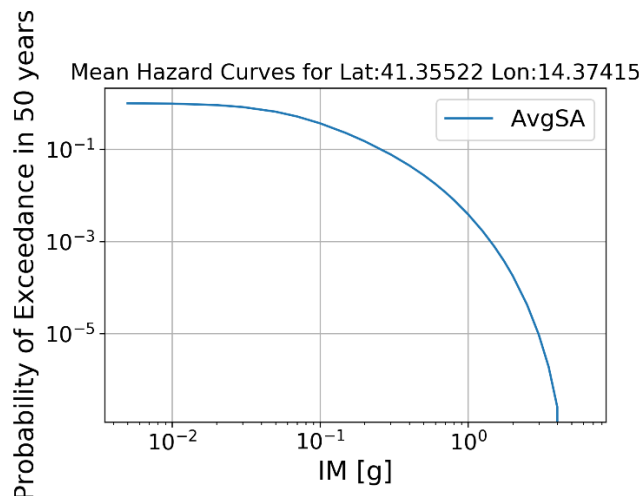


Figure 18 Hazard Curve

The table below reports the values of the AvgSa for some probabilities of exceedance in 50 years, that represent different return periods.

Table 8 AvgSa for different return periods

Return Period	22	42	72	140	224	475	975	2475	4975	9975
PoE in 50 years	0.897	0.696	0.501	0.300	0.200	0.100	0.050	0.020	0.010	0.005
AvgSa (g)	0.021	0.044	0.072	0.123	0.166	0.268	0.383	0.577	0.746	0.945

3.3 RECORD SELECTION

The selection of the ground motions that will be used in the NLTH analyses must be done carefully since they represent the link between the seismic hazard and the structural response modules (Lin et al., 2013). On the early stages of seismic risk assessment, records were selected and scaled to match a specific ordinate of the uniform hazard spectrum of the site, estimated from PSHA. The focal point remained only in one period of interest, usually the fundamental period of the structure. However, it has been proven that this method results in overly conservative structural responses (Lin et al., 2013).

As an alternative the conditional spectrum method was developed (Lin et al., 2013). The Conditional Spectrum (CS) is a target spectrum that captures both the mean and variability of ground motions expected at the site, to select records that have spectral shapes somehow similar to the one of the uniform hazard spectra determined by the PSHA, as shown in Figure 19. The process of selecting the records involves first performing seismic hazard analysis and disaggregation to identify key characteristics such as magnitude and distance of the type of records that will be selected. Then, using the CS as the target, ground motions are picked from a database to match the mean and variance of the target spectrum at the specified periods.

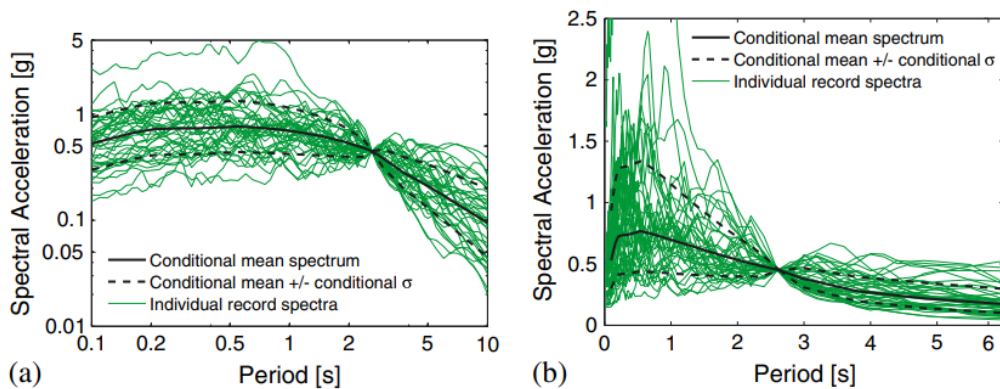


Figure 19 Example of response spectra of selected ground motions with CS as target spectra for $Sa(2.6s)$ in log scale (a) and linear scale (b) (Adapted from Lin et al., 2013)

The CS was the method used on the case study to select the records for performing the MSA, as will be explained in Chapter 4. It is important to mention that in this case the CS doesn't have a particular conditioning period but a range of periods between 0.12s and 1.82s, given that the chosen IM for the analysis was the AvgSa at that particular period range, as discussed in Section 3.1. Different records were selected for each of the IM levels

corresponding to the return periods shown in Table 8, with 40 records chosen to match a target spectrum of the mean \pm two times the standard deviation. An example of the comparison between the target spectrum and the spectra of the selected records is shown in Figure 20, in which the data for a return period of 22 years is presented.

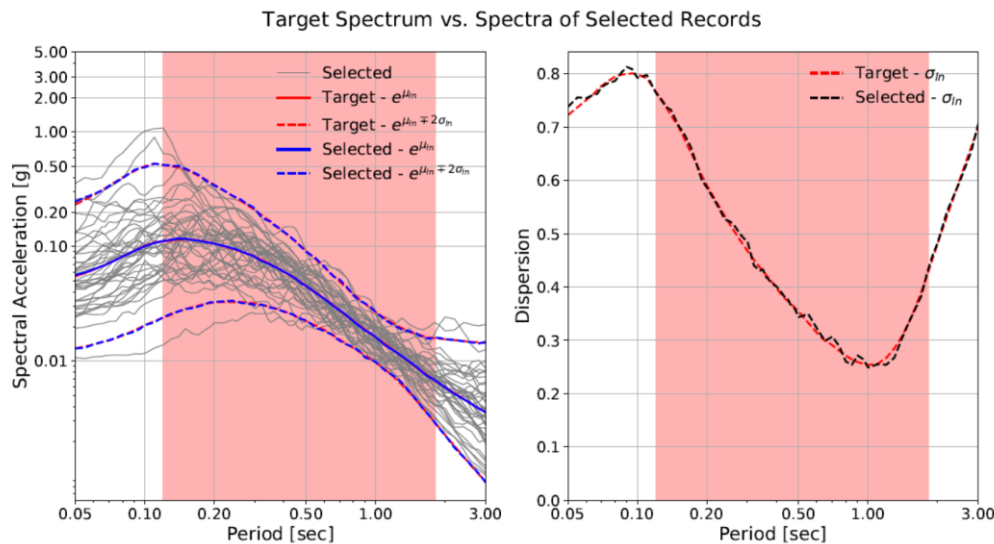


Figure 20 Target Spectrum vs Spectra of Selected Records for Return Period of 22 years

No filtering of the records was performed based on magnitude and distance to source. The spectrum of each of the records was calculated considering both directional components of the recorded event. The scale factor of the records was limited to have a minimum value of 0.25 and a maximum of 4.00. The selected records for the different return periods, as well as the comparison between the Target Spectrum and the Spectra of the selected records are presented on Appendix A.

4. BUILDING RESPONSE AND DAMAGE QUANTIFICATION

In this section, the focus shifts to the building response and damage estimation within the regional performance-based earthquake engineering (RPBEE) framework. These steps are essential for evaluating the effects of seismic events on multiple structures across a region, extending the information obtained from the earlier hazard module. The building response module examines how buildings respond to various levels of ground shaking, using engineering demand parameters (EDPs) such as peak interstory drift and floor acceleration. On the other hand, the damage estimation module in regional seismic risk assessment emphasises the global performance of buildings rather than the sum of the individual components. Global damage states (DS) are defined based on the EDP values estimated in the building response module. For example, a building might be classified in DS1, light damage, if the peak interstory drift ratio exceeds a value of 1.0%; in DS2, moderate damage, if it exceeds a value 2.5% and a DS3, collapse, if the interstory drift is larger than 8%. Fragility curves, then, are a tool that connects the hazard and damage models, using the building response module as an intermediary, as shown in the following sections.

4.1 FRAGILITY CURVES

Fragility curves describe the probability of exceeding a set of damage states conditional to a ground shaking intensity and are fundamental for the assessment of damage in earthquake scenarios (Martins & Silva, 2021). As previously mentioned, on regional seismic risk assessment, these damage states are linked to a global response of the building, generally being defined by the exceedance of a given threshold of the peak interstory drift ratio (PIDR) in the building. An example of fragility curves and what they represent is shown in Figure 21.

The concept behind fragility curves is quite simple. Considering, for instance, the case presented in Figure 21, fragility curves are presented for a building considering three damage state: DS1, that is defined as the case in which the peak interstory drift ratio of the building exceeds a 0.5%; DS2, when it exceeds 1.5%; and DS3, when it is larger than 10%. In this example the selected IM for the analysis is AvgSa. If the fragility curves intersect at a given AvgSa value, for example, 0.5g, the probability of exceeding each damage state individually corresponds to the value on the y-axis, as shown in the figure. However, in a regional analysis, where it is possible to observe all damage states across various buildings,

the probability of each DS is calculated as the difference between the value of its curve and the curve for the immediately lower damage state.

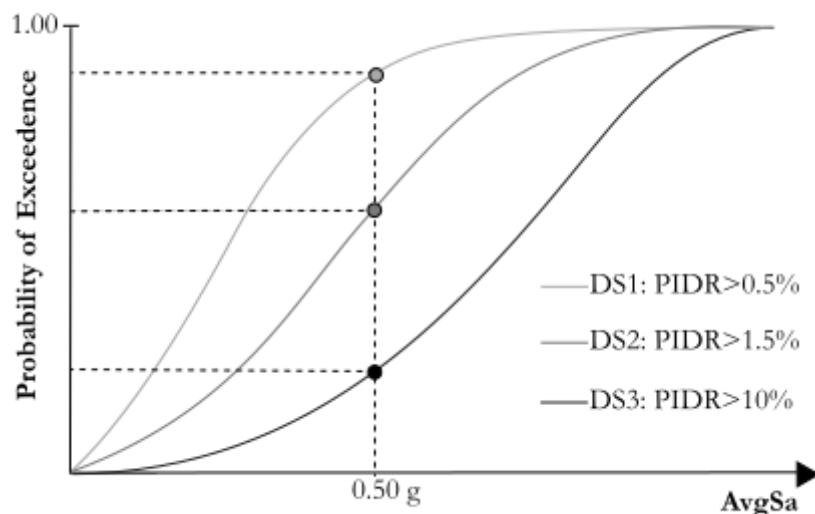


Figure 21 Example of Fragility Curves

There are three different methods commonly used for deriving fragility curves: the empirical, the judgemental and the analytical (Amir M. Kaynia (Editor) et al., 2013). The empirical method estimates curves based on actual data observed from past events, making the results specific to a particular site, considering its unique seismic conditions and building characteristics. Judgmental fragility curves, on the other hand, are derived from the opinions and experiences of experts, who estimate fragilities according to their criteria. Finally, analytical methods simulate damage distributions based on statistical results obtained from performing analysis on structural models.

Even though it would be preferred to use empirical fragility functions, due to their basis in actual observations from previous events and their site-specific nature, they are not commonly found because of the scarcity of the data required to derive them. However, some efforts have been made in the past (i.e., Nafeh & O'Reilly, (2024)). On the other hand, the reliability of the curves obtain by the judgement of experts can be debatable because of their subjective nature and deeply dependence on the experience of the consulted expert. Analytical fragility functions, then, are more extensively used in seismic risk assessment, as they are derived from actual building data and have been shown to produce reliable results in estimating vulnerabilities (Amir M. Kaynia (Editor) et al., 2013).

The analytical derivation of fragility functions on single buildings requires a certain level of knowledge of its specific structural characteristics. The most accurate results are obtained by performing several nonlinear time history analyses on a structural model of the building, which requires detailed information of the geometry and mechanical properties of the different structural elements. Additionally, this method is extremely time consuming and computationally demanding, making it impractical to be applied to all buildings on a regional scale.

This is why many simplifications are usually done to estimate fragilities at a regional level. The most used practice involves assuming a common fragility curve for all buildings within the same taxonomy. Building taxonomies are therefore defined in a way that ensures similar structural responses from the buildings grouped together. Several efforts, for instance, have been made by the GEM foundation to derive fragility functions for commonly used building taxonomies worldwide, such as the work developed by Martins and Silva (2021). However, in the case study presented here, the GEM-derived fragility functions are not used, as it is possible to determine the fragility curves for each building directly.

Analytical derivation of fragility curves generally consists of two steps. In the first step the response of the building is quantified by performing a series of nonlinear time history analysis (NLTH). Different records are used to obtain the distribution of the observed values of different EDPs conditioned on the intensity level of the selected IM for the analysis. Then, after defining the considered global damage states and the thresholds of the selected EDP that constitute them, different statistical tools are used to fit a probability distribution to the data to obtain the correspondent curve.

The building simulator tool used to generate each of the buildings, as described in Section 2, provides a detailed model of the structure in OpenSees, with the actual characteristics of the buildings and sufficient information to account for the nonlinearities of the structure. This makes it possible to directly perform NLTH on each building. Additionally, since only 62 buildings are being considered, this computationally demanding procedure is still feasible. Finally, performing NLTH on all buildings will ultimately allow for the estimation of structure-to-structure damage correlation, as will be discussed in the following sections.

4.2 BUILDING RESPONSE ESTIMATION

4.2.1 IDA vs MSA

Different methodologies based on nonlinear time history analysis are generally used to quantify the building response on performance-based earthquake engineering. The most commonly used methods are cloud analysis, incremental dynamic analysis and multiple stripe analysis, being the latter two the ones usually used by FEMA P-58. Clouds analysis

consists of performing a regression on the results obtained from NLTH analysis to obtain an equation that relates the value of the EDP with the selected IM.

Incremental dynamic analysis (IDA) was proposed by Vamvatsikos and Cornell (2002). It is equivalent to an incremental pushover analysis but uses dynamic analyses instead of a static load shape. The procedure involves performing nonlinear time history analyses on a set of ground motion records, incrementally scaling each of them until observing a collapse. Since the same records are used for all the IM levels, it is possible to create a plot, known as the IDA curve, that relates the value of a selected EDP obtained from the analysis to the corresponding IM level. For IM values for which the analysis was not performed, the value of the EDP is linearly interpolated.

Although IDA has been very useful in performance-based earthquake engineering, it has some limitations that must be addressed. One major issue is the selection of ground motion records for the analysis, since different studies have proven that the results are significantly affected by the chosen set of records (Kohrangi, Vamvatsikos, et al., 2017). Additionally, there is some bias on the results of nonlinear time history analysis when records are significantly scaled. This bias is caused by the fact that the characteristics of low intensity ground motions, such as the frequency content, differ from the ones of high intensity events (Baker, 2007). Having this in mind, scaling records like the IDA proposes might lead to not realistic results for some levels of the selected IM.

These issues have been solved by the implementation of the multiple stripe analysis method (MSA) (Jalayer, 2003). MSA shares the same principle as IDA, with the difference than in MSA the records are selected to be hazard consistent at each level of the IM (stripe), limiting the scaling factor to avoid bias in the results. This is the main reason why, even if the use of both methods is accepted, generally the implementation of the MSA is preferred. It is important to know, however, that with the MSA it is not possible to create IDA curves, since a different set of records is used for each stripe of the analysis.

A graphical representation on both methods and how the results obtained look like can be seen in Figure 22. It can be observed how the results for the IDA are continuous in function of the IM for a given ground motion record while the results of the MSA are discrete and lumped at certain intensity levels that correspond to the defined stripes, each comprising different ground motion records. In any case, statistics can be estimated in the same way with both methods, being possible to calculate values like the median EDP at different intensity levels, as shown, or the values of certain percentiles. It is also possible to estimate at certain IM level the probability of exceeding given threshold of the EDP by counting the number of records for which the condition is satisfied. Are this type of statistics then that are later used to fit a probability distribution to the data to obtain the fragility curve.

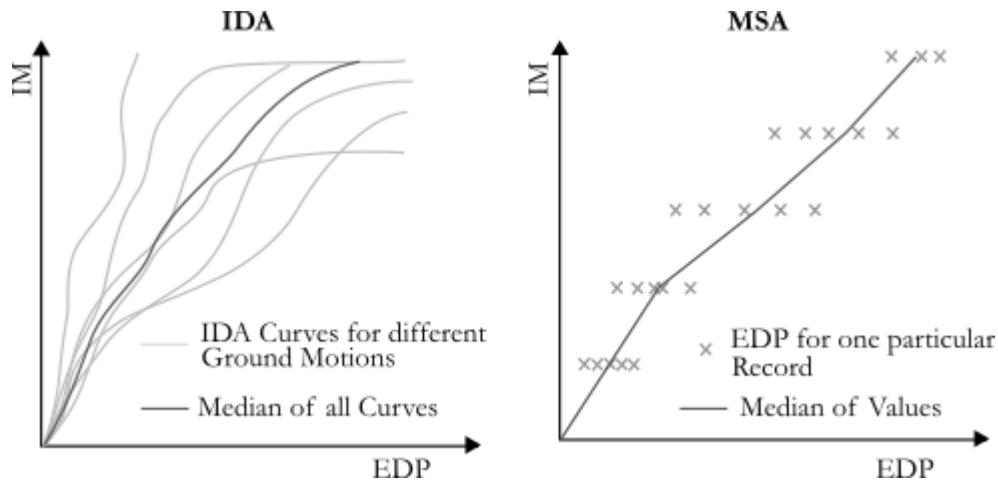


Figure 22 Visual representation of IDA and MSA

Considering then the characteristics and limitation of each of the presented methods for estimating the building response of the buildings, on the case study it was decided to use MSA. The decision was made considering that it has been observed that MSA produces more efficient fragility estimations than IDA (Baker, 2015). The process of selecting records that are hazard consistent in each of the stripes is fundamental to obtain results that are representative for the site in which the analysis is being performed and the structural characteristics of the buildings that are being analysed. The selection of the records to be used in the analysis was presented on Section 0.

4.2.2 MSA on Case Study

As previously mentioned, a MSA was performed on all 62 buildings presented on Table 5. The software OpenSeesPy was used to run all 40 selected records at each of the considered IM levels. For each record the component defined as Direction 1 during the record selection process was applied as the ground acceleration on direction 1 on the model, and the Direction 2 was applied on direction 2. Rayleigh Damping was considered for the model of the structure, considering a value of 5% on Mode 1 and 3.

The displacements and accelerations were recorded to finally estimate the peak floor acceleration and peak interstory drift ratio for each story, in each direction for each of the records selected on the considered return periods. It is possible then to calculate statistics of the results, like the median value of the EDP at each stripe. In this case the focus will remain solely on the MSA results of the global maximum peak interstory drift ratio (PIDR) on all stories for each direction, since this is the EDP in which the definition of the damage state commonly relies on in regional seismic risk assessment.

An example of the type of results obtained is shown in Figure 23, where the values of the PIDR are shown for each of the records on all return periods, along with the estimated median at each stripe. The results obtained for each direction of the 62 buildings that were analysed are shown on Appendix B. It was decided to stop the analysis when the interstory drift reached a value of 10%, since it was considered that at this point the structure can already be assumed to have collapsed, this is why there are no EDP values shown in the plot with a PIDR larger than this value.

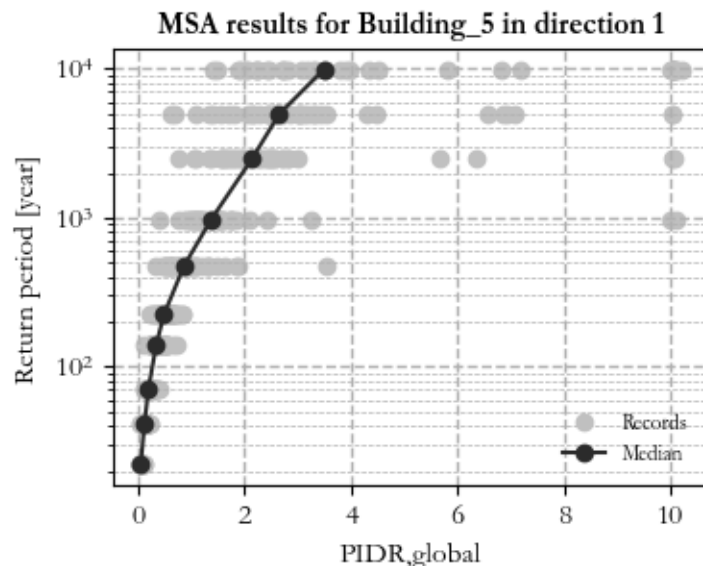


Figure 23 Example of MSA results

4.3 STATISTICAL FITTING OF FRAGILITY CURVES

4.3.1 Maximum Likelihood Method

It is a commonly accepted practice to use a cumulative lognormal distribution to define fragility functions, as done by Baker (2015). This distribution is represented by the following equation.

$$P(DS|IM = x) = \Phi\left(\frac{\ln(x/\theta)}{\beta}\right) \quad (2)$$

where $P(DS|IM = x)$ is the probability that a ground motion with an IM equal to x will cause given damage state (DS), $\Phi(\cdot)$ is the cumulative probability function of a normal standard distribution, θ is the median of the lognormal distribution that represent the IM

level with a probability of 50% of having the considered DS and β is the standard deviation of IM (Baker, 2015). The purpose is then estimating the parameters of the distribution (θ and β) from the results of the structural analyses described in the previous section, that will be referred to as $\hat{\theta}$ and $\hat{\beta}$.

A common method for estimating statistical parameters is the maximum likelihood method. It consists of finding the values that maximize the likelihood function, which measures how well the model explains the observed data. For the case in which MSA is being used, Baker (2015) considered that at each IM level, the probability of obtaining certain number of observations of given damage state (z_j) out of a known number of ground motions (n_j) follows a binomial distribution, assuming that the observation of the damage state is independent for each record.

Working on this assumption, and considering again that the probability of that a ground motion with a given IM equal will cause certain damage state is calculated by Equation (2), the maximum likelihood method can be applied so that:

$$\{\hat{\theta}, \hat{\beta}\} = \arg \max_{\theta, \beta} \sum_{j=1}^m \left\{ \ln \binom{n_j}{z_j} + z_j \ln \Phi \left(\frac{\ln(x_j/\theta)}{\beta} \right) + (n_j - z_j) \ln \left(1 - \Phi \left(\frac{\ln(x_j/\theta)}{\beta} \right) \right) \right\} \quad (3)$$

where m is the number of stipes and x is the IM associated at each stripe. By finding the values of θ and β that satisfy the equation, is possible to determine the parameters of the lognormal distribution to constitute the fragility curve.

4.3.2 Fragility estimation on Case Study

Working on the principles and methodologies previously discussed, this section focuses on applying these concepts to the specific case study. The first step is to define the Damage States that will be used for the analysis. For example, it is possible to focus on collapse fragility, which is typically defined in the literature as a situation where the PIDR reaches a value of 8%. It was possible then to go to the MSA results for each of the buildings and count the exact number of records for which the threshold PIDR was exceeded, to estimate the probability of collapse for every return period analysed, as observed in Figure 24 for Building 10.

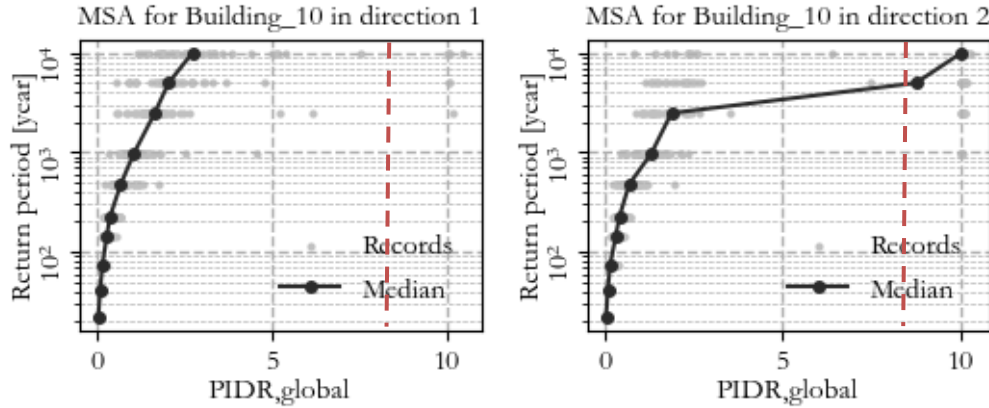


Figure 24 Estimation of probability of collapse at every IM level

It is possible then to fit the lognormal distribution to the data using Equation (3), knowing then that in total 40 records were considered at each return period for the analysis (n_i), and having counted the number of cases in which the threshold of 8% was exceeded ($\tilde{\gamma}_i$). The value of the AvgSa associated with each return period (x_i) is also known from the PSHA as shown in Table 8.

In the framework of the case study two different DS were considered. DS1 is defined as the case in which the PIDR exceeds a value of 1.0%, consistent with what could usually be defined as light damage. DS2, on the other hand, corresponds to the collapse of the structure, and is defined as the case in which the PIDR exceeds a value of 8.0%. A summary of the different DS considered in the analysis is presented on Table 9.

Table 9 Definition of damage states

Damage State	Condition
DS1 (Light Damage)	$\text{PIDR} \geq 1.0\%$
DS2 (Collapse)	$\text{PIDR} \geq 8.0\%$

As an example, Figure 25 shows the derived fragility curve for DS2 for Building 10. The estimated probability of collapse obtained by the results of MSA is shown, calculated for each IM level by dividing the values of $\tilde{\gamma}_i$ and n_i . It can be seen then how the estimated

lognormal distribution fits the data on an accurate way. The process to estimate other damage states is the same, only varying the PIDR threshold as defined for each case.

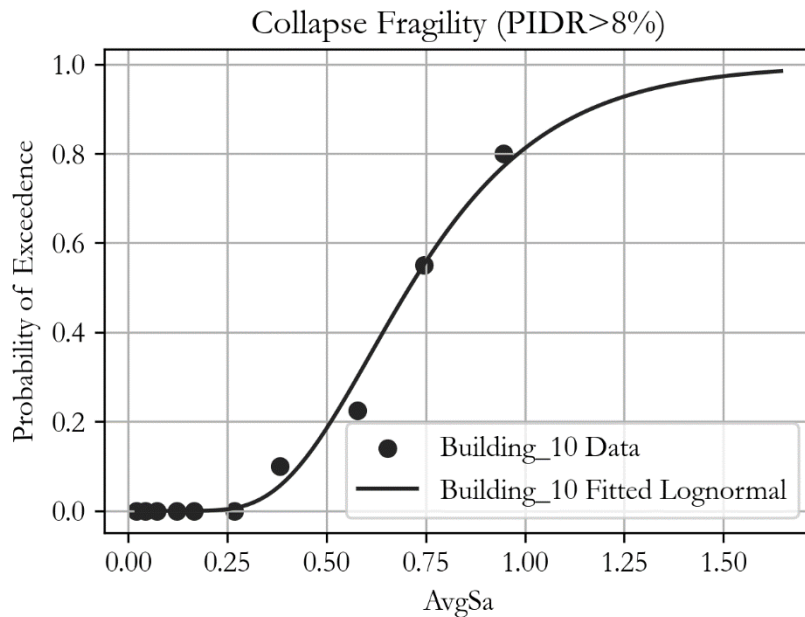


Figure 25 Collapse Fragility Fitting for Building 10

The parameters for the lognormally fitted fragility curves for all buildings in the two considered DS are presented on Table 10. The plot of the fragility curves for DS2 for all buildings are presented on Figure 26. The colour of the curve for each building is given by its corresponding class, as defined in Table 4. It is evident that buildings represented by lighter colours tend to exhibit higher collapse fragility compared to those shown in darker colours. This aligns with expectations, as lighter-coloured buildings were designed with more vulnerable design codes and lateral force factors. However, variability in the results is still noticeable. For instance, some buildings in more vulnerable classes are stronger than others in less vulnerable classes.

Table 10 Parameters of fitted lognormal distribution to fragility curves

Building	DS1		DS2		Building	DS1		DS2	
	θ	β	θ	β		θ	β	θ	β
1	-1.325	0.236	-0.357	0.562	32	-1.427	0.226	-0.476	0.388
2	-1.285	0.190	-0.277	0.342	33	-1.433	0.322	-0.489	0.386
3	-1.369	0.100	-0.341	0.482	34	-1.188	0.597	0.162	0.789
4	-1.463	0.248	-0.597	0.296	35	-1.203	0.595	0.090	0.737
5	-1.321	0.175	-0.349	0.355	36	-1.481	0.467	0.407	1.126
6	-1.477	0.249	-0.710	0.395	37	-1.500	0.421	-0.379	0.509
7	-1.481	0.298	-0.310	0.634	38	-1.327	0.424	-0.387	0.590
8	-1.491	0.294	-0.565	0.538	39	-1.245	0.519	0.273	0.740
9	-1.340	0.179	-0.358	0.515	40	-1.591	0.262	-0.599	0.389
10	-1.211	0.270	-0.344	0.389	41	-1.455	0.336	-0.495	0.443
11	-1.377	0.100	-0.655	0.401	42	-1.264	0.454	-0.161	0.407
12	-1.515	0.298	-0.303	0.520	43	-1.371	0.558	0.355	0.506
13	-1.322	0.263	-0.339	0.384	44	-1.258	0.633	0.541	0.706
14	-0.889	0.865	5.689	3.484	45	-1.513	0.295	0.095	0.581
15	-1.616	0.317	-0.689	0.555	46	-1.513	0.320	0.468	0.926
16	-1.505	0.263	-0.600	0.429	47	-1.545	0.448	-0.031	0.503
17	-1.479	0.302	-0.488	0.499	48	-1.337	0.425	0.176	0.587
18	-1.489	0.273	-0.180	0.552	49	-1.258	0.628	0.807	0.786
19	-1.379	0.327	0.046	0.712	50	-1.250	0.541	0.799	0.781
20	-1.242	0.255	-0.419	0.475	51	-1.355	0.494	0.029	0.637
21	-1.372	0.276	-0.424	0.418	52	-0.832	0.861	1.732	1.313
22	-1.223	0.247	-0.297	0.454	53	-1.410	0.375	0.248	0.690
23	-1.344	0.402	0.251	0.903	54	-1.341	0.523	0.965	1.012
24	-1.311	0.287	-0.311	0.482	55	-1.388	0.436	0.177	0.629
25	-1.369	0.100	-0.480	0.433	56	-1.298	0.306	-0.479	0.310
26	-1.392	0.216	-0.546	0.425	57	-1.277	0.356	-0.359	0.423
27	-1.581	0.369	-0.609	0.580	58	-0.732	0.720	1.155	0.957
28	-1.525	0.252	-0.019	0.767	59	-1.046	0.598	0.633	0.945
29	-1.342	0.203	-0.031	0.655	60	-1.247	0.387	-0.307	0.355
30	-1.273	0.399	-0.474	0.464	61	-1.340	0.275	-0.256	0.569
31	-1.472	0.390	-0.031	0.882	62	-1.171	0.489	-0.093	0.650

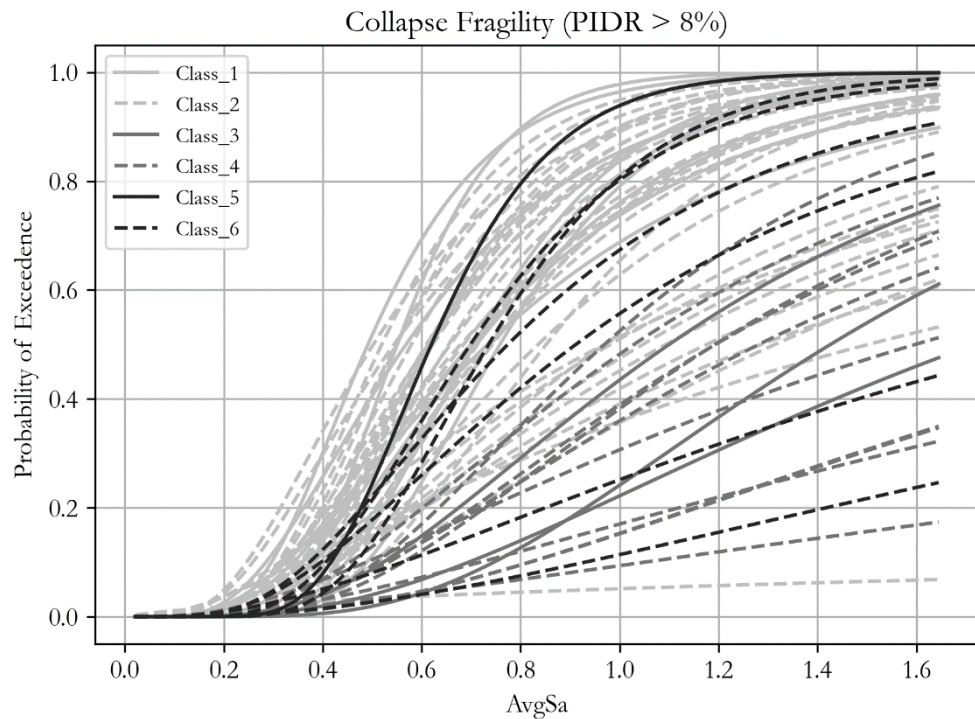


Figure 26 Collapse Fragility of Buildings by Class

5. DETERMINATION OF STRUCTURE-TO-STRUCTURE DAMAGE CORRELATION

As previously discussed, the primary goal of this study is to examine the effects of incorporating structure-to-structure damage correlation within the regional PBEE framework through a case study analysis. Up until now, it was shown how each of the modules that compose the regional PBEE framework are considered for the analysis and an assessment could already be done without incorporating the damage correlation. This chapter then focuses on studying how such correlation has been considered in the past through a literature review in order to determine how it can be estimated in this study. From this information, a method based on the statistical equation for the correlation between Bernoulli trials and the analytical procedure to determine fragility functions is proposed. Finally, an alternative to decrease the computational demand of the method is presented with the use of equivalent single-degree-of-freedom oscillators.

5.1 OVERVIEW

According to Heresi and Miranda (2023) one of the main challenges in extending the PBEE framework to a regional scale is incorporating the correlation between the damage of different structures, also known as structure-to-structure damage correlation. Unlike the spatial correlation of intensity measures in the hazard module, which has been extensively studied with several mathematical models developed to quantify it (i.e., Bodenmann et al., 2023; Esposito & Iervolino, 2011; Jalayer & Cornell, 2009), damage correlation has received comparatively less attention. It is often either completely neglected in the analyses or treated approximately by assigning a constant value for all structures. Some efforts, however, have been made in the last few years to study and understand the problem.

One of the first studies on the topic was conducted by Lee and Kiremidjian (2007), who analyzed the effects of considering the structure-to-structure damage correlation on spatially distributed systems, primarily focusing on transportation networks. Specifically, the damage correlation was estimated for bridges within network, assuming an equi-correlated scenario, in which the correlation is equal to one in the diagonal of the matrix and a constant value between 0 and 1 in all the other cases. The correlation value was considered to be independent of the ground motion intensity level but not on the damage level and was estimated mathematically as an optimization problem using a least squares adjustment and considering the marginal probabilities of each bridge as constraints. A

sensitivity analysis demonstrated that the variation in total loss increases with the estimated value of the correlation.

Kang et al. (2021) employed a different approach, focusing on estimating the correlation of engineering demand parameters (EDPs) rather than directly correlating the damage of structures. In this case, instead of estimating the damage of each building from fragility curves, the value of the interstory drift was calculated probabilistically as a function of the IM. Then, a damage state was assigned depending on its value, for example, if the interstory drift ratio exceeded 4%, the building was classified in damage state 4. The value of the correlation of the EDPs of different buildings was estimated from the results of IDAs performed on the structures.

From a statistical standpoint, correlation represents the linear relation of two variables, so Kang et al. derived it from the trendline of the scatter plot between the natural logarithm of the EDP of one building with that of another building. Each point of the plot corresponds to the results for one record amongst the ones selected to perform the IDA at the intensity measure experienced by that building, and the results for the same record on the second building for its simulated intensity measure. It can be seen then that in this approach, unlike Lee and Kiremidjian's, the value of the correlation depends on the level of the ground motion experienced by each of the structures.

Xiang et al. (2024), on the other hand, developed a model to derive the structure-to-structure correlation analytically based on the dynamic properties and the spatial distance of the structures. To do so, equivalent SDOF models were subjected to consistent and spatially varying white noise, to calibrate a mathematical equation in which the value of the correlation decreases with the distance between the structures. The proposed model was compared with the results of the method proposed by Kang et al. (2021), obtaining similar results.

Heresi & Miranda (2022) approached the problem considering that the random variable damage of the structure can be represented by a Bernoulli trial. The correlation between two Bernoulli trials can be derived from their marginal probabilities and the joint probability of both buildings experiencing damage. The authors modelled the joined distribution with a Gaussian copula, a bivariate normal distribution with mean equal to zero and a given correlation matrix. However, selecting an appropriate correlation factor for the copula remains challenging. The authors proposed an equation inversely proportional to the distance between structures and the difference in their construction years. Although this equation was not validated, it illustrated how different values of structure-to-structure correlation can significantly affect regional risk assessment outcomes.

Among the methods previously discussed, the approach proposed by Heresi and Miranda is the most suitable for the regional seismic risk assessment undertaken in this study. It not only allows the use of fragility curves widely accepted in the literature, like the ones derived by GEM, but also acknowledges that the correlation value should not be uniform across all buildings, given their varying characteristics. Additionally, the challenge of selecting the correlation for the Gaussian copulas can be addressed by developing mathematical models performing regressions with data from real historical events or derived from simulated scenarios. Alternatively, direct determination of the joint distribution may be possible based on nonlinear time history analyses, as will be demonstrated in the following sections.

5.2 ANALYTICAL DERIVATION OF STRUCTURE-TO-STRUCTURE CORRELATION

Having highlighted the importance of structure-to-structure damage correlation within the regional PBEE framework and reviewed existing approaches, this section presents the method for estimating these correlations in the frame of the case study. The method is based on the statistical principles of Bernoulli trials and incorporates nonlinear time history analyses to estimate joint probabilities of damage. To address computational challenges, an alternative approach using equivalent single-degree-of-freedom (SDOF) oscillators is also presented. This method aims to balance accuracy and efficiency, ensuring reliable regional risk assessments while effectively managing computational resources.

5.2.1 Correlation between Bernoulli trials

A Bernoulli trial is an experiment whose outcome is random but has one of only two possible outcomes: success or failure (Tsokos & Wooten, 2016). The probability of success is typically denoted as p . In the context of seismic events, a structure experiencing certain damage state can be visualized as a Bernoulli trial, where a successful outcome corresponds to the structure being damaged, and a failure corresponds to the structure remaining undamaged. This probability can be obtained by the fragility curve for a given IM value. This assumption was also made by Baker (2015) to develop the equation for fitting a lognormal distribution to MSA results, as shown in Section 4.3.1.

It is possible then to estimate the structure-to-structure damage correlation of two buildings from the equation of the correlation (ρ) between two Bernoulli trials as follows:

$$\rho_{1,2} = \frac{P[D_1 = 1, D_2 = 1] - p_1 p_2}{\sqrt{p_1(1-p_1)p_2(1-p_2)}} \quad (4)$$

where p_1 and p_2 correspond to the marginal probability of building 1 and 2 to experience a given damage state, and $P[D_1=1, D_2=1]$ is the joint probability of both buildings experiencing damage simultaneously.

Even though the marginal probabilities are already known by the fragility curves of the buildings, which are usually derived for each building taxonomy, there is generally not enough information regarding the joint probability of damage of the buildings. This is the reason why Heresi and Miranda proposed the use of gaussian copulas in their method. However, in cases where sufficient data exists to perform nonlinear time history analyses on all buildings in a region, it may be possible to analytically determine the joint distribution, and consequently, the structure-to-structure damage correlation for that set of buildings.

5.2.2 Determination of joint probability distribution

As discussed in Section 4.2.1, nonlinear time history analysis is a common methodology in performance-based earthquake engineering for computing fragility curves. These analyses not only estimate the probability of a building experiencing a certain level of damage at a given intensity measure (IM) but can also be extended to determine the joint probability of damage between structures, which is crucial for calculating structure-to-structure damage correlation (as per Equation (4)). However, specific criteria must be met during these analyses to ensure accurate results.

Following the same methodology used to estimate the probability of a particular building reaching a certain damage state for a given IM, it is possible to estimate joint probability of damage of two buildings from the results of either an IDA or MSA. If the same set of records is used for all buildings, the probability of two buildings reaching a damage state can be estimated by counting the records for which the corresponding limit EDP was exceeded for both buildings simultaneously and dividing by the total number of records. It should be noted that the value of the joint probability, and consequently, the correlation factor, is conditioned on the value of the IM experienced by the buildings, as in the approach presented by Kang et al. (2021), since the records are counted for a specific level of the IM.

Given the limitations of IDA discussed earlier, the ideal approach would involve using the results of MSA on all buildings. However, as previously mentioned, MSA requires a different set of records for each stripe, making it difficult to interpolate the EDP results for IM values other than those corresponding to the one for which the records were selected. This limitation means that MSA can only be used in a hypothetical scenario where all buildings experience a constant level of ground motion, with an IM corresponding to that of a particular stripe. The process followed to estimate the joined probability distribution from MSA is shown in Figure 27. It can be seen in the figure that to use this method AvgSa_1 must be equal to AvgSa_2 .

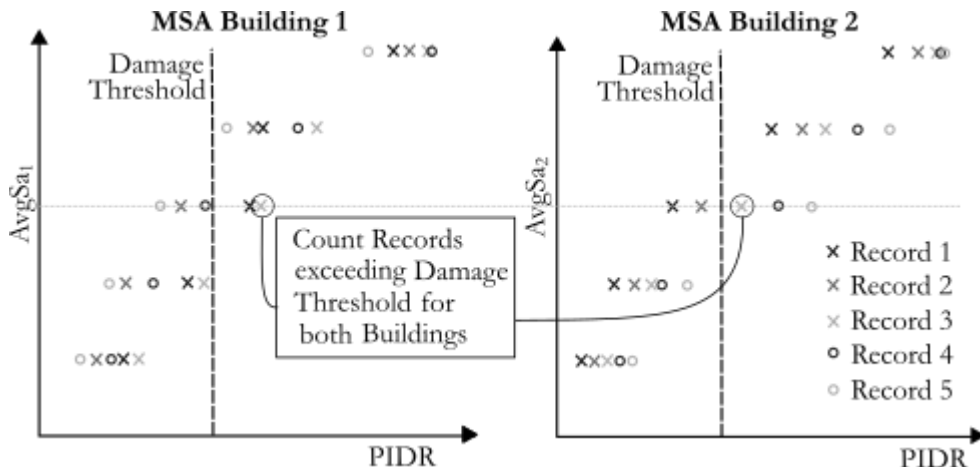


Figure 27 Estimation of joined probability distribution from MSA results

In reality, where each building experiences a different ground motion level, the only viable alternative is to use the results obtained by performing an IDA on the buildings. This involves modelling the expected IM level at each site and then interpolating the EDP values for each building at the corresponding IM level for each record. Once this is done, the joint probability can be estimated by counting the records where the limit EDP for that damage state was simultaneously exceeded for both buildings at their respective IM levels, as shown in Figure 28. It can be observed graphically in the figure below how using IDA allows to consider scenarios where the IM value is different at both sites. It should be noted that this approach of using IDA involves scaling the ground motions to different intensity levels for both structures, hence the inherent assumption is that the results are not biased by scaling factor, which is may not always be the case.

It is important to say that in the particular case of the case study, the marginal probabilities used to estimate the correlation from Equation (4) were not taken from the fragility curves, but were directly calculated from the results of either MSA or IDA depending on each case, as seen on Equation (5) and Equation (6). This was done to avoid having an unrealistic mathematical distributions of probability, since marginal probabilities from fragility curves come from a fitted lognormal distribution of the data. Estimating the marginal probability distribution by counting the records in which the damage threshold is exceeded and dividing by the total number of records is consistent with the way in which the joined probability distribution is calculated.

$$p_1 = \frac{z_1}{n} \quad (5)$$

$$p_2 = \frac{z_2}{n} \quad (6)$$

where z_i is the number of observations of given damage state and n is the number of ground motions.

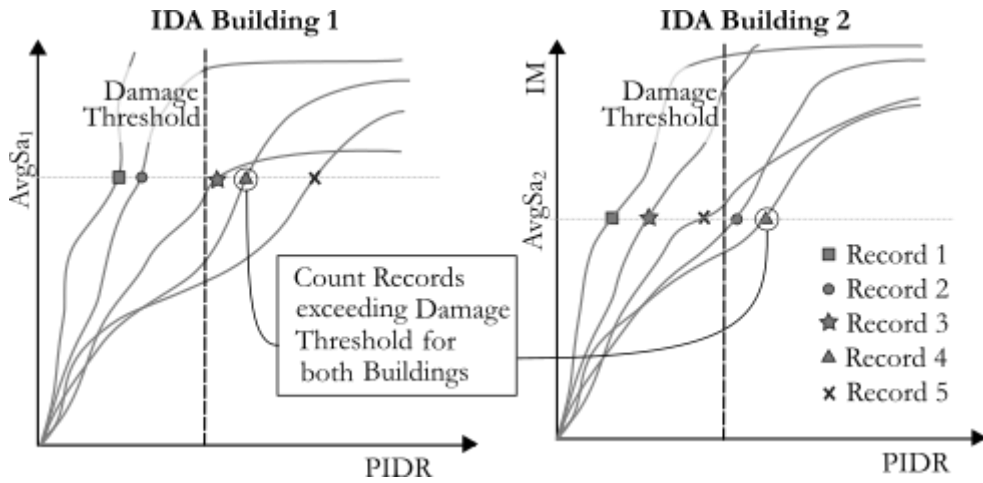


Figure 28 Estimation of joined probability distribution from IDA results

It is important to note that the application of this method is very computationally demanding, as it requires running several records at various IM levels on all buildings of the region under assessment. It is possible, however, to explore the applicability in this specific context of different approaches commonly used to simplify the process of generating fragility curves. One of the most common approaches, as done by Martins and Silva (2021), is using SDOF nonlinear oscillators based on the capacity curve of the building, to approximate the behaviour of a multiple degree of freedom building. This methodology was also employed as a simplified method for assessing infilled structures by Nafeh et al. (2020), using equivalent SDOF oscillators with properties derived from the pushover curve of the buildings.

5.2.3 Equivalent SDOF nonlinear oscillators

In the modelling of nonlinear SDOF oscillators the backbone that simulates the hysteretic behavior of the element is estimated by transforming the force-displacement relation given by the pushover curve of the multiple degree of freedom building into an equivalent SDOF, assuming a response dominated by the first mode of vibration of the structure. Given the limitations of common software used to run this type of analysis, the backbone of the hysteretic behavior can only be input as a multilinear function of the force vs the displacement of the element, requiring the use of an idealized linearization of the curve.

There are different standards for linearizing the pushover, or capacity curve of a building. ATC-19 (ATC, 1995) recommends two common approaches to do it. The first one is based on the methodology developed by (Paulay & Priestley, 1992) which assumes an elastic-perfectly plastic behaviour with a known yield strength, where the elastic stiffness is calculated as the secant stiffness for a force of 75% of the yield strength. In the second approach, known as the equal energy method, the linearized curve is selected in a way that the area enclosed by it is equal to the area beneath the pushover curve. A graphical representation of both methods is shown in Figure 29.

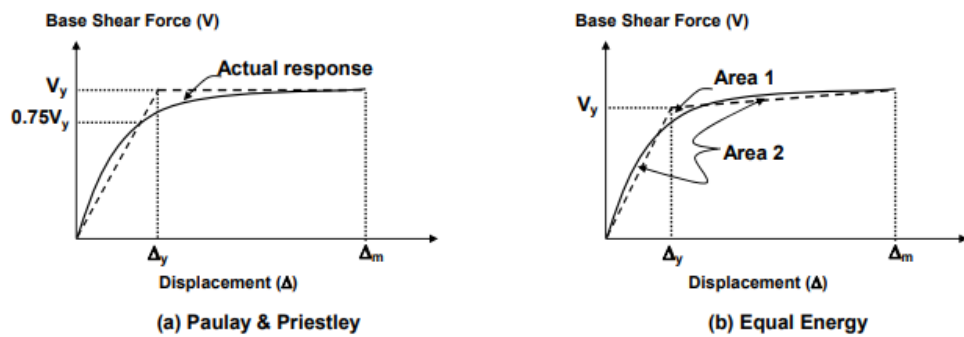


Figure 29 Linearization methods according to ATC-19

The transformation into a SDOF is done by transforming the forces (V) and displacements (Δ) of the linearized capacity curve into its equivalent values, F^* and Δ^* respectively. The equivalent mass of the oscillator (m^*) is also calculated. The equations to estimate these parameters are the following:

$$F^* = \frac{V}{\Gamma} \quad (7)$$

$$\Delta^* = \frac{\Delta}{\Gamma} \quad (8)$$

$$m^* = \sum_{i=1}^{nst} m_i \Phi_i \quad (9)$$

where m_i is the mass and Φ_i is the first mode shape ordinate at a given story. It is important to note that the first mode shape vector must be normalized so that the displacement of the top story is equal to 1. On the other hand, the value of Γ corresponds to the first mode transformation factor, which can be estimated as:

$$\Gamma = \frac{m^*}{\sum_{i=1}^{nst} m_i \Phi_i^2} \quad (10)$$

It is important to consider that the same transformations should be done inversely to the displacements obtained after running the time history analysis on the equivalent SDOF to obtain the displacements of the top story of the MDOF building. The interstory drift ratios can be estimated then assuming that the building will maintain a deformed shape proportional to the first mode of vibration of the structure, which tends to work well for regular low- to mid-rise framed structures.

The previously outlined method of transforming the building into an equivalent SDOF is very useful for simplifying the nonlinear dynamic analysis of complex structures. Even though it has been used to appropriately deriving fragility curves, it is still not clear how good it might be for estimating the structure-to-structure damage correlation. To further explore its applicability on this context, it is applied on the case study.

5.3 STRUCTURE-TO-STRUCTURE DAMAGE CORRELATION ON CASE STUDY

Two different approaches were considered to estimate the structure-to-structure damage correlation on the framework of the case study, using always the method proposed on Section 5.2. The first one involves using the results of MSA on the full 3D models of the buildings, which were already used to determine the fragility functions of each structure as shown on Section 4.2.2. This approach has the limitation previously described of only being applicable in the cases in which the ground motion intensity is constant on all buildings. The second approach consists of the realization of IDA on the equivalent SDOF, that can be used for cases in which ground motion intensities are different in all sites, with the additional advantage of being less computationally demanding.

There are two important aspects of the second method that must be studied. The first one consists of how deeply the bias caused by excessive scaling of the records associated with the use IDA affects the estimation of the correlation at different IM levels. The second involves identifying how good are the results obtained by using the SDOF oscillators when comparing with the results of the full 3D model. Having this in mind, it was decided to use the records previously selected for a return period of 475 years for the IDA, since it is one of the intermediate IM levels considered so it requires the use of less extreme scale factors both for the lower and higher intensity levels.

In this way, if the results are analysed for the intensity level associated with that return period, since the scaling factors and the records are exactly the same for the MSA and the IDA estimations, the only difference in the results is caused by the use of the SDOF oscillators. This allows then to determine how deeply this simplification modifies the

estimation of the structure-to-structure damage correlation. When comparing the results for the highest considered return periods is possible to observe how much the bias due to excessive scaling of the records can affect the results.

The process of performing IDAs on the equivalent SDOF involves several steps. First, the pushover curves in each direction of the buildings must be linearized to model the oscillators by transforming the backbone curve into that of the equivalent SDOF. Next, a series of NLTH should be conducted to obtain the IDA curves for each building. Afterwards, the results must be converted back to reflect the original MDOF building. Once this is completed, the damage correlation can be estimated.

5.3.1 Linearization of Pushover Curve

The linearization of the pushover curves of the buildings was made considering three different stages of the building: the initial elastic behaviour, the post yield portion, and the final softening of the building until loosing completely its capacity. Each of these stages is represented by one segment of the linearized backbone, as shown in Figure 30. It is fundamental, however, to consider the limitations of the type of elements used on OpenSeesPy to model the SDOF elements, since they condition the type of linearizations that can be made to the buildings.

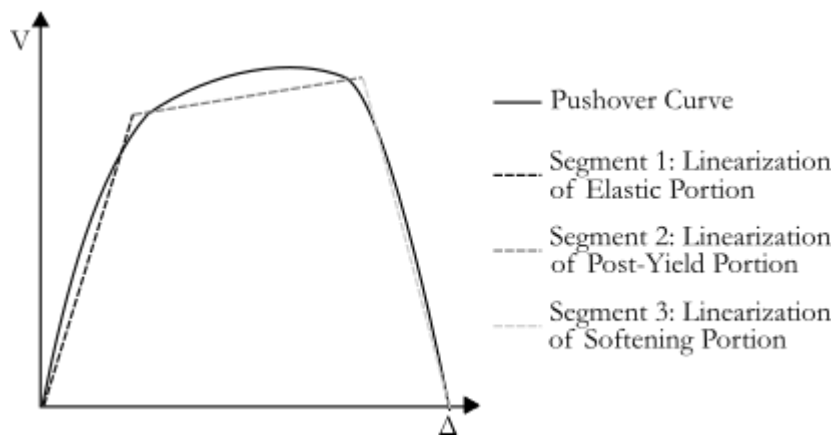


Figure 30 Type of Linearization of Pushover Curve

The oscillators were modelled as zero length elements with a hysteretic material on OpenSeesPy. This type of material model simulates the nonlinear, path-dependent behaviour of materials under cyclic loading, capturing effects like energy dissipation and stiffness degradation. One of the input parameters for this type of material is the backbone, that is equivalent to the linearization of the pushover curve. A limitation of the model of

the material is that it doesn't allow to have more than one segment of the backbone curve with a negative slope. This doesn't represent a problem for the cases in which the post-yield portion presents hardening, like in the example shown on Figure 30, but requires special considerations when the post-yield portion presents softening.

For those cases in particular, it was not possible to linearize the pushover curve of the structure both capturing the maximum strength of the building and maintaining the equal energy rule, as presented on Section 5.2.3, given that the post-yield portion had to be linearized with a horizontal slope. It was decided then to prioritize maintaining the maximum strength of the building, since it was considered to be a more representative parameter of its mechanical behaviour. This meant then that the area between the pushover curve and the linearized backbone were not going to be equal. An example of how the pushover was linearized in this type of buildings is shown in Figure 31.

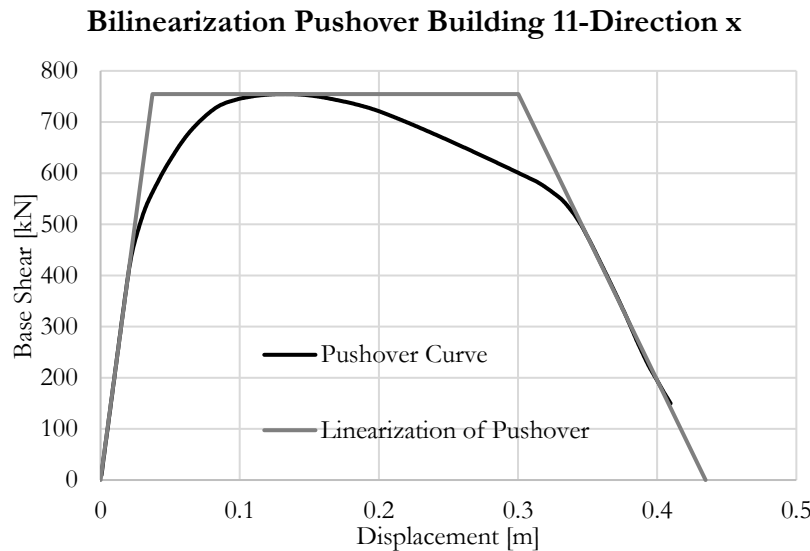


Figure 31 Linearization of Pushover for Direction x of Building 11

This procedure was done for all directions of the considered 62 buildings in the analysis. As an example, the linearization of both directions of Building 1 are shown in Figure 32 and Figure 33. As it can be seen from the figures, the initial stiffness was maintained in all the cases to avoid a modification of the elastic period of the oscillator.

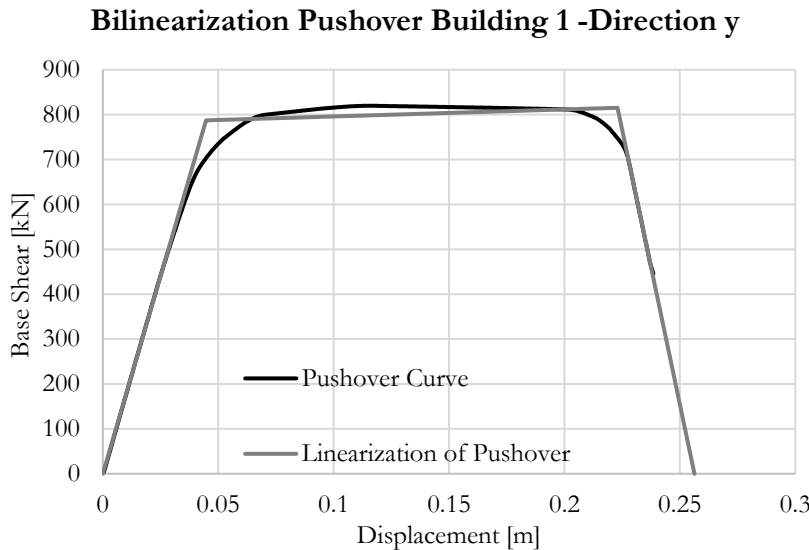


Figure 32 Linearization of Pushover for Direction x of Building 1

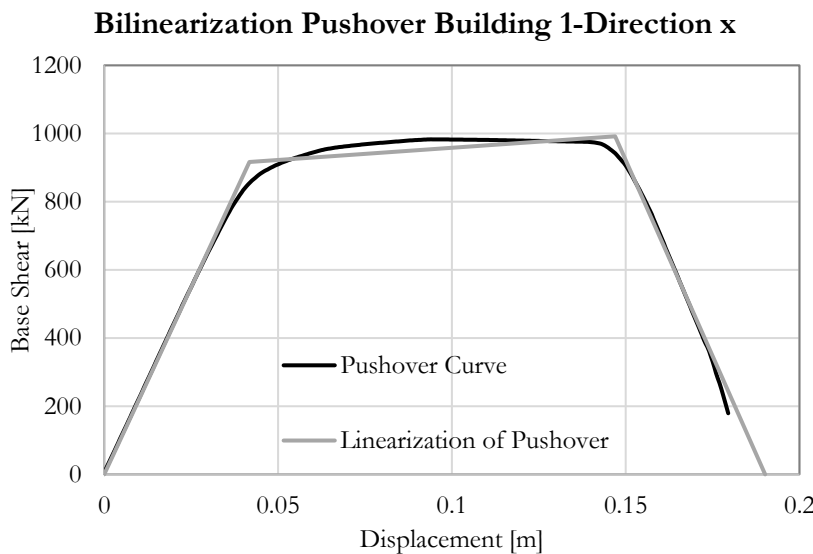


Figure 33 Linearization of Pushover for Direction y of Building 1

5.3.2 IDA on equivalent SDOF oscillators

After linearizing the pushover curve of the building, it needs to be converted to the equivalent SDOF with the procedure shown in Section 5.2.3. The value of Γ , as calculated by Equation (10), was estimated for each building and each direction as a function of the modal shape corresponding to each particular case. Then, the linearized pushover curves of the buildings are transformed to the equivalent SDOF by dividing by Γ . The results for each direction of the calculated yield force and displacements, ultimate force and displacements, and displacements after the softening branch when the building has lost completely its strength to resist lateral forces are presented on Table 11 and Table 12.

Table 11 Parameters of equivalent SDOF oscillator in direction 1

Building	Γ_1	$F_{y,1}^*$ [kN]	$\Delta_{y,1}^*$ [m]	$F_{u,1}^*$ [kN]	$\Delta_{u,1}^*$ [m]	$\Delta_{0,1}^*$ [m]
1	1.276	755.9	3.45E-02	768.6	1.16E-01	1.49E-01
2	1.313	1481.1	3.84E-02	1586.4	1.46E-01	1.64E-01
3	1.29	1048.3	2.30E-02	1048.3	1.14E-01	1.66E-01
4	1.303	1062.8	2.57E-02	1062.8	1.47E-01	2.98E-01
5	1.298	960.5	2.98E-02	1028.2	1.59E-01	2.59E-01
6	1.265	927.2	2.52E-02	927.2	7.96E-02	1.04E-01
7	1.289	758.5	3.18E-02	758.5	1.38E-01	1.65E-01
8	1.241	571.0	3.31E-02	611.0	1.11E-01	1.45E-01
9	1.312	631.0	3.07E-02	631.0	1.76E-01	3.37E-01
10	1.323	1127.8	3.92E-02	1147.6	1.82E-01	4.27E-01
11	1.298	581.4	2.87E-02	581.4	2.31E-01	3.35E-01
12	1.303	491.8	3.93E-02	491.8	2.57E-01	3.29E-01
13	1.318	1716.4	3.79E-02	1716.4	1.87E-01	3.68E-01
14	1.322	3124.4	2.67E-02	3124.4	5.57E-02	6.83E-02
15	1.264	464.9	2.90E-02	464.9	8.94E-02	1.19E-01
16	1.327	1303.6	3.17E-02	1321.1	8.18E-02	9.80E-02
17	1.269	613.4	3.79E-02	613.4	1.83E-01	2.36E-01
18	1.305	2376.4	4.10E-02	2376.4	1.74E-01	1.89E-01
19	1.327	1506.1	2.58E-02	1597.1	8.02E-02	1.01E-01
20	1.3	1085.6	4.03E-02	1193.1	1.23E-01	1.59E-01
21	1.282	985.6	3.68E-02	985.6	1.01E-01	1.25E-01
22	1.311	1520.0	3.61E-02	1520.0	2.08E-01	3.19E-01
23	1.286	1087.5	3.09E-02	1087.5	9.21E-02	1.10E-01
24	1.32	1204.3	3.11E-02	1204.3	1.66E-01	3.58E-01

25	1.291	1106.6	3.83E-02	1106.6	1.97E-01	3.29E-01
26	1.314	848.7	3.99E-02	894.9	1.90E-01	2.86E-01
27	1.282	1143.7	2.97E-02	1143.7	8.91E-02	1.07E-01
28	1.281	974.7	4.01E-02	974.7	1.83E-01	2.01E-01
29	1.289	411.9	3.56E-02	411.9	2.04E-01	2.56E-01
30	1.315	3126.2	1.82E-02	3401.8	5.94E-02	8.33E-02
31	1.297	1142.3	3.65E-02	1142.3	1.11E-01	1.25E-01
32	1.295	599.8	3.76E-02	599.8	2.06E-01	2.64E-01
33	1.331	2281.8	2.87E-02	2397.7	8.33E-02	1.05E-01
34	1.316	843.5	2.73E-02	843.5	2.42E-01	3.67E-01
35	1.327	1427.2	2.84E-02	1427.2	1.14E-01	1.69E-01
36	1.333	2353.0	2.55E-02	2353.0	6.68E-02	8.69E-02
37	1.305	873.8	2.04E-02	873.8	1.40E-01	1.60E-01
38	1.319	2178.1	1.94E-02	2204.9	7.81E-02	1.04E-01
39	1.325	1080.3	2.68E-02	1080.3	2.27E-01	3.93E-01
40	1.31	775.5	3.05E-02	775.5	2.43E-01	3.43E-01
41	1.302	629.3	2.52E-02	629.3	1.51E-01	2.78E-01
42	1.301	1152.7	2.61E-02	1152.7	1.33E-01	1.60E-01
43	1.331	753.2	2.28E-02	758.5	1.94E-01	2.22E-01
44	1.345	993.6	3.15E-02	993.6	1.80E-01	3.91E-01
45	1.331	773.7	2.89E-02	773.7	1.42E-01	1.79E-01
46	1.322	741.9	5.56E-02	741.9	3.14E-01	3.44E-01
47	1.327	691.0	2.65E-02	691.0	1.47E-01	2.00E-01
48	1.36	1067.1	3.90E-02	1102.9	1.11E-01	1.23E-01
49	1.274	903.9	5.41E-02	903.9	1.87E-01	2.05E-01
50	1.274	1730.1	4.30E-02	1730.1	1.61E-01	1.95E-01
51	1.343	2209.0	3.64E-02	2220.7	1.54E-01	1.71E-01
52	1.313	1776.9	3.66E-02	1892.9	1.22E-01	1.71E-01
53	1.3	1051.8	4.00E-02	1051.8	1.45E-01	1.59E-01
54	1.323	2408.7	2.78E-02	2408.7	1.13E-01	1.46E-01
55	1.328	1023.4	6.07E-02	1023.4	1.85E-01	1.91E-01
56	1.313	1446.3	3.01E-02	1490.8	1.62E-01	2.95E-01
57	1.309	1822.6	4.68E-02	1914.0	1.59E-01	2.31E-01
58	1.326	1361.3	3.91E-02	1361.3	1.52E-01	2.31E-01
59	1.272	1153.3	4.05E-02	1252.2	9.65E-02	1.14E-01

60	1.364	1293.4	3.22E-02	1372.0	2.19E-01	3.29E-01
61	1.331	1095.9	5.16E-02	1127.5	2.21E-01	2.94E-01
62	1.284	756.6	3.47E-02	756.6	1.43E-01	1.60E-01

Table 12 Parameters of equivalent SDOF oscillator in direction 2

Building	Γ_2	$F_{y,2}^*$ [kN]	$\Delta_{y,2}^*$ [m]	$F_{u,2}^*$ [kN]	$\Delta_{u,2}^*$ [m]	$\Delta_{0,2}^*$ [m]
1	1.295	607.7	3.45E-02	629.4	1.72E-01	1.98E-01
2	1.321	1481.6	3.62E-02	1647.0	1.52E-01	1.66E-01
3	1.301	995.6	2.34E-02	995.6	1.79E-01	2.11E-01
4	1.264	1438.1	2.00E-02	1458.0	6.77E-02	8.79E-02
5	1.3	1075.3	3.00E-02	1093.6	1.44E-01	1.51E-01
6	1.293	565.1	3.07E-02	565.1	1.71E-01	3.19E-01
7	1.301	412.6	3.33E-02	412.6	1.96E-01	3.32E-01
8	1.267	511.3	3.75E-02	511.3	1.46E-01	1.94E-01
9	1.32	999.7	3.43E-02	1013.7	1.58E-01	1.89E-01
10	1.31	1158.0	4.43E-02	1182.9	1.55E-01	1.68E-01
11	1.282	1127.8	3.26E-02	1148.0	8.44E-02	9.74E-02
12	1.294	930.3	4.24E-02	930.3	1.61E-01	2.39E-01
13	1.317	2137.9	4.12E-02	2214.1	1.03E-01	1.27E-01
14	1.342	901.6	3.02E-02	901.6	2.60E-01	3.90E-01
15	1.291	180.5	3.13E-02	180.5	2.63E-01	3.68E-01
16	1.327	508.0	3.67E-02	508.0	2.49E-01	3.38E-01
17	1.277	750.2	4.43E-02	750.2	1.75E-01	1.94E-01
18	1.308	1553.6	3.77E-02	1553.6	1.73E-01	2.81E-01
19	1.335	768.5	2.83E-02	768.5	2.22E-01	4.26E-01
20	1.315	1110.7	3.91E-02	1134.0	1.75E-01	2.16E-01
21	1.29	573.9	3.92E-02	573.9	1.86E-01	3.40E-01
22	1.301	1618.8	4.04E-02	1739.7	1.38E-01	1.64E-01
23	1.306	501.5	3.45E-02	501.5	2.57E-01	3.53E-01
24	1.334	1693.3	2.84E-02	1693.3	1.70E-01	4.37E-01
25	1.296	1544.9	4.29E-02	1544.9	1.47E-01	1.80E-01
26	1.328	1332.7	3.99E-02	1392.7	8.33E-02	9.62E-02
27	1.292	421.2	2.87E-02	421.2	2.35E-01	3.11E-01
28	1.282	673.5	4.19E-02	673.5	1.93E-01	2.74E-01

29	1.321	907.7	3.74E-02	922.5	1.71E-01	2.26E-01
30	1.336	1162.0	2.20E-02	1162.0	2.11E-01	4.52E-01
31	1.31	615.5	3.50E-02	615.5	2.18E-01	3.20E-01
32	1.313	1439.1	3.53E-02	1515.3	8.99E-02	1.09E-01
33	0.507	2254.8	1.27E-01	2254.8	5.91E-01	7.87E-01
34	1.325	1882.9	2.84E-02	1882.9	8.88E-02	2.19E-01
35	1.3	530.3	3.01E-02	530.3	2.11E-01	2.70E-01
36	1.317	1062.7	3.27E-02	1062.7	2.27E-01	3.14E-01
37	1.321	400.2	2.41E-02	400.2	2.21E-01	3.50E-01
38	1.302	632.3	2.23E-02	632.3	2.59E-01	4.11E-01
39	1.334	2493.1	2.64E-02	2619.3	6.29E-02	6.71E-02
40	1.326	1528.2	3.14E-02	1547.6	8.06E-02	1.02E-01
41	1.311	733.3	2.99E-02	733.3	1.88E-01	2.17E-01
42	1.323	838.6	3.47E-02	838.6	2.54E-01	3.12E-01
43	1.374	572.8	2.93E-02	572.8	2.15E-01	4.82E-01
44	1.34	1089.7	2.78E-02	1143.6	7.80E-02	1.07E-01
45	1.355	634.9	2.91E-02	634.9	1.76E-01	2.81E-01
46	1.317	776.7	6.21E-02	776.7	2.00E-01	2.57E-01
47	1.38	491.3	2.54E-02	491.3	2.17E-01	4.06E-01
48	1.386	1060.9	4.41E-02	1117.5	1.63E-01	1.74E-01
49	1.286	881.3	6.18E-02	881.3	3.08E-01	4.42E-01
50	1.3	1373.9	5.56E-02	1373.9	2.60E-01	2.78E-01
51	1.339	2427.8	3.67E-02	2477.9	1.39E-01	1.42E-01
52	1.367	1233.7	4.41E-02	1233.7	2.06E-01	3.95E-01
53	1.315	847.9	5.20E-02	847.9	2.15E-01	3.13E-01
54	1.329	1865.4	4.38E-02	1865.4	1.61E-01	2.11E-01
55	1.314	916.6	6.15E-02	916.6	2.35E-01	3.08E-01
56	1.292	1605.1	2.68E-02	1657.7	1.07E-01	1.31E-01
57	1.294	1993.8	4.45E-02	2078.6	1.30E-01	1.62E-01
58	1.31	1533.0	4.24E-02	1533.0	7.95E-02	9.12E-02
59	1.313	1083.6	6.24E-02	1154.4	1.40E-01	1.81E-01
60	1.341	1673.0	3.57E-02	1752.7	1.12E-01	1.59E-01
61	1.321	1238.5	4.36E-02	1296.6	9.55E-02	1.02E-01
62	1.292	783.3	3.98E-02	783.3	1.24E-01	1.74E-01

It is possible then to run the NLTH analysis on the oscillators. As previously mentioned, the set of records chosen for the return period of 475 years are used for the analysis. Unlike typical IDA analysis, in which the records are scaled until reaching collapse, in this case the records were scaled to match the intensity levels associated with the return periods used for the MSA. This was done to have the data exactly on the same intensity levels on both methods to compare easier the results when verifying the constant shaking scenarios that will be evaluated in the following sections.

The displacements obtained by the running the analysis on the equivalent SDOF oscillator needs to be converted back to the original MDOF building. For that, each of the displacements were multiplied again by the Γ factor used on each direction and presented on Table 11, obtaining the roof displacement for each record. Then, it is assumed that the building maintains a constant deformed shape proportional to fundamental eigenvector in each direction, so the maximum interstory drifts were calculated accordingly. This assumption, however, might lead to not accurate results for large intensity levels, in which the building might have already yielded, and soft story mechanisms might have developed.

An example of the type of results obtained after transforming the equivalent SDOF back to the MDOF Building are shown in Figure 34. The obtained IDA for all the buildings in all directions are presented on Appendix C.

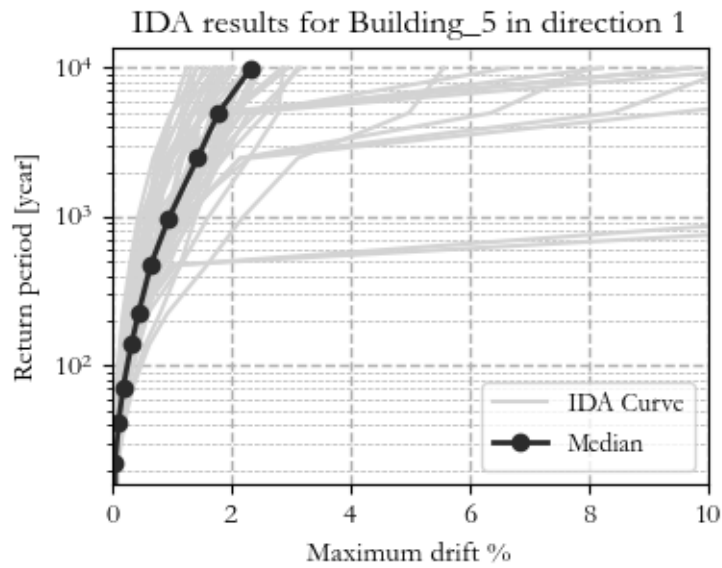


Figure 34 Example of IDA results

5.3.3 Calculation of correlation matrix

After obtaining the results of both the MSA on the full 3D models of the buildings and of the IDA on the equivalent SDOF oscillators is possible then to proceed with the calculation of the correlation matrix. As previously explained, the correlation between each pair of buildings was computed by applying Equation (4), estimating the joint probability either from the results of MSA or IDA. There are two different factors that condition the result of the estimation, one is the drift threshold that is defined in the damage state, and the other is the IM level that is being considered. This is due to the fact that the value of the marginal probability of damage of the building as well as the joint distribution depend on those two parameters.

Some special considerations must be made on the mathematical applicability of that equation in this context. In the case in which either of the marginal probabilities p_1 and p_2 is equal to 0 or 1, the denominator of Equation (4) is equal to zero rendering the correlation mathematically undefined. It is important to see however what this means in the context in which the correlation is being applied. In practical terms, when p_1 or p_2 equals 0, it means that the probability of the structure experiencing damage is zero; thus, regardless of its correlation with other structures, it will never get damaged. Therefore, any value for the correlation is arbitrary, as it will not impact the outcome. Similarly, if p_1 or p_2 are equal to 1, the structure will inevitably sustain damage, and any correlation value can be assumed without affecting the result.

The correlation matrix calculated for DS1 ($\text{PIDR} \geq 1.0\%$), as defined on Table 9, is presented. This level of drift can be seen as indicating light to moderate damage. To compare the results from MSA and IDA, a scenario where the Intensity Measure (IM) level is the same for all buildings was used, and the results across different IM levels is examined. For cases where the correlation is mathematically undefined because of the issue described above, the corresponding rows and columns in the matrix were left blank.

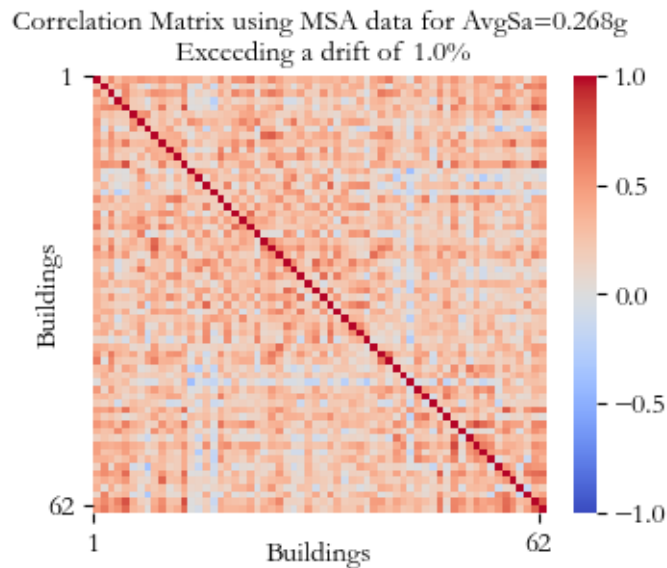


Figure 35 Correlation Matrix estimated from MSA Exceeding a drift of 1.0%.
AvgSa=0.268 g

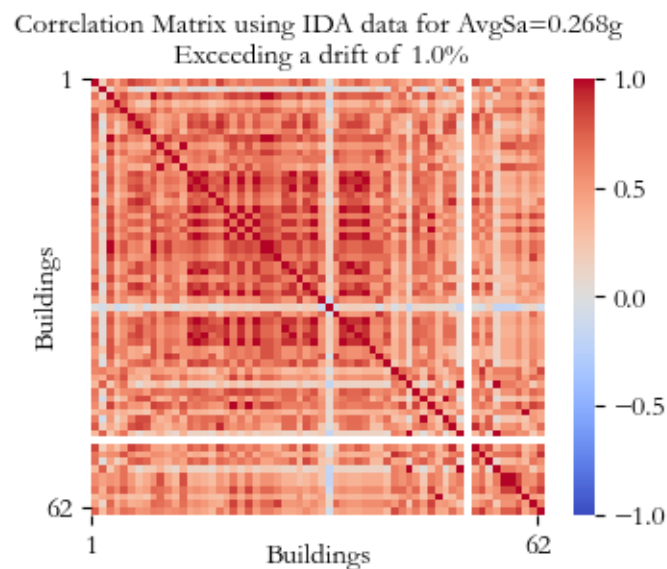
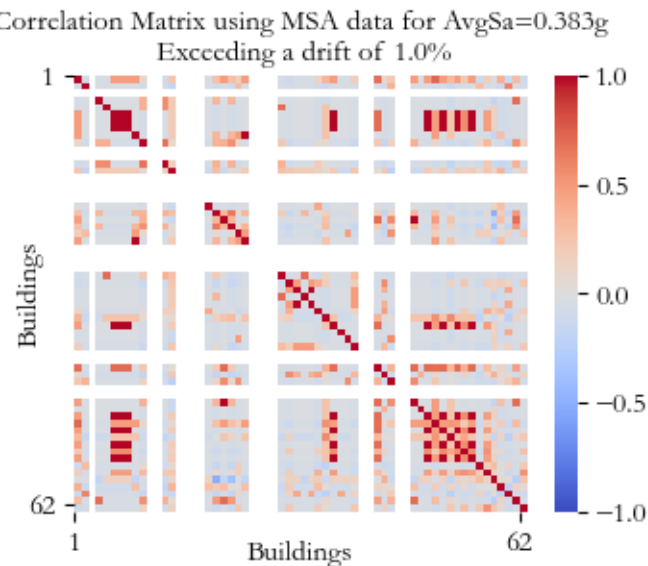
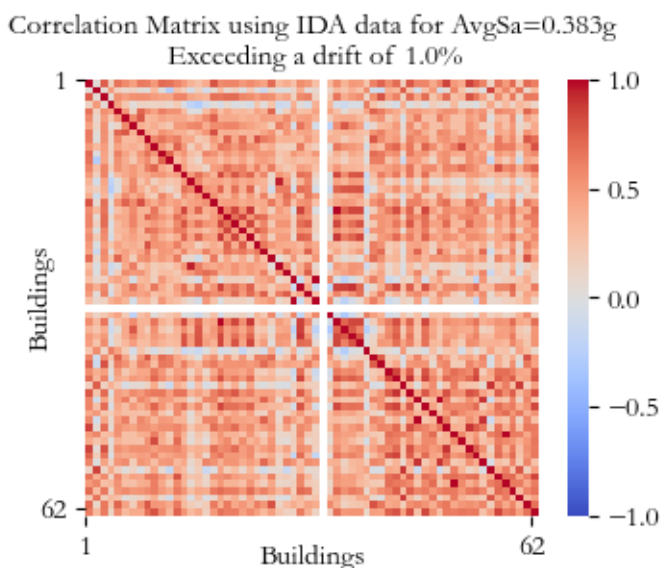


Figure 36 Correlation Matrix estimated from IDA Exceeding a drift of 1.0%.
AvgSa=0.268 g



**Figure 37 Correlation Matrix estimated from MSA Exceeding a drift of 1.0%.
AvgSa=0.383 g**



**Figure 38 Correlation Matrix estimated from IDA Exceeding a drift of 1.0%.
AvgSa=0.383 g**

Several observations can be made from the previous figures. The first one is that typically the IDA on equivalent SDOF overestimates the value of the correlation, as it can be seen by comparing Figure 35 and Figure 36. Additionally, MSA results tend to reach mathematically undefined values more quickly, which is evident when comparing Figure 37 and Figure 38. This occurs because IDA on equivalent SDOF systems often underestimates the maximum interstory drift ratios, as shown in Appendix B compared to Appendix C. This causes the results of MSA to reach at lower values of AvgSa marginal probabilities equal to 1, leading to a mathematically indeterminate solution to the equation. It could be analysed in a future work if this issue could be solved by using the marginal probabilities obtained by the lognormally fitted fragility curve for each building instead of using those directly estimated from the results of NLTH analyses.

To further explore how different are the results, the correlation between Building 1 and other buildings is presented below as in illustrative example.

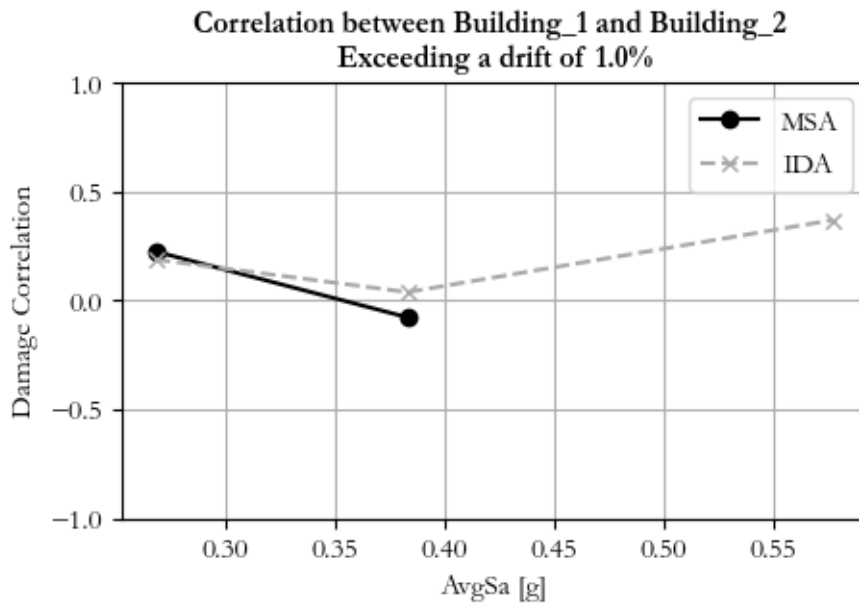


Figure 39 Correlation between Building 1 and Building 2 for a drift limit of 1.0%

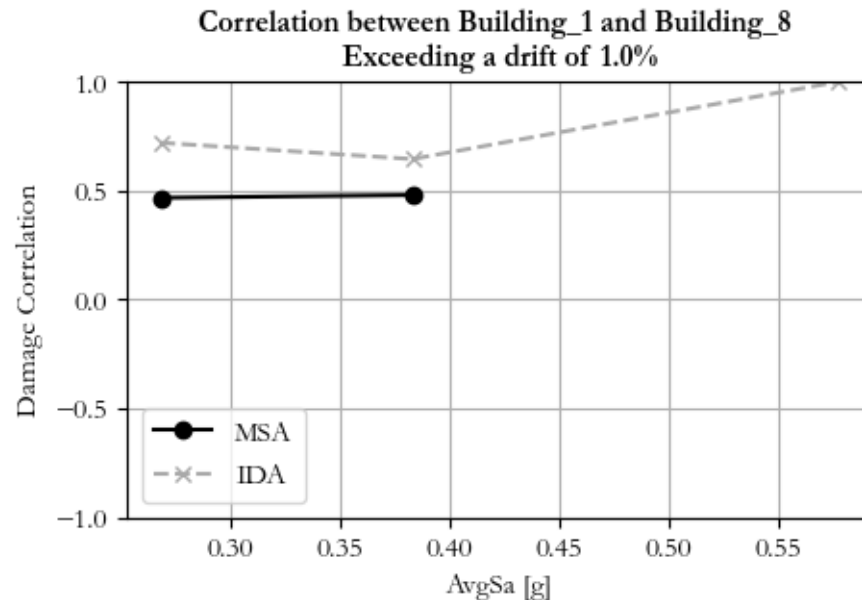


Figure 40 Correlation between Building 1 and Building 8 for a drift limit of 1.0%

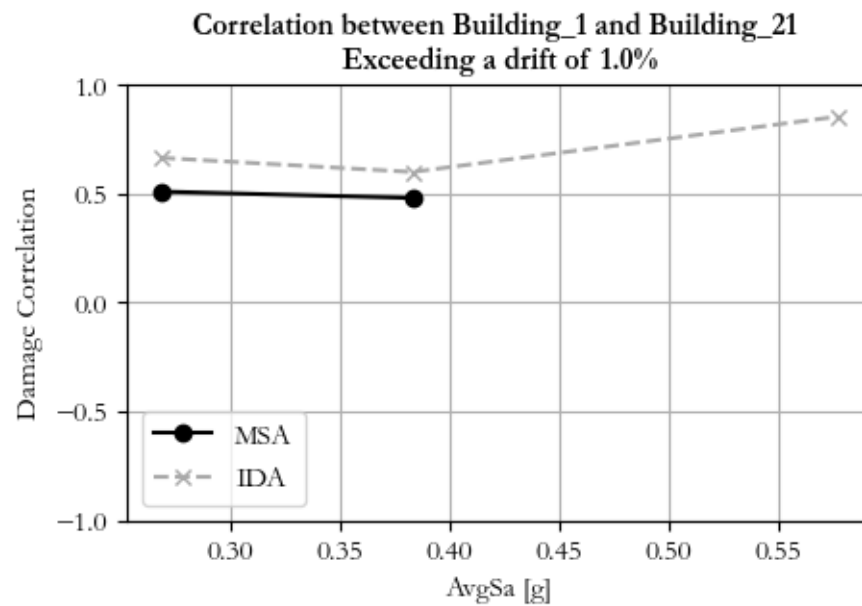


Figure 41 Correlation between Building 1 and Building 21 for a drift limit of 1.0%

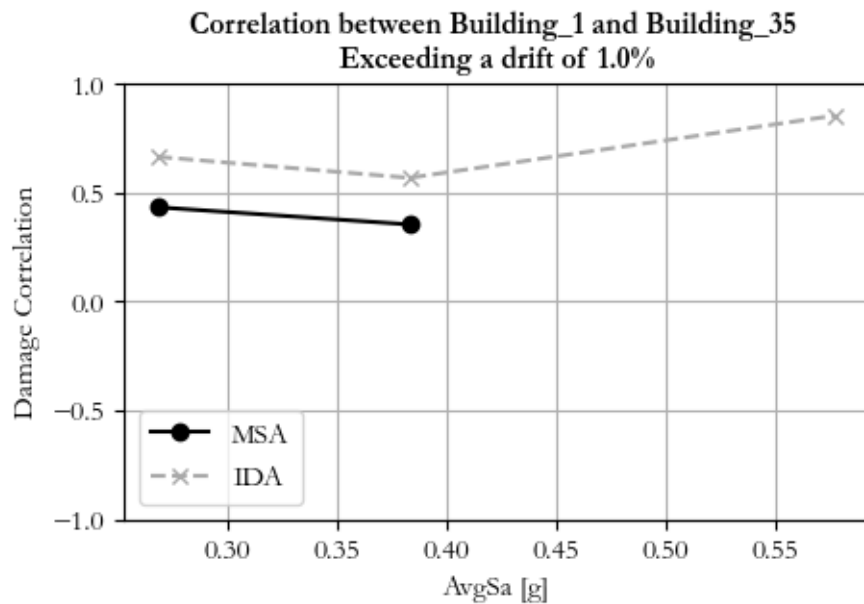


Figure 42 Correlation between Building 1 and Building 35 for a drift limit of 1.0%

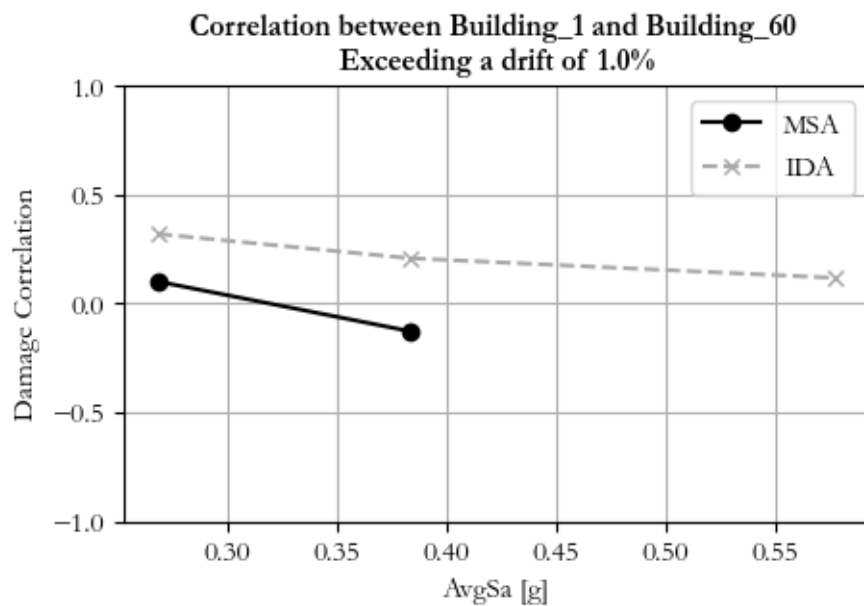


Figure 43 Correlation between Building 1 and Building 60 for a drift limit of 1.0%

It can be seen from the figures above that, in general, the correlations estimated from MSA are slightly lower than the ones estimated with IDA on SDOF oscillators. Focusing particularly on the results for an AvgSa of 0.268g, in which the same records with the same scale factors are used, the difference in some of the cases is quite significant. Taking as an example the correlation with Building 60, the value estimated with MSA is equal to 0.102 and with IDA is 0.320, which means a difference of 214%. This proves then what was previously indicated that the difference in the estimation is caused by the underestimation of the drifts from the use of equivalent SDOF. This is likely due to the key assumption that the buildings are assumed to respond solely in the first mode of vibration and neglects any contribution or impacts of the higher modes of vibration, which MSA does include. Furthermore, the bilinearisation procedure adopted to create the equivalent SDOFs is anticipated to have had an impact.

Another observation is that in some of the cases the values of the correlations are negative, as seen on Figure 35 through Figure 38, which doesn't make sense for the phenomenon being studied. This was particularly evident in the results of Building 1 with Building 2 (Figure 39) and with Building 60 (Figure 43), where the correlation was negative for some of the results with the MSA for an AvgSa of 0.383 g. To understand this condition, the actual values of the marginal and joint probabilities were examined. Specifically, the correlation between Building 1 and Building 60 was analysed.

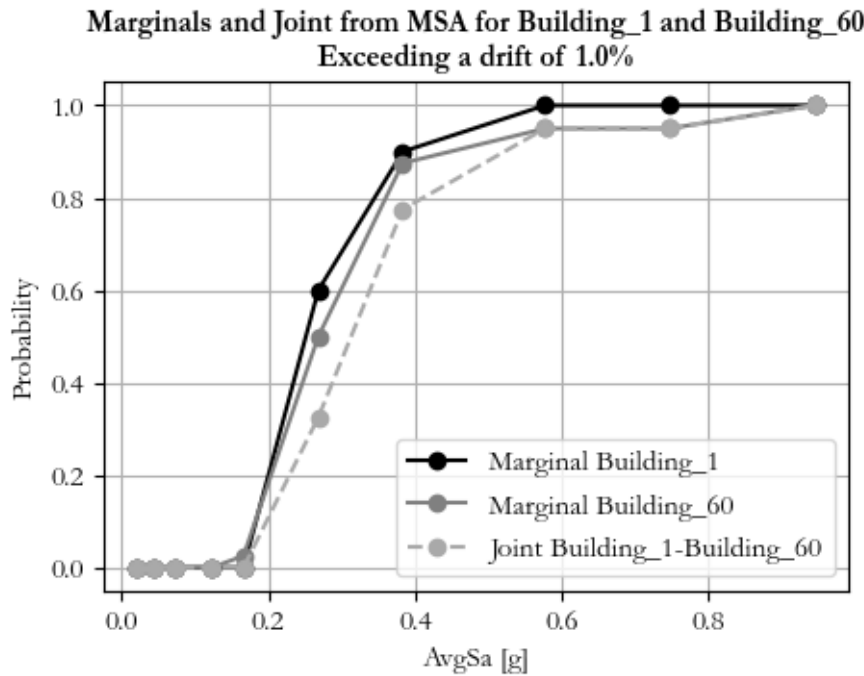


Figure 44 Marginal and Joint Probabilities for Building 1 and Building 60

It can be observed that at an AvgSa of 0.383g the joint distribution is two low comparing to the marginal distributions. As a result, when estimating the correlation with Equation (4), the value of the subtraction on the numerator is negative. Further analysis should be done to determine if this is an issue related with using very few records on the analysis, or if it is indeed a limitation of the method that is being proposed.

Now, to further explore how the value of the correlation changes by the use of IDA instead of MSA and identify possible bias due to scaling, the correlation is estimated for DS2, as defined in Table 9, corresponding to a case of collapse. The results are again shown for different values of AvgSa, assuming scenarios of constant shaking. The estimated correlation matrices are shown below.

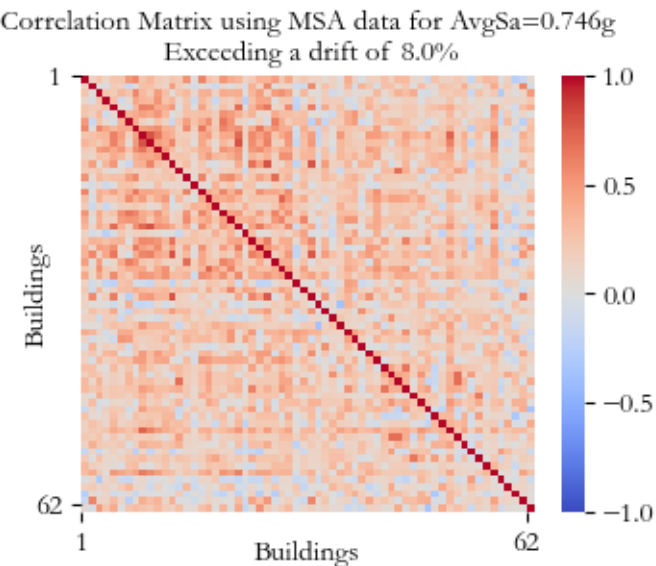


Figure 45 Correlation Matrix estimated from MSA Exceeding a drift of 8.0%.
AvgSa=0.746 g

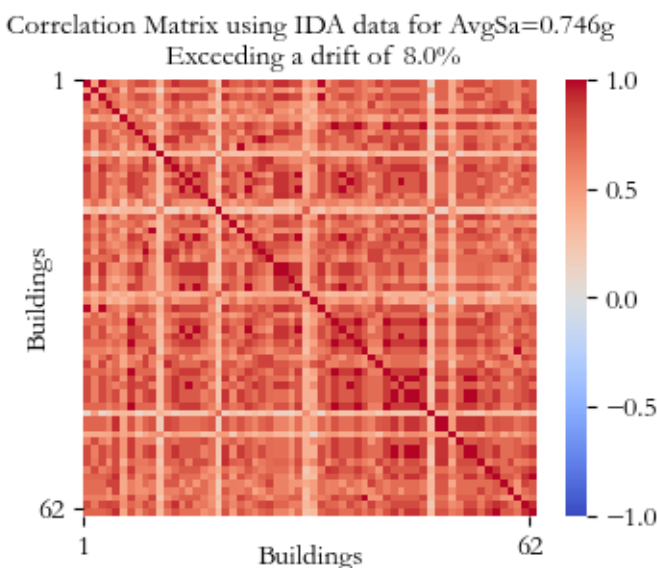


Figure 46 Correlation Matrix estimated from IDA Exceeding a drift of 8.0%.
AvgSa=0.746 g

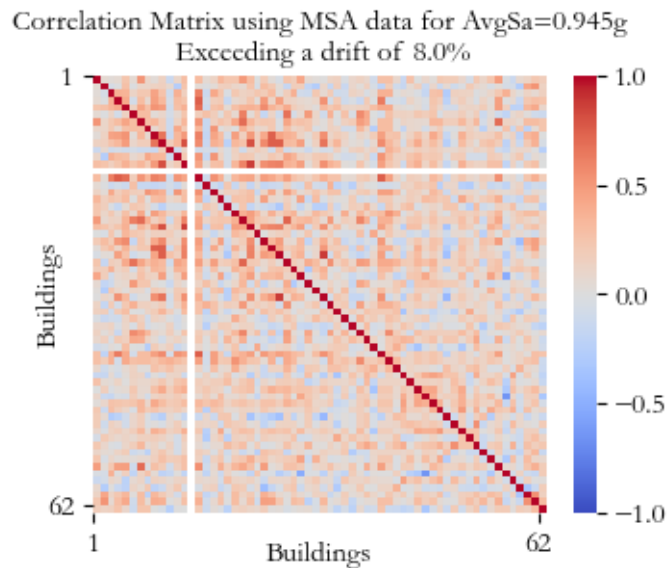


Figure 47 Correlation Matrix estimated from MSA Exceeding a drift of 8.0%.
AvgSa=0.945 g

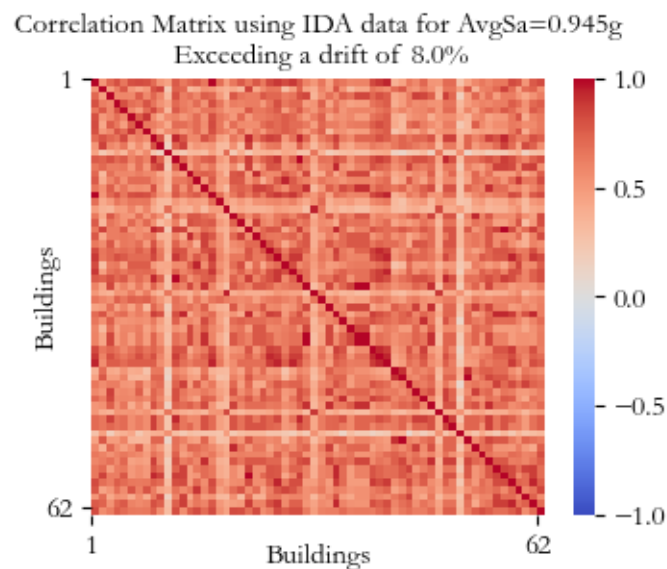


Figure 48 Correlation Matrix estimated from IDA Exceeding a drift of 8.0%.
AvgSa=0.945 g

It can be noted, once again, that the correlation values are overestimated with the application of the IDA on equivalent single degree of freedom oscillators. As in the previous case, there are also some negative values, which require further investigation to determine if they are due to the limited number of records used. To understand how much the use of excessive scale factors associated with the use of IDA modifies the estimation of the correlation, the calculated values at different IM levels for both approaches are shown for Building 1 in comparison with Buildings 2, 8, 21, 35, and 60.

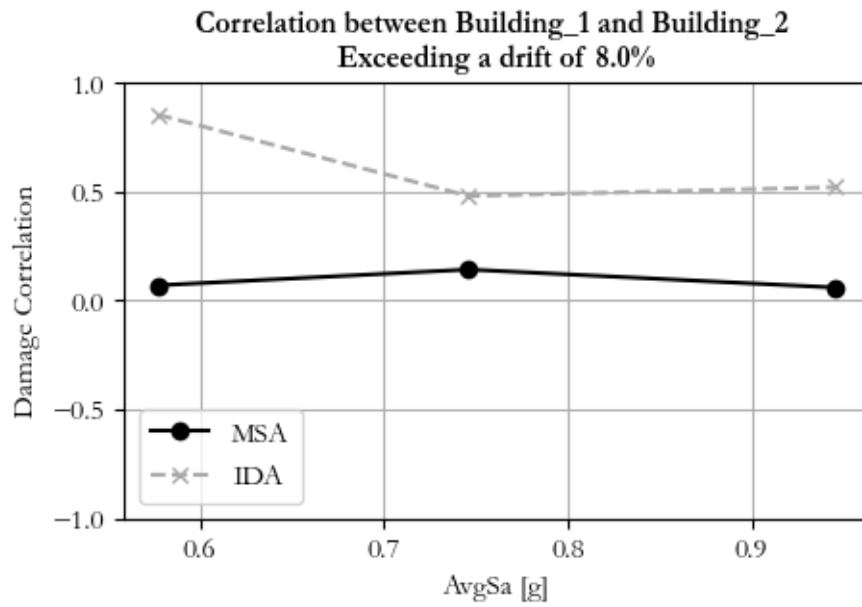


Figure 49 Correlation between Building 1 and Building 2. Drift limit of 8.0%

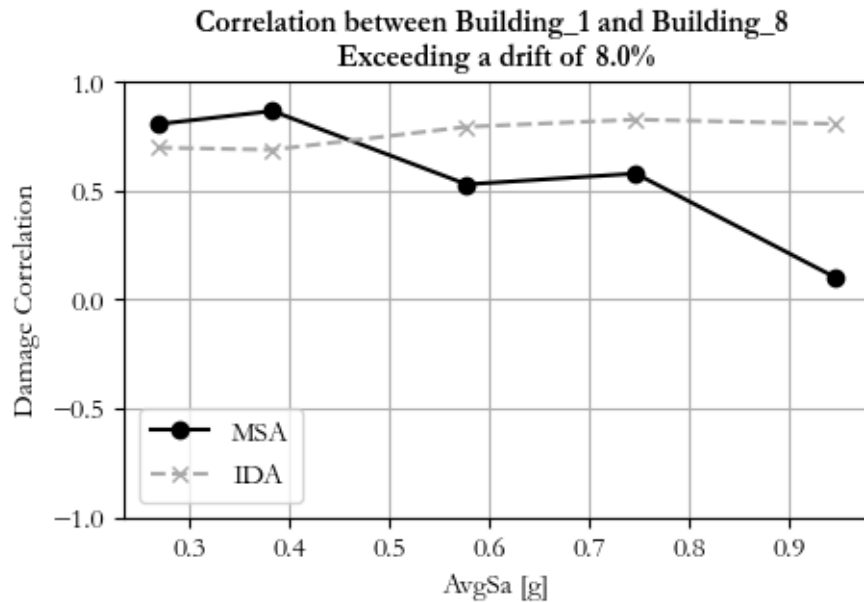


Figure 50 Correlation between Building 1 and Building 8. Drift limit of 8.0%

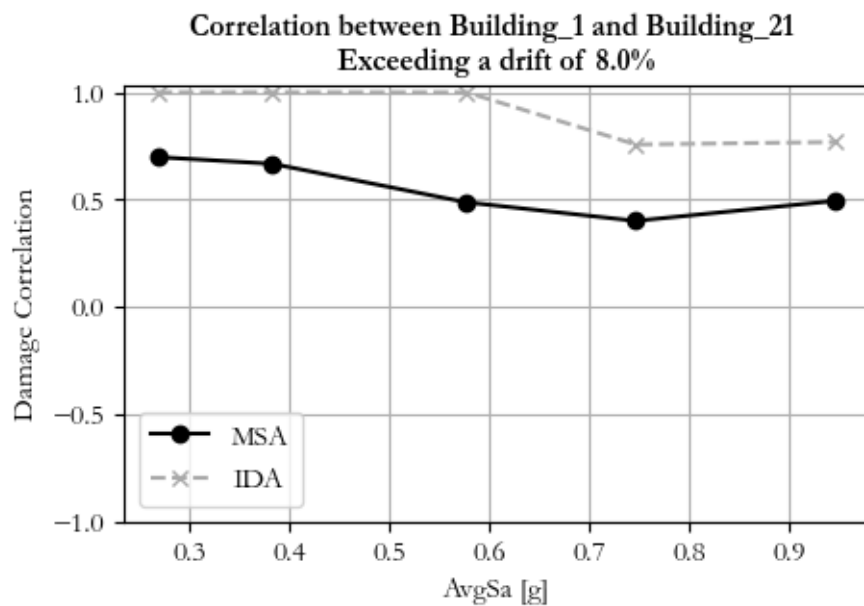


Figure 51 Correlation between Building 1 and Building 21. Drift limit of 8.0%

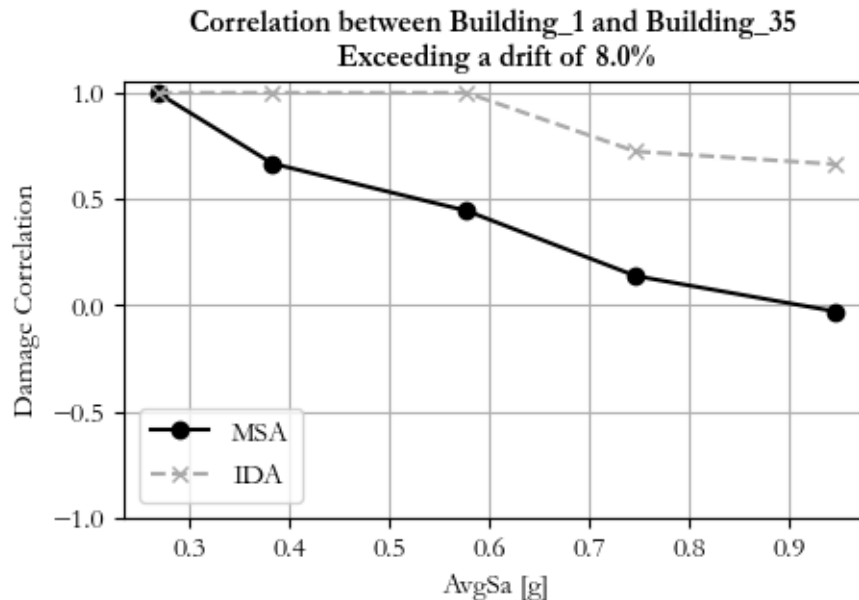


Figure 52 Correlation between Building 1 and Building 35. Drift limit of 8.0%

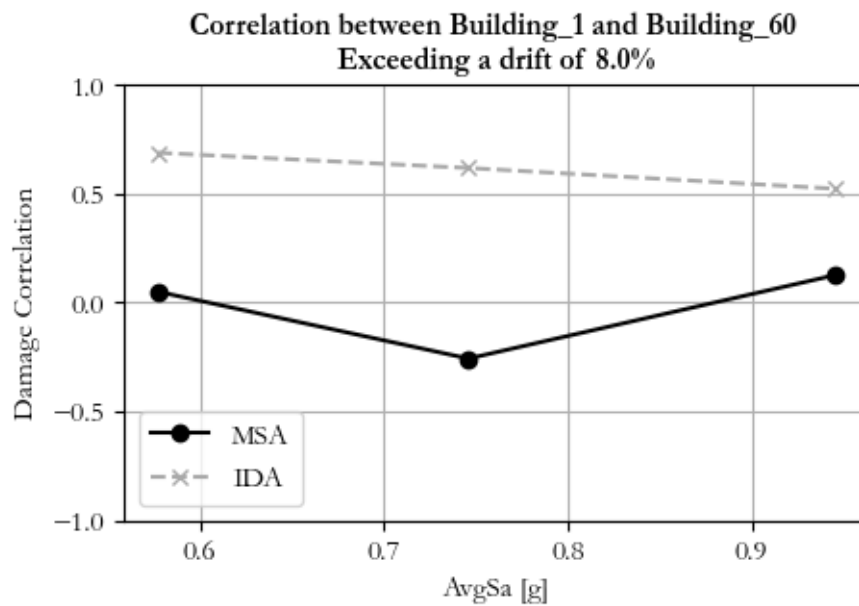


Figure 53 Correlation between Building 1 and Building 60. Drift limit of 8.0%

It is confirmed that the correlation estimated with the results of IDA on equivalent SDOF is considerably larger than the one calculated from the results of MSA. Even though the shape of the plot with both approaches follows similar tendencies, in cases like the correlation between Building 1 and Building 60 for an AvgSa of 0.746 g, there is a difference of 340% between both values (0.618 for IDA and -0.257 with MSA). This shows that in general the error of the estimation is larger for higher IM levels, having not only an overestimation of the calculations due to the use of equivalent SDOF, as shown by the results on Figure 35 through Figure 38, but also due to the bias associated with the use of IDA due to excessive scaling. It is noted that other factors may contribute to this difference but that the scaling is likely to be the largest contributor.

One particular situation that was observed is that in some of the cases the correlation between both buildings was equal to 1, as observed for the pairing of Building 1 and 21 (Figure 51). To understand the cause of this result, the marginal and joint probabilities for both buildings were examined, as shown in Figure 54. It was observed that, for the lowest values of AvgSa, both the marginal and joint probabilities were identical, meaning that the same records caused collapse in both buildings. It must be explored, then, if this result is a consequence of using very few records or if this is a reasonable result.

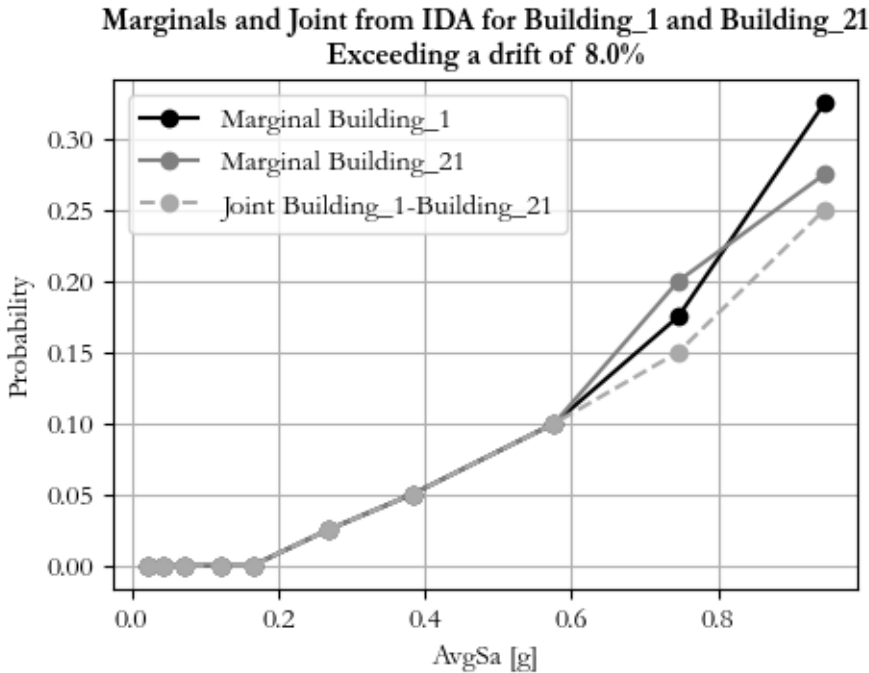


Figure 54 Marginal and Joint Probabilities for IDA on Building 1 and Building 60

It was shown then that in general the results obtained by running IDA on equivalent SDOF are overestimated when comparing to the ones obtained by MSA on the full 3D models. This overestimation is initially caused by the use of the equivalent SDOF, but for larger IM levels is increased probably by the bias caused by excessive scaling of the records associated with the use of IDA and because of the assumption of maintaining a deformed shape proportional to the first modal shape. Even though the difference of the values is significant, its actual impact on the estimation of damage is unknown, so the previously shown correlation matrices are used to actually estimate damage on different scenarios, both with constant shaking and an earthquake rupture scenario, as will be shown in the following chapter.

6. CASE STUDY EVALUATION

To evaluate the impacts of the correlation models previously described in Chapter 5, a case study was investigated to estimate damage both with and without considering the structure-to-structure damage correlation and subsequently analyse the impacts.

First, constant shaking scenarios were considered to estimate the correlation using the results of MSA on the full 3D model of the building and compare it with the results of IDA on equivalent SDOF. An initial constant shaking scenario with the AvgSa at all sites equal to the one associated with a return period of 475 years was used. Through this analysis, the impacts of using equivalent SDOF oscillators to estimate the damage correlation on the number of damaged buildings can be quantified. Then, a second shaking scenario was analysed, considering collapse fragility at an AvgSa equivalent to the return period of 4975 years. In general terms, even though this kind of scenarios are not realistic, they help to determine how good are the estimation of the correlation of the proposed method when compared with the ones from MSA and the overall impacts that these models can have.

Second, an earthquake rupture scenario was considered, to observe the impacts of considering the structure-to-structure damage correlation on a more realistic seismic shaking situation. The occurrence of an event is simulated at a given location and magnitude relative to the case study previously presented in Southern Italy. Then using GMMs, the ground motion at each of the locations of the buildings is estimated both considering and neglecting the spatial correlation. The damage correlation is estimated for each pair of buildings based on the previously simulated AvgSa at their locations, to finally simulate the damages both considering and neglecting such correlation. By comparing the results is possible then to estimate how deeply the consideration of the correlations can impact the results of the number of damaged buildings in regional seismic risk assessment.

A summary of all the different cases that are being considered is shown on Table 13. The constant shaking scenarios can be considered as special cases of the earthquake rupture scenario in which the spatial correlation (ρ_{sp}) is equal to one on all buildings. The method used to estimate the damage correlation (ρ_{dm}) is also shown in each particular case is also presented. The considered DS are the ones defined on Table 9.

Table 13 Considered Scenarios for Damage Estimation

Scenario	Ground Shaking	Damage State	Case	Spatial Correlation (ρ_{sp})	Damage Correlation (ρ_{dm})
1	Constant, equivalent to the one of a Return period of 475 years	DS1: PIDR larger than 1.0% (Light Damage)	1.1	Considered, equal to 1.0	Not Considered
			1.2	Considered, equal to 1.0	Considered, from MSA.
			1.3	Considered, equal to 1.0	Considered, from IDA on SDOF
2	Constant, equivalent to the one of a Return period of 4975 years	DS2: PIDR larger than 8.0% (Collapse)	2.1	Considered, equal to 1.0	Not Considered
			2.2	Considered, equal to 1.0	Considered, from MSA.
			2.3	Considered, equal to 1.0	Considered, from IDA on SDOF
3	Calculated based on an earthquake rupture scenario	DS1: PIDR larger than 1.0% (Light Damage)	3.1	Not Considered	Not Considered
			3.2	Considered	Not Considered
			3.3	Not Considered	Considered, from IDA on SDOF
			3.4	Considered	Considered, from IDA on SDOF

6.1 CONSTANT SHAKING SCENARIOS

As previously stated, the constant shaking scenarios were used to compare the results of using MSA on the full 3D numerical models of the buildings and those obtained by performing IDAs on the equivalent SDOF oscillators. Monte Carlo simulations were used to estimate the number of damaged buildings using the fragility functions derived as presented on Chapter 4. The damage correlations, on the other hand, were calculated according to the methods as presented Chapter 5.

To account for the correlation between the random variables when using Monte Carlo simulations, the Cholesky decomposition method was used. This method starts with a correlation matrix, which is factorized into a lower triangular matrix through Cholesky decomposition. When this triangular matrix is multiplied by its transpose, the original correlation matrix is obtained. A set of uncorrelated standard normal random variables is then generated and transformed by multiplying them with the lower triangular matrix, resulting in a new set of correlated random variables that maintain the relationships defined by the original correlation matrix. This correlation-controlled simulation has been used in past studies such as O'Reilly & Sullivan (2018) among others. It is important to note that the Cholesky decomposition method requires the correlation matrix to be symmetric and positive definite, which means that its eigenvalues are all positive. Since it is already guaranteed that the correlation matrix is always going to be symmetrical, a regularization process is conducted to ensure that the results are always positive symmetrical. This process consists of adding a very small value to the elements in the diagonal to ensure that its eigenvalues of the matrix are all positive.

These correlated normal variables were then transformed into uniform random variables by using the cumulative distribution function of a standard normal distribution. These obtained uniform random variables were used to simulate damage on each building, considering the probability of damage given by the fragility curve of each structure at the considered damage state conditioned for the AvgSa at the site, as presented in Figure 55. The total number of damaged buildings was estimated by counting how many buildings exceeded the damage state threshold. After repeating this procedure multiple times, histograms were generated to estimate the probability distribution of the number of damaged buildings for each case on each scenario.

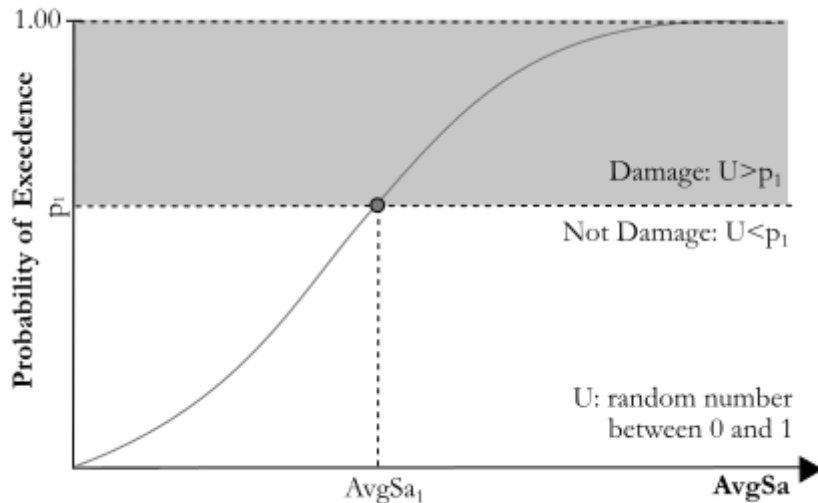


Figure 55 Monte Carlo Simulation of Damage

Two different constant shaking scenarios were analysed, Scenario 1 and Scenario 2, as described on Table 13. The results of the simulated number of damaged buildings for both scenarios and their associated cases are presented in the following sections.

6.1.1 Scenario 1: Exceeding a PIDR of 1% at an AvgSa of 0.268g

In this scenario, the number of damaged buildings estimated using the damage correlation matrix calculated based on the results from the full 3D model is compared to the estimation obtained using equivalent SDOF oscillators. An AvgSa of 0.268g was considered since it corresponds to the ground motion intensity for a return period of 475 years. On this intensity level the records used for calculating the correlation matrix both with MSA and IDA are the same, with identical scale factors. Therefore, the only difference in the results is caused by the method to compute the correlation using of the equivalent SDOF oscillators, naas the intensity and the ground motions were identical. A damage state of light damage was defined as the case in which the peak interstory drift ratio exceeded a threshold of 1.0%, so the correlation matrices used are the ones shown in Figure 35 and Figure 36 depending on the method used to estimate it.

Histograms of the different cases described in Table 13 were plotted on Figure 56 through Figure 58, illustrating the probability distribution function of the number of damaged buildings for each case. Additional statistics like the mean, median and standard deviation were also computed. A total number of 100000 realizations were performed to obtain an accurate estimation of the data.

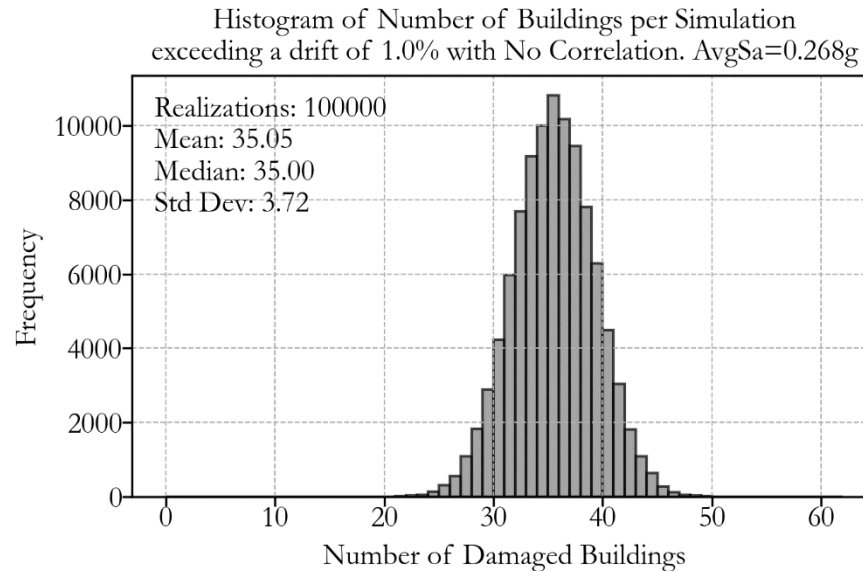


Figure 56 Histogram damaged buildings for Case 1.1

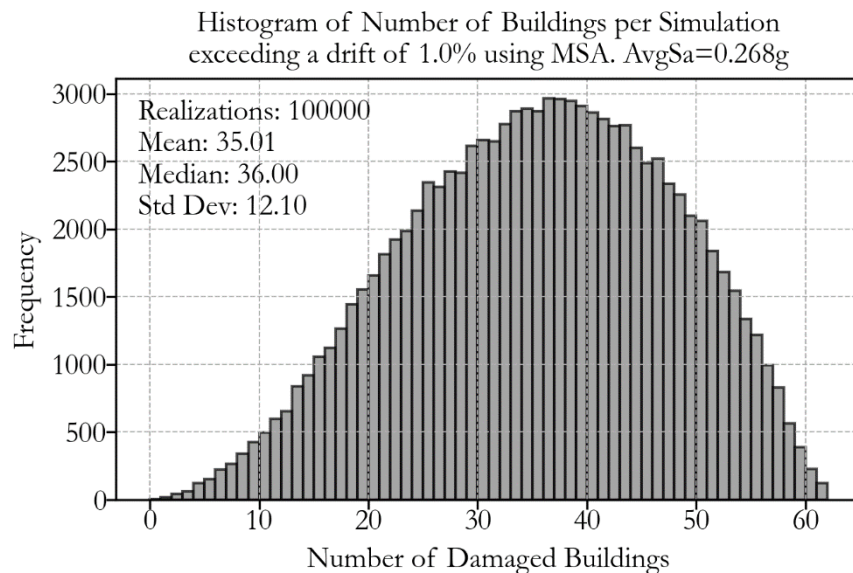


Figure 57 Histogram Damaged Buildings for Case 1.2

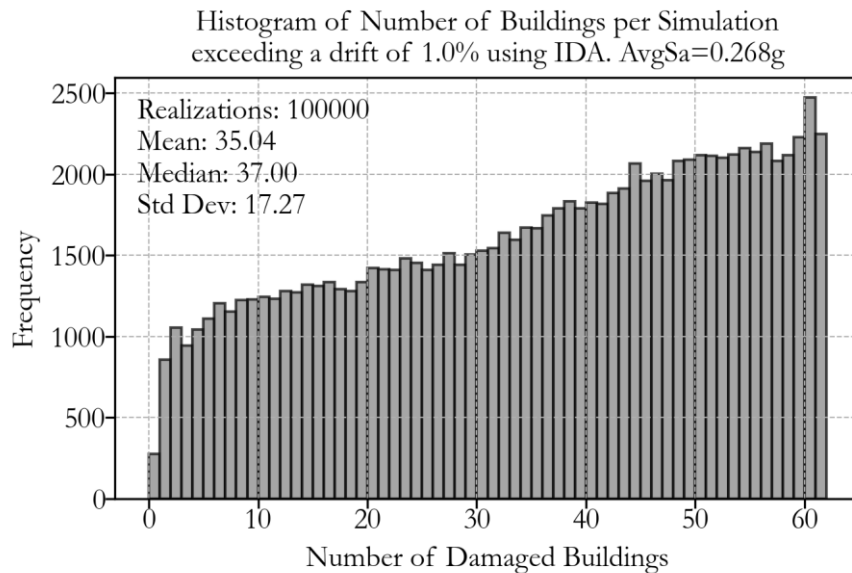


Figure 58 Histogram Damaged Buildings for Case 1.3

It can be observed that in general the mean number of damaged buildings is essentially the same in all three cases, having a value close to 35 buildings. Regarding the median, the difference between the three cases is very similar, with 35 buildings for Case 1.1, 36 buildings for Case 1.2 and 37 buildings for Case 1.3. The most significant change, however, is observed on the value of the standard deviation, increasing from 3.72 for Case 1.1 to 12.10 for Case 1.2 and 17.27 for Case 1.3. These results are consistent with what would have been expected given that the correlation matrix estimated with the equivalent SDOF was considerably larger than the one from the full 3D models.

When comparing the probability distribution functions between Case 1.1 and Case 1.2, it can be noted that they have very similar shapes, with a notable difference in the scatter of the data due to the increase of the standard deviation in Case 1.2. On the other hand, the distribution of the data observed for Case 1.3, presented on Figure 58, is completely different to the one of the other two cases, looking more like a triangular distribution than a normal or lognormal distribution.

What the previous analysis proves is that considering the structure-to-structure damage correlation into the analysis doesn't modify the estimated mean or median number of damaged buildings. Instead, it has a notable impact on the estimation of the tails of the distribution, increasing the observed probabilities of obtaining a large number of damaged buildings, which in the context of regional seismic risk assessment might be a very

interesting decision variable for the governments to create risk mitigation strategies. To explore on depth how the probabilities of observing a large number of buildings differs for each of the cases the probability of exceeding a certain number of buildings is presented on Figure 59 and in Table 14.

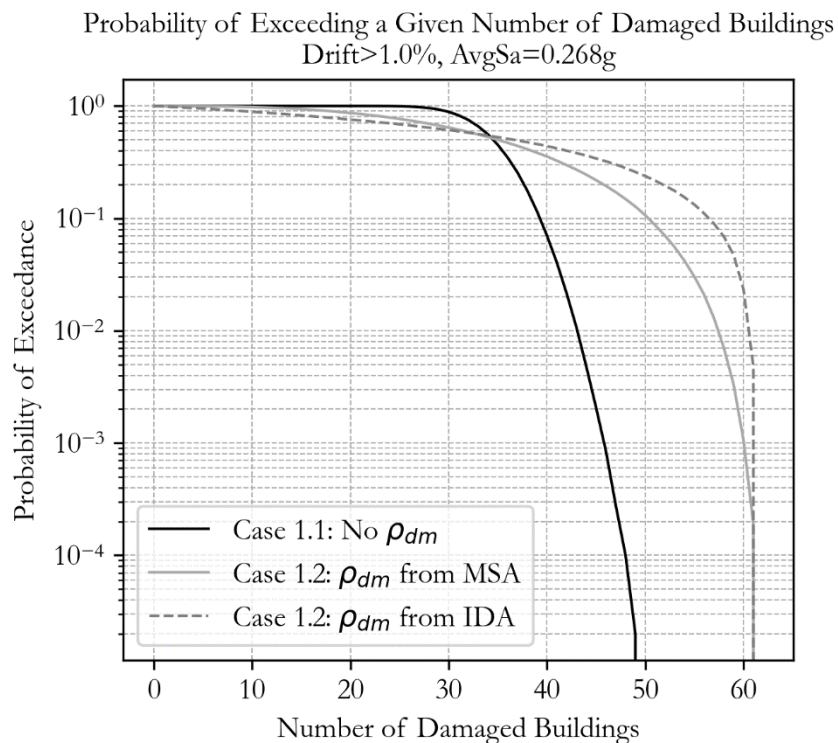


Figure 59 Comparison of Probability of Exceeding a Given Number of Damaged Building for Scenario 1

Table 14 Probability of Exceeding a Given Number of Buildings for Scenario 1

Probability of Exceeding more than X damaged buildings	Case 1.1: No Correlation	Case 1.2: Correlation from MSA	Case 1.3: Correlation from IDA on SDOF
X=30	88.7%	64.2%	61.0%
X=35	45.4%	49.9%	52.9%
X=40	6.9%	35.5%	43.9%
X=45	0.2%	21.9%	34.2%

It can be observed that there is a significant difference between the results obtained by neglecting the structure-to-structure damage correlation and those calculated using either of the two methods employed. When comparing the results from Case 1.2 and Case 1.3, the difference increases as the number of damaged buildings rises, approaching the maximum number of buildings in the portfolio (61), where both curves converge once again. For example, as shown in Table 11, the probability of exceeding more than 45 damaged buildings is 34.2% in Case 1.3. In comparison, Case 1.2 yields a probability of 21.9%, reflecting a significant difference of 56%. Despite this, Case 1.3 provides a better estimate than ignoring the correlation altogether, as done in Case 3.1.

In conclusion, using equivalent SDOF oscillators to calculate the structure-to-structure damage correlation results in an overestimation of the total number of damaged buildings. However, it still offers a more accurate estimate compared to completely ignoring this correlation.

6.1.2 Scenario 2: Exceeding a PIDR of 8% at an AvgSa of 0.746g

This scenario was analysed to evaluate the potential bias in damage estimation at higher intensities potentially caused by excessive scaling of records associated with IDAs used to calculate the structure-to-structure damage correlation. To do this, the total number of damaged buildings obtained from this method was compared with those estimated using MSA on the full 3D models. An AvgSa of 0.746g was selected, corresponding to an intensity associated with a return period of 4975 years, one of the highest values considered in the analysis, which required considerable scaling of the records of up until a value of 34.5.

A damage state of collapse was considered, associated with exceeding a peak interstory drift ratio of 8.0%. In consequence, the correlation matrices used for the analysis are the ones presented in Figure 45 and Figure 46. Once again 1,000,000 realizations were performed to calculate the histograms for each of the considered cases, that represent the probability distribution function of the total number of collapsed buildings in the scenario. The results are presented in Figure 60, Figure 61 and Figure 62 for Case 2.1, Case 2.2 and Case 2.3 respectively.

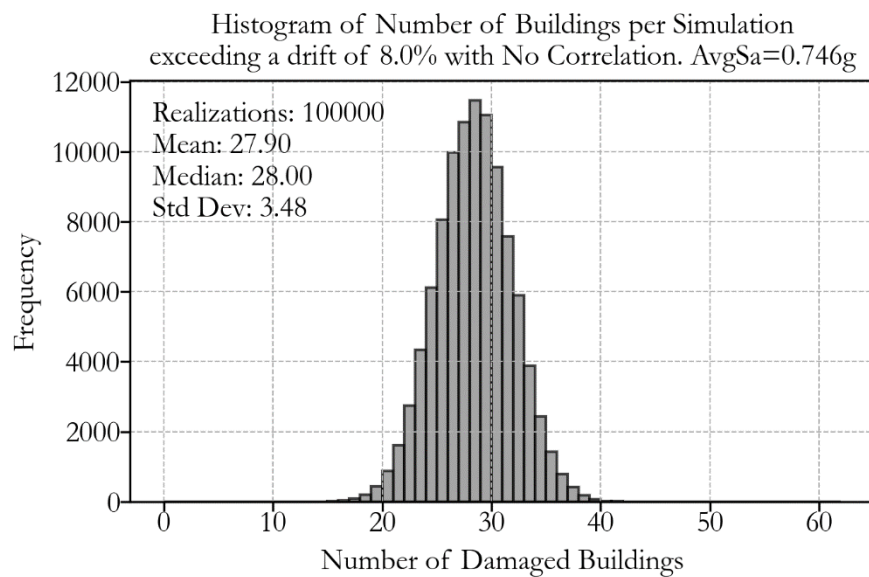


Figure 60 Histogram damaged buildings Case 2.1

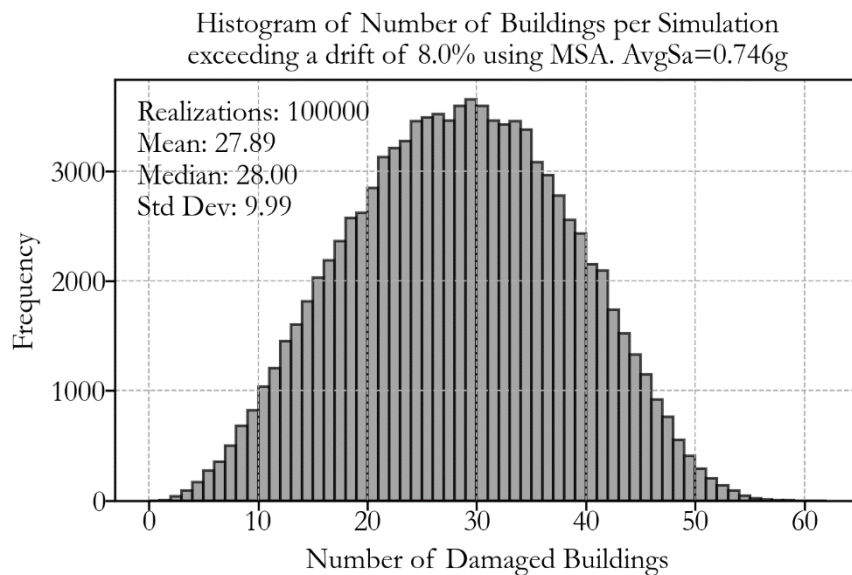


Figure 61 Histogram Damaged Buildings Case 2.2

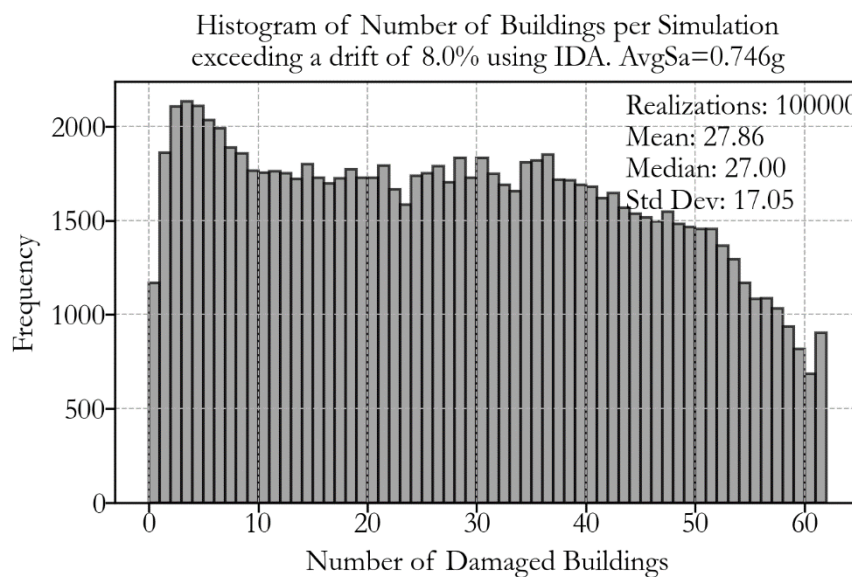


Figure 62 Histogram Damaged Buildings Case 2.3

As in the previous scenario the mean number of buildings is essentially the same in all cases, being approximately 27.9 buildings. There is also a very small variation in the obtained results for the median, that is equal 28 buildings for Cases 2.1 and 2.2, and 27 buildings for Case 2.3. Once again, the main difference can be observed in the values of the standard deviations, that increase significantly from 3.48 on Case 2.1, to 9.99 on Case 2.2 and 17.05 on Case 2.3. The shape of the distribution is also considerably different for Case 2.3 when compared to the one of the other two Cases. As a result, once again the main consequence of this differences is associated with the probability of exceeding a large number of damaged buildings, which is presented on Figure 63 and Table 15.

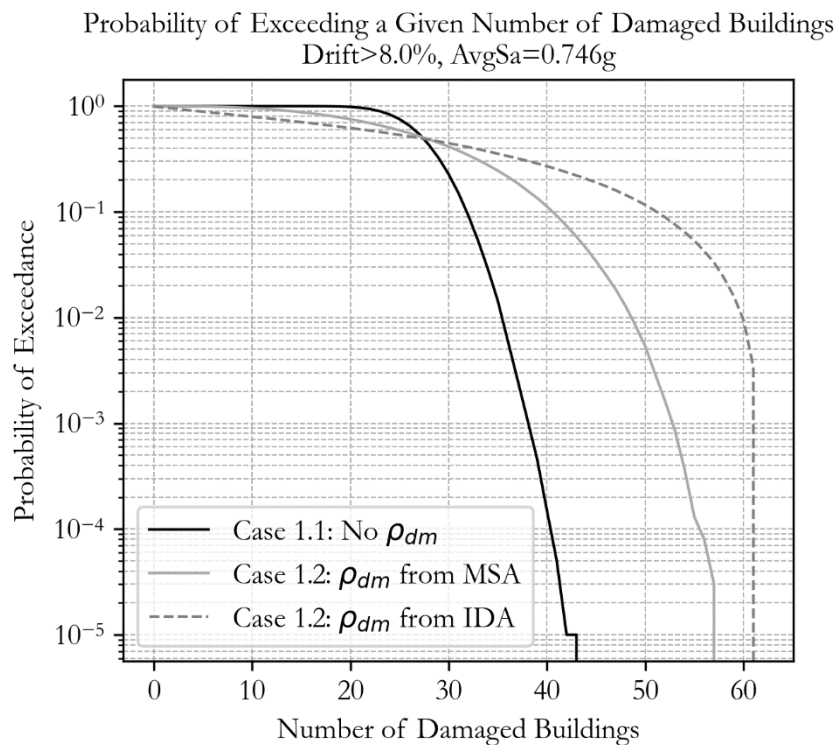


Figure 63 Comparison of Probability of Exceeding a Given Number of Damaged Building Scenario 2

Table 15 Probability of Exceeding a Given Number of Buildings Scenario 2

Probability of Exceeding more than X damaged Buildings	Case 1.1: No Correlation	Case 1.2: Correlation from MSA	Case 1.3: Correlation from IDA on SDOF
X=25	75.5%	58.8%	53.4%
X=30	22.6%	41.0%	44.5%
X=35	1.46%	24.2%	35.8%
X=40	0.01%	11.3%	27.2%

It can be noted that there is a significant difference in the results of considering and neglecting the structure-to-structure correlation, with the difference increasing as the probability of exceedance decreases. When comparing the results shown in Figure 63 with the ones in Figure 59, it can be observed that the difference between the cases that use MSA and the cases that use IDA on equivalent SDOF are greater in this, which requires substantial scaling of the records to maintain hazard consistency compared to Scenario 1. This proves once again that there is indeed a bias on the results of damage estimation due to this phenomenon.

When looking at some data in particular, for example at the probability of exceeding more than 40 damaged buildings in the scenario, as presented in Table 15, a significant difference is observed. The result obtained for Case 2.3 (27.2%) and results in a considerable difference of 143% when compared to the ones for Case 2.2 (11.3%). It is still, however, a better approximation to the result than completely neglecting the correlation, for which the probability of exceeding a total number of damaged buildings is nearly negligible (0.01%).

6.2 EARTHQUAKE RUPTURE SCENARIO

Following the previous section's consideration of an uniform level of ground shaking, here an earthquake rupture scenario was considered to observe the impacts of considering the structure-to-structure damage correlation in a more realistic seismic shaking context. After selecting a rupture scenario, Monte Carlo simulations were used to model different shaking maps caused by the same event, using a specific GMM and both considering and neglecting the spatial correlation depending on each specific case. Then, damage was also modelled with Monte Carlo simulations using the fragility functions previously derived for the damage state and conditioned on the AvgSa simulated for that particular realization.

Once again Cholesky's decomposition method was used to consider the structure-to-structure damage correlation in the analysis, estimated based on the results of IDAs on the equivalent SDOF oscillators. Since the value of the correlation depends on the value of AvgSa at the location of each building, the correlation matrix had to be computed specifically for the modelled ground motion intensities on each realization. After running several realizations, it was possible then to estimate the probability distribution of the number of damaged buildings, comparing the results for the cases presented on Table 13.

6.2.1 Scenario 3: Definition of earthquake rupture

Since it was already verified comparing the results of Scenarios 1 and 2 that the estimations of damage with the structure-to-structure correlation matrix calculated from IDA on equivalent SDOF oscillations are better for intensities closer to a return period of 475 years, the earthquake rupture scenario was defined from the disaggregation for that return period. This data, shown in Figure 64 was obtained from the PSHA of the site performed on OpenQuake and described in Section 3.2. The scenario was selected as the modal value of the disaggregation data, consisting of a rupture at 5km from the point with mean coordinates of the location of the buildings and with a magnitude of 6.25.

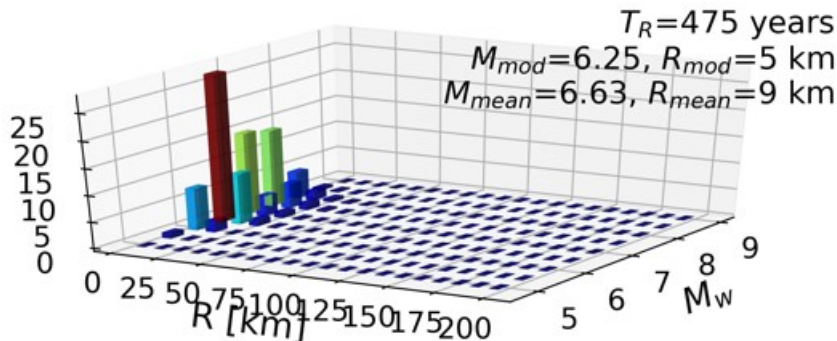


Figure 64 Disaggregation for return period of 475 years

The location of the rupture itself was determined by moving 5km from the mean coordinates of the buildings in the direction to the closer fault system, resulting in a point with latitude:14.3965 and longitude: 41.3958. The location of the rupture on the map is presented on Figure 65. A damage state of light damage was considered for the analysis, defined as the case in which the peak interstory drift ratio exceeded a threshold of 1.0%.

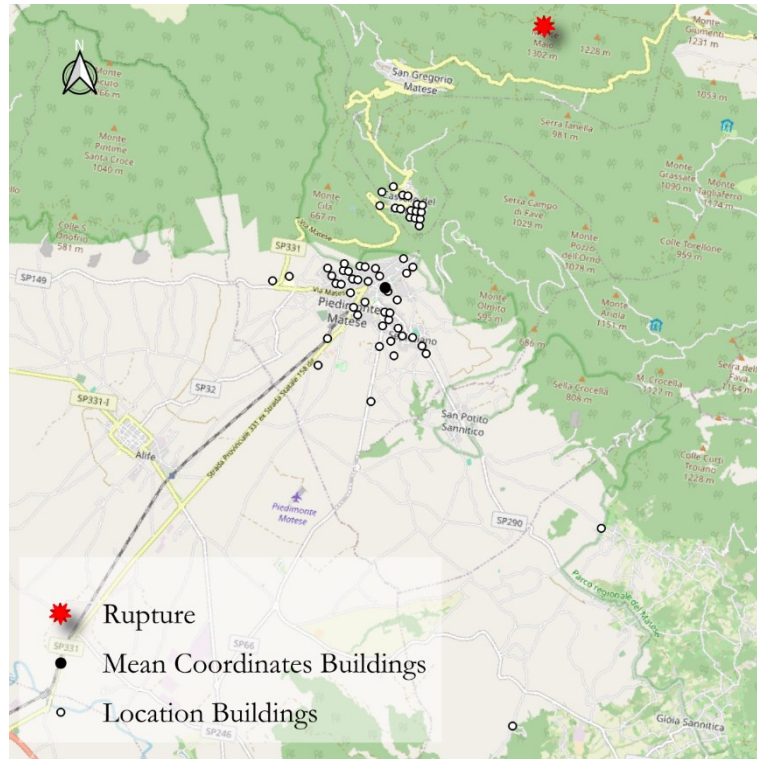


Figure 65 Considered Earthquake Rupture for Scenario 3

6.2.2 Intensity Measure Modelling

The intensity of shaking at the location of each of the buildings was simulated from the assumed rupture using the GMM proposed by Boore et al. (2014), as it was the same model used for the realization of the PSHA of the region. This model estimates the natural logarithm of the spectral acceleration at a given period considering the specific event, path and site effects at each location. The model also accounts for the inter- and intra-event variability of the estimations, as described by Equation (11).

$$\ln(Y) = F_E + F_p + F_s + \varepsilon_n \sigma \quad (11)$$

where Y corresponds to the desired IM, that can be either the PGA, PGV or 5% damped pseudo acceleration for a given structural period. F_E corresponds to the event function, that is estimated with specific coefficients for the considered IM as a function of the magnitude of the considered event and the failure mechanism that generated it. On the other hand, F_p is the path function, that is calculated in terms of the Joyner-Boore distance to the source and the characteristics of the geographic region. The site function, F_s , is

calculated as a function of the characteristics of the region, the magnitude and Joyner-Boore distance to the rupture, the basin depth and the value of $v_{s,30}$ at the site. The total standard deviation (σ) is calculated in terms of the between event variability (τ) and the within event variability (φ) as:

$$\sigma = \sqrt{\varphi^2 + \tau^2} \quad (12)$$

In this case in particular, however, special considerations must be done to model the ground motion intensity, since the chosen IM for the analysis is not the spectral acceleration for a given period but the average of the spectral accelerations between a range of periods (AvgSa). Given that a specific GMM that estimates directly AvgSa was not used, some mathematical calculations must be done to estimate indirectly the value of the desired IM as a function of the spectral accelerations estimated with Equation (11), as proposed by Kohrangi et al. (2018). The mean AvgSa and its standard deviation for a period range consistent of n number of periods can then be computed as:

$$\mu_{\ln AvgSa} = \left(\frac{1}{n} \right) \sum_{i=1}^n \mu_{\ln Sa(T_i)} \quad (13)$$

$$\sigma_{\ln AvgSa} = \sqrt{\left(\frac{1}{n^2} \right) \sum_{i=1}^n \sum_{m=1}^n \rho_{\ln Sa(T_i), \ln Sa(T_m)} \sigma_{\ln Sa(T_i)} \sigma_{\ln Sa(T_m)}} \quad (14)$$

where $\mu_{\ln Sa(T_i)}$ on Equation (13) was calculated from Equation (11) by considering an ε_n equal to 0. On the other hand, the correlation used in Equation (14) corresponds to the correlation between the spectral ordinates for different periods. Given that this is an academic study, the correlation between spectral ordinates for different periods was neglected to avoid overcomplicating the analysis. The standard deviations used on that equation can be computed from Equation (12).

As shown on Table 13, some of the cases of this scenario incorporate the use of spatial correlation in the analysis. This correlation must also be estimated considering that the IM in the analysis is the AvgSa, so the indirect approach developed by Kohrangi et al. (2018) was used to calculate it. The spatial correlation between site j and site k can be estimated from Equation (15), assuming the correlation between the spectral ordinates for different periods is neglected.

$$\rho_{sp}(j, k) = \frac{\left(\frac{1}{n^2}\right) \sum_{i=1}^n \rho_{\ln Sa(T_{j,i}), \ln Sa(T_{k,i})} \sigma_{\ln Sa(T_{j,i})} \sigma_{\ln Sa(T_{k,i})}}{\sigma_{\ln AvgSa_j} \sigma_{\ln AvgSa_k}} \quad (15)$$

The value of $\rho_{\ln Sa(T_{j,i}), \ln Sa(T_{k,i})}$ corresponds to the spatial correlation between two sites for a given spectral ordinate. It was estimated, on this case, from the method proposed by Jayaram and Baker (2009), as a function between the distance of the buildings.

It was possible then to use Monte Carlo simulation to simulate different realizations of the same earthquake rupture scenario, considering the mean and standard deviation for AvgSa on each site as estimated from Equations (13 and (14 respectively, and either considering and neglecting the spatial correlation. One particular realization is presented on Figure 66, in which a scenario modelled neglecting spatial correlation is presented on the right side and another modelled considering spatial correlation is presented on the left side. The two buildings located in Gioia Sannitica are not shown in the figure since they are located far from the other assets and the modeled AvgSa on both cases was in the lower range of values.

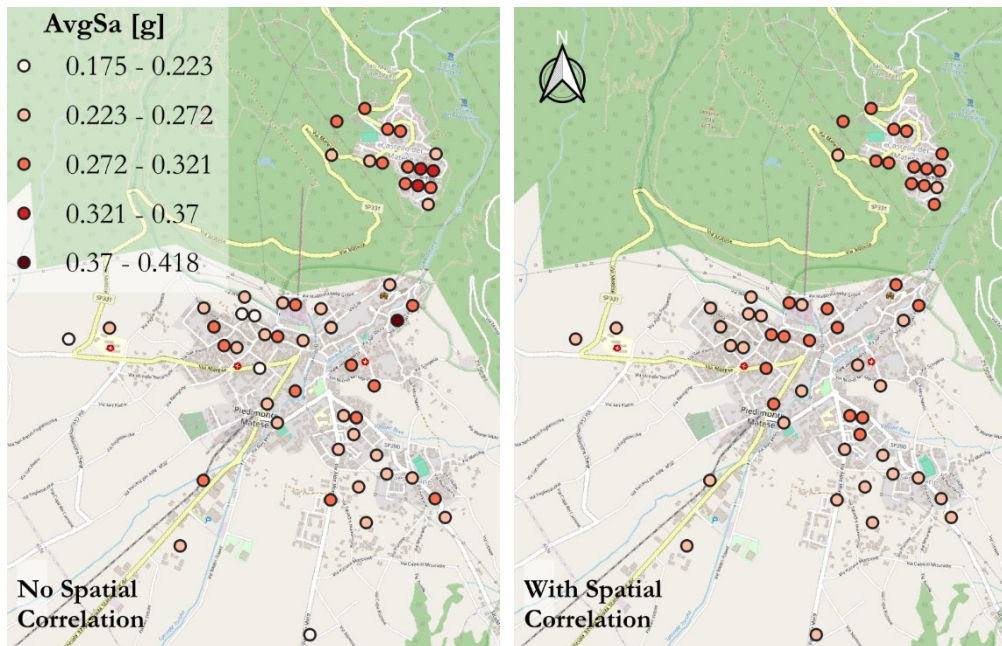


Figure 66 Modelled AvgSa with and without spatial correlation for one realization

The presented realizations have very similar mean AvgSa for all Buildings, with a value of 0.266g for the spatially uncorrelated model and of 0.260 g for the spatially correlated one. It can be seen then that even if the means of the data are similar, the spatially uncorrelated model presents a larger variation of the data, containing the points with both the largest and lowest estimations at random locations. The spatially correlated model, on the other hand, presents a more reasonable estimation of the ground motion intensity, capturing the variability of the results but maintaining a realistic geographical distribution of the data in which similar AvgSa are observed at close locations.

6.2.3 Calculation of structure-to-structure damage correlation

The structure-to-structure damage correlation was estimated from the results of IDA on the equivalent SDOF oscillators. It had to be computed for every particular realization as a function of the modelled intensities for that particular simulation. An example of the correlation matrix calculated for a particular realization is presented in Figure 67.

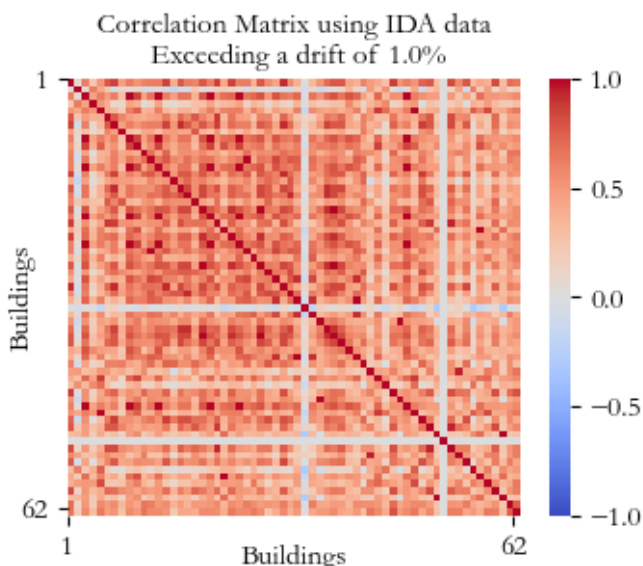


Figure 67 Correlation matrix calculated for one of the realizations

6.2.4 Estimation of number of damaged buildings

The histograms with the estimated number of damaged buildings after running 5000 realizations on each of cases shown on Table 13 are presented on Figure 68 through Figure 71.

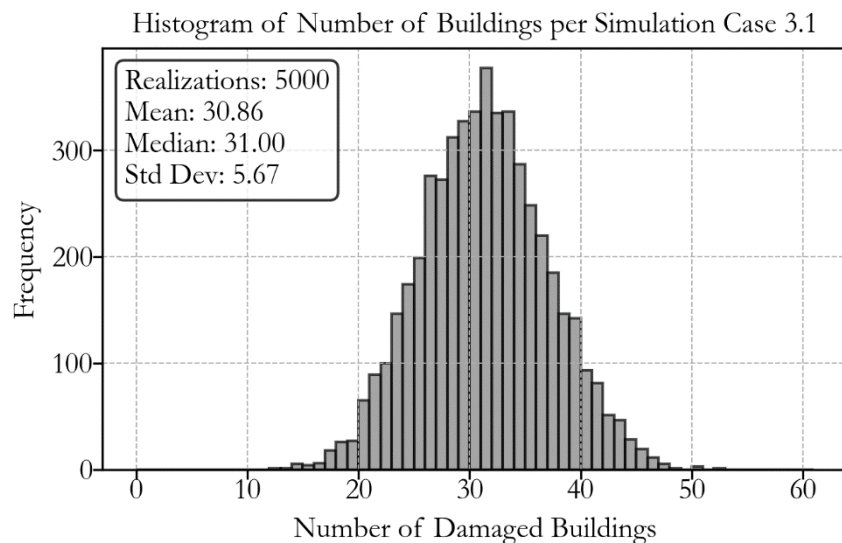


Figure 68 Histogram damaged buildings Case 3.1

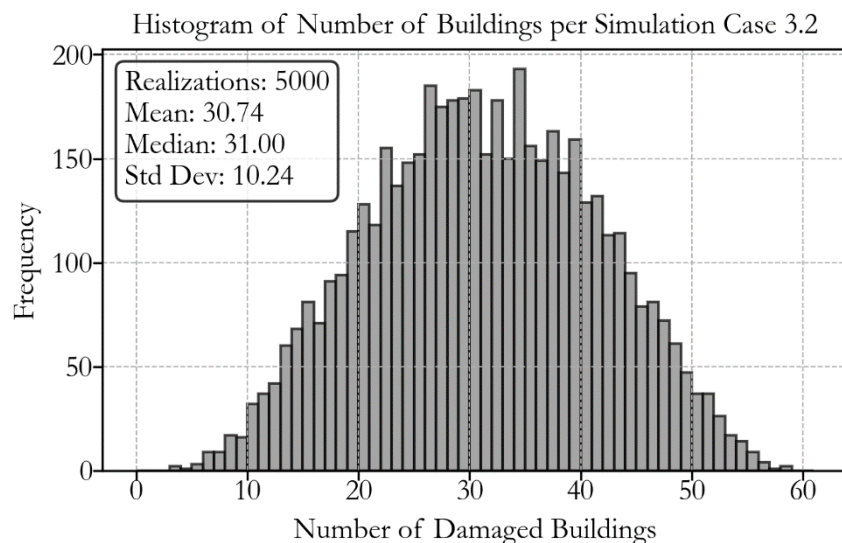


Figure 69 Histogram damaged buildings Case 3.2

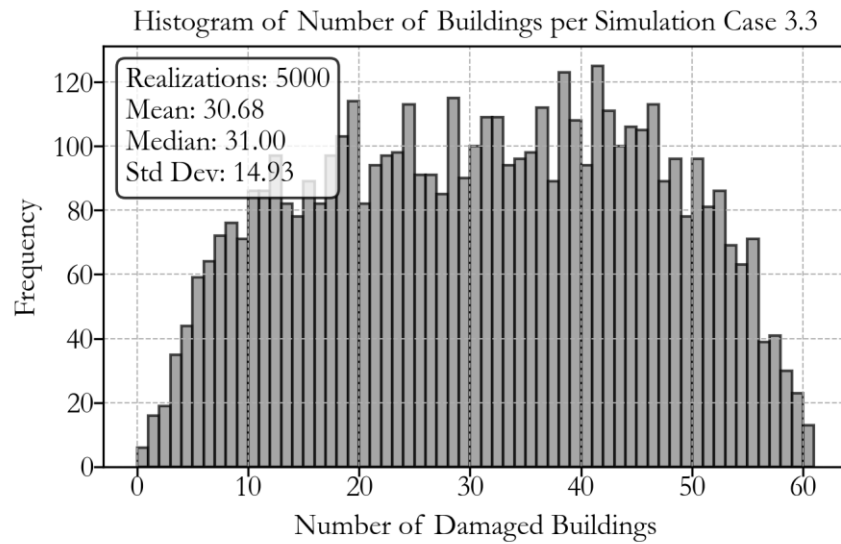


Figure 70 Histogram damaged buildings Case 3.3

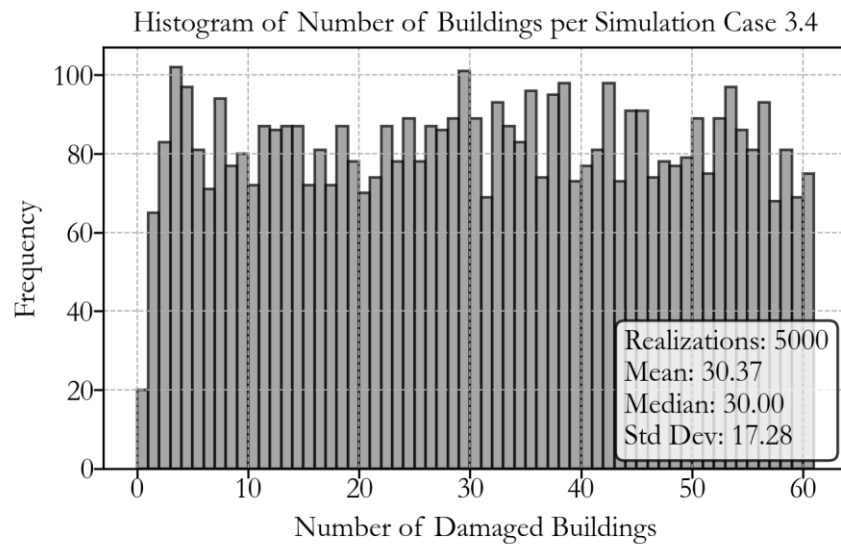


Figure 71 Histogram damaged buildings Case 3.4

It can be observed that also in this scenario the mean and median values for all cases are very similar, with the main difference being the value of the standard deviation and the shape of the probability distribution. As previously stated, these differences have an impact on the probability of exceeding a certain number of buildings, increasing the tails of the distribution, as shown on Figure 72.

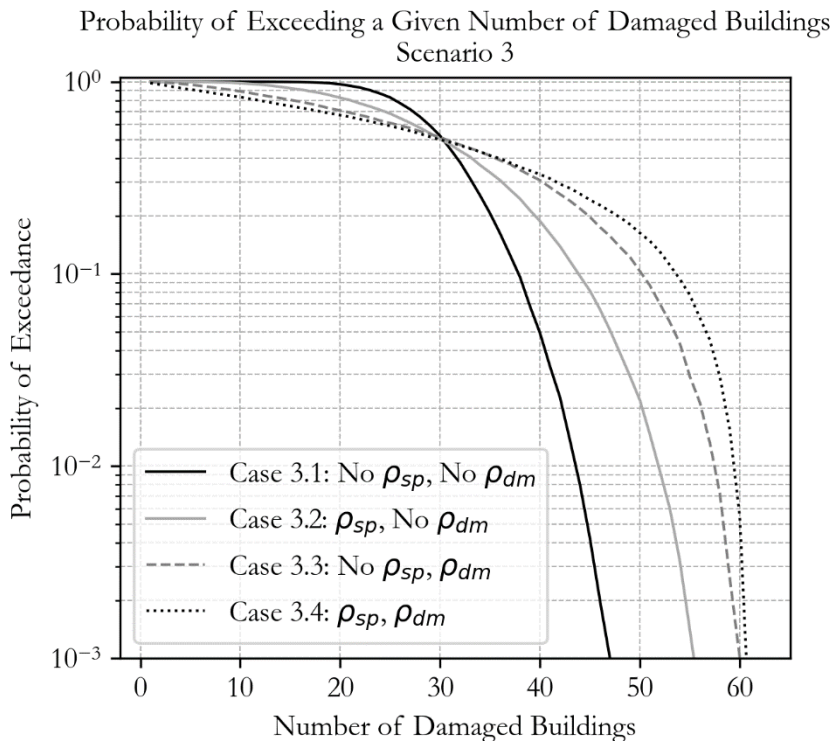


Figure 72 Comparison of Probability of Exceeding a Given Number of Damaged Building Scenario 3

It can be seen that when considering only spatial correlation or damage correlation, the latter has a more significant impact on the results. Therefore, we can deduce that considering the structure-to-structure damage correlation can be as important as considering the spatial correlation on regional seismic risk assessment at least for the case study under examination here. On the other hand, the use or not of the spatial correlation also impacts the calculation of the damage correlation itself, since it depends on the values of the simulated ground motion intensities that are derived based on that variable. To observe the results of the figure on a more comparable way the probability of exceeding a range of buildings between 30 and 35 is presented on Table 16.

Table 16 Probability of Exceeding a Given Number of Buildings Scenario 3

Probability of Exceeding more than X damaged Buildings	Case 3.1	Case 3.2	Case 3.3	Case 3.4
X=30	52.3%	50.3%	51.3%	49.8%
X=35	20.6%	33.7%	41.2%	41.3%
X=40	4.92%	18.8%	30.7%	32.9%
X=45	0.42%	8.16%	19.8%	24.3%

Once again, it can be observed that the differences between the cases increase with the number of damaged buildings. Given that the use of spatial correlation is widely adopted and will likely always be used for this type of analysis, the results were compared using Case 3.2 as the reference. For instance, focusing on Case 3.4, which considers both spatial and damage correlation, the probability of exceeding more than 45 damaged buildings increases from 8.16% to 24.3%, resulting in a difference of almost 200% between the two estimations.

To better understand the real-world implications of this difference, consider a hypothetical scenario in which the government of the Caserta province plans strategies to finance the reconstruction of the three municipalities analysed in this study in the event of an earthquake. Assuming the earthquake scenario presented here is viewed as a "worst-case scenario," the government might decide to secure funds to repair the number of buildings with a 5% probability of being damaged by such an event. If the analyst only considers spatial correlation in the risk assessment, the government would plan to repair 47 buildings. However, if structure-to-structure damage correlation is also considered, as done in this study, the government would need to finance the repair of 57 buildings, resulting in a difference of 10 buildings or a 21.3% increase in required resources. Obviously, these numbers are case study specific and further studies could be conducted to examine the magnitude in other regions, but the fundamental issue is clear.

In conclusion, the data shows that including structure-to-structure damage correlation has a significant effect on the probability of exceeding a certain number of damaged buildings. This correlation can lead to much higher probability estimates than when only spatial

correlation is considered. This highlights the need to incorporate both types of correlation in risk assessments. For decision-makers, like in disaster planning, using both correlations provides a more accurate estimate of required resources, ensuring better preparation and more effective allocation of funds for recovery efforts.

7. SUMMARY AND CONCLUSIONS

In this study, it was demonstrated how significantly the results of a regional seismic risk assessment can differ when the structure-to-structure damage correlation is either considered or neglected. Using a case study where the probability distribution of the total number of damaged buildings was estimated, it was verified that even if this parameter doesn't affect the estimations of the mean and median values, it does heavily influence the standard deviation and shape of distribution. These parameters heavily impact the probability of exceeding a large number of buildings, which can be a variable of particular interest to government for planning mitigation strategies.

The proposed method for estimating analytically the damage correlation from the results of performing IDA on equivalent SDOF oscillators proved to result in a considerable overestimation of the total number of damaged buildings when compared with the more adequate method of using the results of MSA on the full 3D models. However, it was also verified that this method still provides better estimates than completely neglecting the correlation, as it is commonly done for this type of analysis. The use of MSA on full 3D models, however, is not an approach that could be used in real life, since it not only requires having a full nonlinear model of the building, but also is very computationally demanding and time consuming, and can only be applied on the special scenarios of constant shaking that do not occur in reality.

Further exploration is needed to understand the sensitivity of the results to the number of ground motions used in the analysis. Since the joint distribution of probability of damage was estimated from the results of NLTH, in some cases had too few ground motions causing both structures to get damaged, which lead to having some negative values of the correlation. On the context of the phenomenon that is being studied, this means that if a structure gets damaged it is less likely than the other structure also gets damage, which is which is not a realistic outcome. It must be verified then if this is an issue related with the number of ground motions used for the analysis or if it is a limitation of the method itself.

It could also be determined how good are the results of the calculation if the results of IDA are on the full 3D models are used, to verify if the use of this approach leads to better estimations of the correlation, as recent studies on the topic have explored. The results should also be validated with information from actual events to assess whether the

analytical approach proposed here can be used to develop mathematical models of correlation as a function of different building characteristics that influence their vulnerability. However, doing this validation might be difficult, given that the available data may be sparse and challenging to interpret. In this way, approximated equations could be generated to approximate the correlation on real life cases, where a full nonlinear model of all buildings are not available.

In conclusion, this study underscores the significant impact of considering structure-to-structure damage correlations in earthquake risk assessments. By integrating this variable into the analysis, the probability of exceeding a large number of damaged buildings increases, leading to higher resource estimates for recovery efforts. As demonstrated in the case of the Caserta province, in a hypothetical scenario where the government plans resources based on the number of buildings with a 5% probability of exceeding damage from the earthquake defined as Scenario 3, the government would need to prepare for a 21.3% increase in building repairs if both the damage and the spatial correlations are considered, compared to when only the latter is accounted for. This finding emphasizes the importance for decision-makers to incorporate both correlations in risk modelling to ensure accurate resource estimation and efficient allocation of funds for recovery during disaster planning. While the specific figures in this study are case-dependent, the broader implication is clear: a more complete risk assessment leads to better preparedness in real-world scenarios.

REFERENCES

- Amir M. Kaynia (Editor), Iunio Iervolino (Reviewer), Fabio Taucer (Publishing Editor), & Ufuk Hancilar (Publishing Editor). (2013). *Guidelines for deriving seismic fragility functions of elements at risk: Buildings, lifelines, transportation networks and critical facilities.* <https://doi.org/10.2788/19605>
- Aristeidou, S., & O'Reilly, G. J. (2024). Exploring the Use of Orientation-Independent Inelastic Spectral Displacements in the Seismic Assessment of Bridges. *Journal of Earthquake Engineering*, 28(12), 3515–3538. <https://doi.org/10.1080/13632469.2024.2343067>
- Aristeidou, S., Shahnazaryan, D., & O'Reilly, G. J. (2024). Artificial neural network-based ground motion model for next-generation seismic intensity measures. *Soil Dynamics and Earthquake Engineering*, 184, 108851. <https://doi.org/10.1016/j.soildyn.2024.108851>
- ATC. (1995). *Structural Response Modification Factors, ATC-19.*
- ATC. (2018). *FEMA P-58: Vol. Volum 1* (2nd ed.).
- Atilla Ansal (Ed.). (2014). *Perspectives on European Earthquake Engineering and Seismology* (Vol. 34). Springer International Publishing. <https://doi.org/10.1007/978-3-319-07118-3>
- Baker, J. W. (2007, December 5). Measuring Bias in Structural Response Caused by Ground Motion Scaling . *8th Pacific Conference on Earthquake Engineering*.
- Baker, J. W. (2015). Efficient Analytical Fragility Function Fitting Using Dynamic Structural Analysis. *Earthquake Spectra*, 31(1), 579–599. <https://doi.org/10.1193/021113EQS025M>
- Bodenmann, L., Baker, J. W., & Stojadinović, B. (2023). Accounting for path and site effects in spatial ground-motion correlation models using Bayesian inference. *Natural Hazards and Earth System Sciences*, 23(7), 2387–2402. <https://doi.org/10.5194/nhess-23-2387-2023>

- Boore, D. M., Stewart, J. P., Seyhan, E., & Atkinson, G. M. (2014). NGA-West2 Equations for Predicting PGA, PGV, and 5% Damped PSA for Shallow Crustal Earthquakes. *Earthquake Spectra*, 30(3), 1057–1085. <https://doi.org/10.1193/070113EQS184M>
- Corlito, V., & De Matteis, G. (2019). Caratterizzazione tipologico-strutturale e valutazione della vulnerabilità sismica degli edifici in cemento armato della Provincia di Caserta attraverso i parametri della scheda CARTIS. *XVIII CONVEGNO ANIDIS “L’Ingegneria Sismica in Italia,”* 96–104.
- Crowley, H., Despotaki, V., Silva, V., Dabbeek, J., Romão, X., Pereira, N., Castro, J. M., Daniell, J., Veliu, E., Bilgin, H., Adam, C., Deyanova, M., Ademović, N., Atalic, J., Riga, E., Karatzetzou, A., Bessason, B., Shendova, V., Tiganescu, A., ... Hancilar, U. (2021). Model of seismic design lateral force levels for the existing reinforced concrete European building stock. *Bulletin of Earthquake Engineering*, 19(7), 2839–2865. <https://doi.org/10.1007/s10518-021-01083-3>
- D. Giardini et al. (2013). *Seismic Hazard Harmonization in Europe (SHARE): Online Data Resource*.
- Dávalos, H., & Miranda, E. (2021). A Ground Motion Prediction Model for Average Spectral Acceleration. *Journal of Earthquake Engineering*, 25(2), 319–342. <https://doi.org/10.1080/13632469.2018.1518278>
- Eads, L., Miranda, E., & Lignos, D. G. (2015). Average spectral acceleration as an intensity measure for collapse risk assessment. *Earthquake Engineering & Structural Dynamics*, 44(12), 2057–2073. <https://doi.org/10.1002/eqe.2575>
- Esposito, S., & Iervolino, I. (2011). PGA and PGV Spatial Correlation Models Based on European Multievent Datasets. *Bulletin of the Seismological Society of America*, 101(5), 2532–2541. <https://doi.org/10.1785/0120110117>
- GEM. (2021, May 12). *Exposure Spatial Disaggregation*. GitHub Repository.
- H. Crowley, V. Despotaki, D. Rodrigues, V. Silva, C. Costa, D. Toma-Danila, E. Riga, A. Karatzetzou, S. Fotopoulou, L. Sousa, S. Ozcebe, P. Gamba, J. Dabbeek, X. Romão, N. Pereira, J.M. Castro, J. Daniell, E. Veliu, H. Bilgin, ... U. Hancilar. (2021). *European Exposure Model Data Repository (v1.0)*. <https://doi.org/10.5281/ZENODO.5730071>
- Heresi, P., & Miranda, E. (2022). Structure-to-structure damage correlation for scenario-based regional seismic risk assessment. *Structural Safety*, 95, 102155. <https://doi.org/10.1016/j.strusafe.2021.102155>

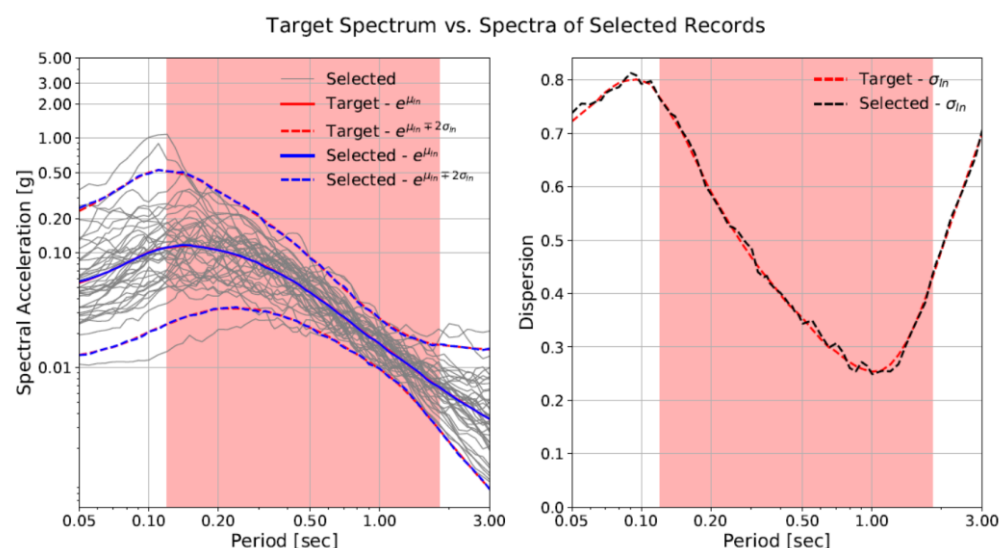
- Heresi, P., & Miranda, E. (2023). RPBEE: Performance-based earthquake engineering on a regional scale. *Earthquake Spectra*, 39(3), 1328–1351. <https://doi.org/10.1177/87552930231179491>
- Jalayer, F. (2003). *Direct Probabilistic Seismic Analysis: Implementing Non-Linear Dynamic Assessments*. Stanford University.
- Jalayer, F., & Cornell, C. A. (2009). Alternative non-linear demand estimation methods for probability-based seismic assessments. *Earthquake Engineering & Structural Dynamics*, 38(8), 951–972. <https://doi.org/10.1002/eqe.876>
- Jayaram, N., & Baker, J. W. (2009). Correlation model for spatially distributed ground-motion intensities. *Earthquake Engineering & Structural Dynamics*, 38(15), 1687–1708. <https://doi.org/10.1002/eqe.922>
- Kang, C., Kwon, O.-S., & Song, J. (2021). Evaluation of correlation between engineering demand parameters of structures for seismic system reliability analysis. *Structural Safety*, 93, 102133. <https://doi.org/10.1016/j.strusafe.2021.102133>
- Kohrangi, M., Bazzurro, P., Vamvatsikos, D., & Spillatura, A. (2017). Conditional spectrum-based ground motion record selection using average spectral acceleration. *Earthquake Engineering & Structural Dynamics*, 46(10), 1667–1685. <https://doi.org/10.1002/eqe.2876>
- Kohrangi, M., Kotha, S. R., & Bazzurro, P. (2018). Ground-motion models for average spectral acceleration in a period range: direct and indirect methods. *Bulletin of Earthquake Engineering*, 16(1), 45–65. <https://doi.org/10.1007/s10518-017-0216-5>
- Kohrangi, M., Vamvatsikos, D., & Bazzurro, P. (2017). Site dependence and record selection schemes for building fragility and regional loss assessment. *Earthquake Engineering & Structural Dynamics*, 46(10), 1625–1643. <https://doi.org/10.1002/eqe.2873>
- Lee, R., & Kiremidjian, A. S. (2007). Uncertainty and Correlation for Loss Assessment of Spatially Distributed Systems. *Earthquake Spectra*, 23(4), 753–770. <https://doi.org/10.1193/1.2791001>
- Lin, T., Haselton, C. B., & Baker, J. W. (2013). Conditional spectrum-based ground motion selection. Part I: Hazard consistency for risk-based assessments. *Earthquake*

- Engineering & Structural Dynamics*, 42(12), 1847–1865.
<https://doi.org/10.1002/eqe.2301>
- Luco, N., & Cornell, C. A. (2007). Structure-Specific Scalar Intensity Measures for Near-Source and Ordinary Earthquake Ground Motions. *Earthquake Spectra*, 23(2), 357–392. <https://doi.org/10.1193/1.2723158>
- Martins, L., & Silva, V. (2021). Development of a fragility and vulnerability model for global seismic risk analyses. *Bulletin of Earthquake Engineering*, 19(15), 6719–6745. <https://doi.org/10.1007/s10518-020-00885-1>
- Nafeh, A. M. B., & O'Reilly, G. J. (2024). Fragility functions for non-ductile infilled reinforced concrete buildings using next-generation intensity measures based on analytical models and empirical data from past earthquakes. *Bulletin of Earthquake Engineering*, 22(10), 4983–5021. <https://doi.org/10.1007/s10518-024-01955-4>
- O'Reilly, G. J. (2021a). Limitations of Sa(T1) as an intensity measure when assessing non-ductile infilled RC frame structures. *Bulletin of Earthquake Engineering*, 19(6), 2389–2417. <https://doi.org/10.1007/s10518-021-01071-7>
- O'Reilly, G. J. (2021b). Seismic intensity measures for risk assessment of bridges. *Bulletin of Earthquake Engineering*, 19(9), 3671–3699. <https://doi.org/10.1007/s10518-021-01114-z>
- O'Reilly, G. J., & Sullivan, T. J. (2018). Quantification of modelling uncertainty in existing Italian RC frames. *Earthquake Engineering & Structural Dynamics*, 47(4), 1054–1074. <https://doi.org/10.1002/eqe.3005>
- O'Reilly, G., Kohrangi, M., Bazzurro, P., & Monteiro, R. (2018). Intensity Measures for the Collapse Assessment of Infilled RC Frames. *16th European Conference on Earthquake Engineering*.
- Pagani, M., Monelli, D., Weatherill, G., Danciu, L., Crowley, H., Silva, V., Henshaw, P., Butler, L., Nastasi, M., Panzeri, L., Simionato, M., & Vigano, D. (2014). OpenQuake Engine: An Open Hazard (and Risk) Software for the Global Earthquake Model. *Seismological Research Letters*, 85(3), 692–702. <https://doi.org/10.1785/0220130087>
- Paulay, T., & Priestley, M. J. N. (1992). *Seismic Design of Reinforced Concrete and Masonry Buildings*. John Wiley & Sons, Inc.

- Tsokos, C., & Wooten, R. (2016). *The Joy of Finite Mathematics*. Elsevier. <https://doi.org/10.1016/C2014-0-02921-8>
- Vamvatsikos, D., & Cornell, C. A. (2002). Incremental dynamic analysis. *Earthquake Engineering & Structural Dynamics*, 31(3), 491–514. <https://doi.org/10.1002/eqe.141>
- Vamvatsikos, D., & Cornell, C. A. (2005). Developing efficient scalar and vector intensity measures for IDA capacity estimation by incorporating elastic spectral shape information. *Earthquake Engineering & Structural Dynamics*, 34(13), 1573–1600. <https://doi.org/10.1002/eqe.496>
- WorldPop (www.worldpop.org - School of Geography and Environmental Science, U. of S. D. of G. and G. U. of L. D. de G. U. de N. and C. for I. E. S. I. N. (CIESIN), C. U. (2018). *Global High Resolution Population Denominators Project - Funded by The Bill and Melinda Gates Foundation*. [Https://Dx.Doi.Org/10.5258/SOTON/WP00660](https://dx.doi.org/10.5258/SOTON/WP00660).
- Xiang, M., Shen, J., Xu, Z., & Chen, J. (2024). Structure-to-structure seismic damage correlation model. *Earthquake Engineering & Structural Dynamics*, 53(10), 3205–3229. <https://doi.org/10.1002/eqe.4172>

APPENDIX A. RECORD SELECTION

Return period of 22 years

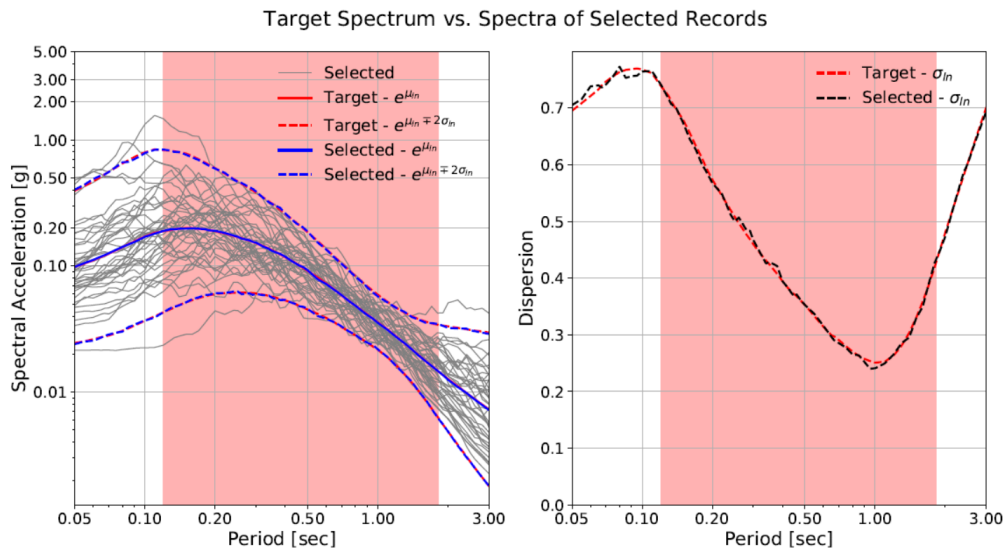


The selected records are:

Record Direction 1	Record Direction 2	Scale Factor
RSN2880_CHICHI.04_TCU105N	RSN2880_CHICHI.04_TCU105E	1.0038
RSN4253_ANCONA.P_E-GEN000	RSN4253_ANCONA.P_E-GEN090	1.58298
RSN5114_CHUETSU_IBRH18NS	RSN5114_CHUETSU_IBRH18EW	3.08575
RSN1890_BEARAFT_RI3090	RSN1890_BEARAFT_RI3360	2.86676
RSN6732_NIIGATA_SIT004NS	RSN6732_NIIGATA_SIT004EW	1.53316
RSN1990_GULFCA_BCR090	RSN1990_GULFCA_BCR360	0.72096
RSN3073_CHICHI.05_ILA064N	RSN3073_CHICHI.05_ILA064W	1.25565
RSN190_IMPVALL.H_H-SUP045	RSN190_IMPVALL.H_H-SUP135	0.33993

RSN10584_10370141_13915360	RSN10584_10370141_13915090	1.73524
RSN6256_TOTTORI.1_KOC009NS	RSN6256_TOTTORI.1_KOC009EW	1.82752
RSN5647_IWATE_IWTH15NS	RSN5647_IWATE_IWTH15EW	0.41493
RSN2677_CHICHI.03_TTN025N	RSN2677_CHICHI.03_TTN025E	3.46187
RSN704_WHITTINGER.A_A-SER000	RSN704_WHITTINGER.A_A-SER270	0.9015
RSN2109_DENALI_FAIFS-90	RSN2109_DENALI_FAIFS360	0.51332
RSN4230_NIIGATA_NIGH13NS	RSN4230_NIIGATA_NIGH13EW	0.32839
RSN4080_PARK2004_36153-90	RSN4080_PARK2004_36153360	1.9475
RSN5281_CHUETSU_NIGH07NS	RSN5281_CHUETSU_NIGH07EW	1.24766
RSN5543_IWATE_FKS002NS	RSN5543_IWATE_FKS002EW	0.5795
RSN2801_CHICHI.04_HWA059N	RSN2801_CHICHI.04_HWA059E	1.61622
RSN5639_IWATE_IWTH07NS	RSN5639_IWATE_IWTH07EW	1.88985
RSN9528_10410337_13881360	RSN9528_10410337_13881090	3.14153
RSN8842_14383980_CIRVRHNN	RSN8842_14383980_CIRVRHNE	2.86221
RSN487_SMART1.33_33I01EW	RSN487_SMART1.33_33I01NS	0.49437
RSN5632_IWATE_IWT025NS	RSN5632_IWATE_IWT025EW	0.85603
RSN2115_DENALI_PS11-66	RSN2115_DENALI_PS11336	0.2562
RSN6711_NIIGATA_NGNH18NS	RSN6711_NIIGATA_NGNH18EW	2.00967
RSN6065_MOHAWK_RF11000	RSN6065_MOHAWK_RF11090	2.47396
RSN6029_SIERRA.MEX_OLP360	RSN6029_SIERRA.MEX_OLP-90	0.83169
RSN403_COALINGA_C-CSU000	RSN403_COALINGA_C-CSU090	1.12736
RSN9619_10410337_24818360	RSN9619_10410337_24818090	2.21479
RSN6470_NIIGATA_CHB003NS	RSN6470_NIIGATA_CHB003EW	0.81744
RSN5893_SIERRA.MEX_13081360	RSN5893_SIERRA.MEX_13081-90	1.68996
RSN3209_CHICHI.05_TCU112N	RSN3209_CHICHI.05_TCU112E	0.31692
RSN6815_NIIGATA_TYM004NS	RSN6815_NIIGATA_TYM004EW	1.65531
RSN4379_UBMARCH.P_I-FSM000	RSN4379_UBMARCH.P_I-FSM090	2.23303
RSN3921_TOTTORI_OKYH03NS	RSN3921_TOTTORI_OKYH03EW	0.33023
RSN9428_14155260_CIWTTHHN	RSN9428_14155260_CIWTTHHE	2.27639
RSN3952_TOTTORI_SMNH06NS	RSN3952_TOTTORI_SMNH06EW	0.48508
RSN670_WHITTINGER.A_A-SUN190	RSN670_WHITTINGER.A_A-SUN280	0.92966
RSN1622_STONECYN_BVF009	RSN1622_STONECYN_BVF099	0.59292

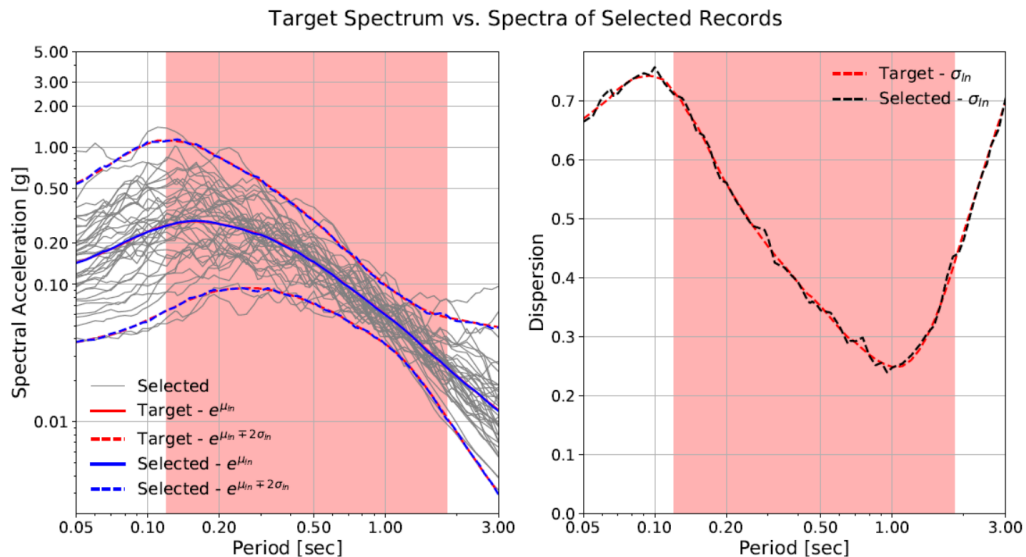
Return period of 42 years



Record Direction 1	Record Direction 2	Scale Factor
RSN2080_NENANA_K220090	RSN2080_NENANA_K220360	2.24063
RSN9594_10410337_14871360	RSN9594_10410337_14871090	3.0044
RSN3941_TOTTORI_SMN009NS	RSN3941_TOTTORI_SMN009EW	1.51178
RSN5480_IWATE_AKTH02NS	RSN5480_IWATE_AKTH02EW	1.46074
RSN3770_NORTH392_3914C145	RSN3770_NORTH392_3914A235	0.88313
RSN4174_NIIGATA_GNM006NS	RSN4174_NIIGATA_GNM006EW	3.51654
RSN542_PALMSPR_H04000	RSN542_PALMSPR_H04090	0.81384
RSN4206_NIIGATA_NIG016NS	RSN4206_NIIGATA_NIG016EW	0.62525
RSN3103_CHICHI.05_KAU069N	RSN3103_CHICHI.05_KAU069E	1.53226
RSN1706_NORTH392_BLD090	RSN1706_NORTH392_BLD360	1.29557
RSN544_CHALFANT.B_B-LAD180	RSN544_CHALFANT.B_B-LAD270	0.3579
RSN4178_NIIGATA_GNM013NS	RSN4178_NIIGATA_GNM013EW	1.02117
RSN534_PALMSPR_H08000	RSN534_PALMSPR_H08090	0.36861
RSN2299_CHICHI.02ILLA067N	RSN2299_CHICHI.02ILLA067E	1.55557
RSN622_WHITTIER.A_A-COM140	RSN622_WHITTIER.A_A-COM230	0.60614
RSN950_NORTHR_NHO180	RSN950_NORTHR_NHO270	0.55065
RSN4123_PARK2004_PG4090	RSN4123_PARK2004_PG4360	0.57551

RSN9838_51182810_54099005	RSN9838_51182810_54099095	0.87737
RSN855_LANDERS_FTI000	RSN855_LANDERS_FTI090	0.38135
RSN5936_SIERRA.MEX_MVI360	RSN5936_SIERRA.MEX_MVI090	2.97752
RSN6513_NIIGATA_FKS014NS	RSN6513_NIIGATA_FKS014EW	2.26833
RSN2123_BEARCTY_FFP180	RSN2123_BEARCTY_FFP270	3.6641
RSN8951_14383980_N5421360	RSN8951_14383980_N5421090	3.94159
RSN385_COALINGA_A-SUB000	RSN385_COALINGA_A-SUB090	0.60692
RSN572_SMART1.45_45EO2EW	RSN572_SMART1.45_45EO2NS	0.28382
RSN6682_NIIGATA_NGN006NS	RSN6682_NIIGATA_NGN006EW	3.15713
RSN1011_NORTHR_WON095	RSN1011_NORTHR_WON185	0.34484
RSN8867_14383980_CITA2HNN	RSN8867_14383980_CITA2HNE	1.94487
RSN633_WHITTINGER.A_A-VER083	RSN633_WHITTINGER.A_A-VER173	0.3568
RSN2004_CABAJA_CAL090	RSN2004_CABAJA_CAL360	2.84116
RSN4114_PARK2004_Z11090	RSN4114_PARK2004_Z11360	0.26245
RSN4075_PARK2004_WORK-90	RSN4075_PARK2004_WORK360	0.70112
RSN3198_CHICHI.05_TCU095N	RSN3198_CHICHI.05_TCU095E	1.22084
RSN4112_PARK2004_Z08090	RSN4112_PARK2004_Z08360	0.28345
RSN3916_TOTTORI_OKY013NS	RSN3916_TOTTORI_OKY013EW	0.66755
RSN6154_TOTTORI.1_EHMH03NS	RSN6154_TOTTORI.1_EHMH03EW	2.30993
RSN3200_CHICHI.05_TCU098N	RSN3200_CHICHI.05_TCU098E	1.28134
RSN6490_NIIGATA_CHBH10NS	RSN6490_NIIGATA_CHBH10EW	3.75651
RSN5253_CHUETSU_NIG007NS	RSN5253_CHUETSU_NIG007EW	1.54105
RSN3036_CHICHI.05_HWA056N	RSN3036_CHICHI.05_HWA056E	2.03684

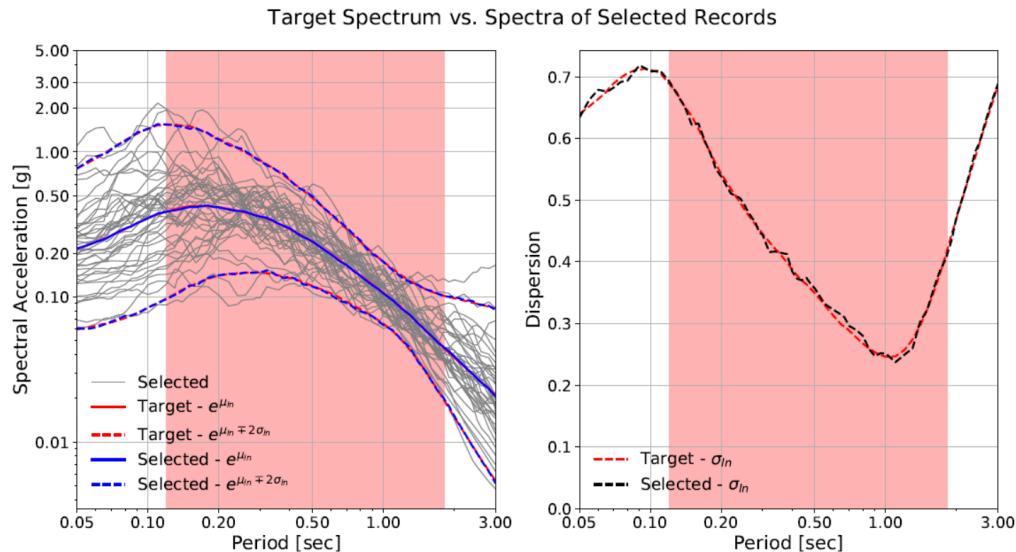
Return period of 72 years



Record Direction 1	Record Direction 2	Scale Factor
RSN2503_CHICHI.03_CHY094N	RSN2503_CHICHI.03_CHY094W	1.49581
RSN18443_21423530_36456360	RSN18443_21423530_36456090	2.54178
RSN3777_NORTH392_CWC180	RSN3777_NORTH392_CWC270	2.37449
RSN3817_HECTOR_RVB090	RSN3817_HECTOR_RVB360	3.19012
RSN3719_WHITTIER.B_B-NYA090	RSN3719_WHITTIER.B_B-NYA180	1.60642
RSN6241_TOTTORI.1_KGW003NS	RSN6241_TOTTORI.1_KGW003EW	0.95362
RSN5124_CHUETSU_ISK009NS	RSN5124_CHUETSU_ISK009EW	3.19191
RSN3018_CHICHI.05_HWA031N	RSN3018_CHICHI.05_HWA031E	1.03548
RSN2782_CHICHI.04_HWA034N	RSN2782_CHICHI.04_HWA034E	2.78257
RSN4112_PARK2004_Z08090	RSN4112_PARK2004_Z08360	0.46383
RSN439_BORAH.MS_TAN260	RSN439_BORAH.MS_TAN350	2.24163
RSN454_MORGAN_GIL067	RSN454_MORGAN_GIL337	2.14558
RSN6375_TOTTORI.1_SMNH07NS	RSN6375_TOTTORI.1_SMNH07EW	2.88101
RSN619_WHITTIER.A_A-GRV060	RSN619_WHITTIER.A_A-GRV330	0.31361

RSN6024_SIERRA.MEX_NPS180	RSN6024_SIERRA.MEX_NPS270	2.14458
RSN8880_14383980_12102360	RSN8880_14383980_12102090	3.08905
RSN622_WHITTINGER.A_A-COM140	RSN622_WHITTINGER.A_A-COM230	0.99186
RSN3631_SMART1.33_33O10EW	RSN3631_SMART1.33_33O10NS	2.49939
RSN3002_CHICHI.05_HWA013N	RSN3002_CHICHI.05_HWA013E	0.8095
RSN9552_10410337_14017360	RSN9552_10410337_14017090	3.14236
RSN4072_PARK2004_REDH-90	RSN4072_PARK2004_REDH360	2.69941
RSN5756_IWATE_YMT013NS	RSN5756_IWATE_YMT013EW	3.92848
RSN5804_IWATE_55446NS	RSN5804_IWATE_55446EW	0.46808
RSN3214_CHICHI.05_TCU119N	RSN3214_CHICHI.05_TCU119E	1.058
RSN5468_IWATE_AKT013NS	RSN5468_IWATE_AKT013EW	2.31428
RSN3093_CHICHI.05_KAU050N	RSN3093_CHICHI.05_KAU050E	1.18184
RSN8919_14383980_U5031360	RSN8919_14383980_U5031090	3.45389
RSN140_TABAS_FER-L1	RSN140_TABAS_FER-T1	1.17057
RSN4386_UBMARCH.P_J-CLC180	RSN4386_UBMARCH.P_J-CLC270	3.3496
RSN8648_40204628_N1825HNN	RSN8648_40204628_N1825HNE	1.17889
RSN1810_HECTOR_MCY090	RSN1810_HECTOR_MCY180	0.39979
RSN3940_TOTTORI_SMN008NS	RSN3940_TOTTORI_SMN008EW	2.04962
RSN412_COALINGA_D-PVY045	RSN412_COALINGA_D-PVY135	0.32647
RSN3175_CHICHI.05_TCU049N	RSN3175_CHICHI.05_TCU049E	2.11401
RSN649_WHITTINGER.A_A-BRC000	RSN649_WHITTINGER.A_A-BRC090	0.68141
RSN2594_CHICHI.03_TCU034N	RSN2594_CHICHI.03_TCU034E	3.47281
RSN3572_SMART1.05_05O03EW	RSN3572_SMART1.05_05O03NS	0.76063
RSN2785_CHICHI.04_HWA037N	RSN2785_CHICHI.04_HWA037E	1.71946
RSN3019_CHICHI.05_HWA032N	RSN3019_CHICHI.05_HWA032E	1.39593
RSN8126_CCHURCH_ROLCS29E	RSN8126_CCHURCH_ROLCS61W	0.81434

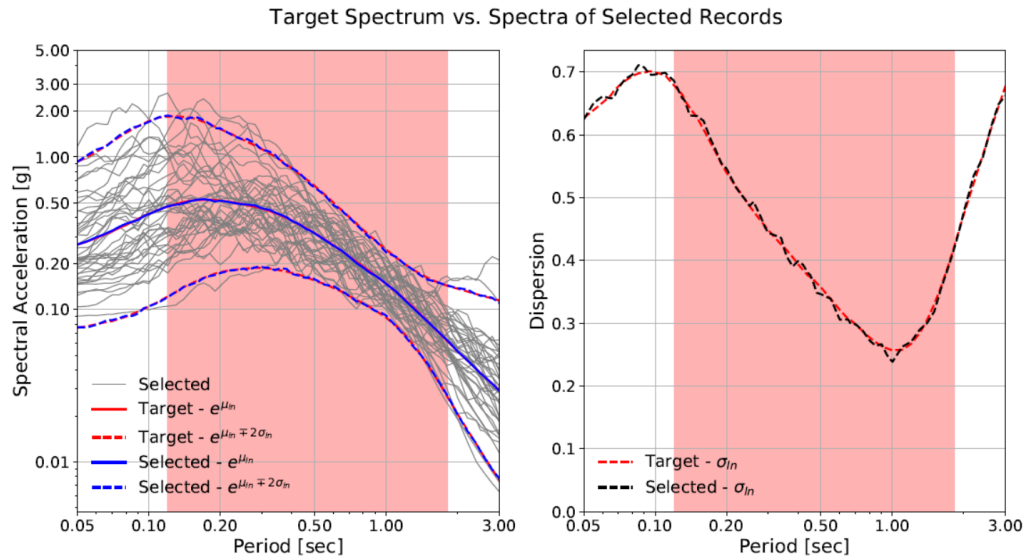
Return period of 140 years



Record Direction 1	Record Direction 2	Scale Factor
RSN2503_CHICHI.03_CHY094N	RSN2503_CHICHI.03_CHY094W	2.55534
RSN1948_ANZA1_LQB360	RSN1948_ANZA1_LQB090	1.71175
RSN213_LIVERMOR_A-FRE075	RSN213_LIVERMOR_A-FRE345	1.95295
RSN9485_10410337_CIDLAHNN	RSN9485_10410337_CIDLAHNE	3.74325
RSN3954_TOTTORI_SMNH10NS	RSN3954_TOTTORI_SMNH10EW	0.73146
RSN5273_CHUETSU_NIG027NS	RSN5273_CHUETSU_NIG027EW	2.11864
RSN3346_CHICHI.06_HWA034N	RSN3346_CHICHI.06_HWA034E	2.30837
RSN5815_IWATE_44BC1NS	RSN5815_IWATE_44BC1EW	0.62519
RSN1627_CALDIRAN_153041	RSN1627_CALDIRAN_153131	2.6997
RSN3926_TOTTORI_OKYH08NS	RSN3926_TOTTORI_OKYH08EW	1.70356
RSN2943_CHICHI.05_CHY025N	RSN2943_CHICHI.05_CHY025E	1.32307
RSN1671_NORTH009_PKC090	RSN1671_NORTH009_PKC360	2.70819
RSN2408_CHICHI.02_TCU107N	RSN2408_CHICHI.02_TCU107E	2.42004
RSN9009_14151344_CIDNRHLN	RSN9009_14151344_CIDNRHLE	1.48587
RSN1836_HECTOR_29P090	RSN1836_HECTOR_29P360	2.43018
RSN4120_PARK2004_PG2090	RSN4120_PARK2004_PG2360	1.12914
RSN288_ITALY_A-BRZ000	RSN288_ITALY_A-BRZ270	0.85753

RSN4480_L-AQUILA_GX066XTE	RSN4480_L-AQUILA_GX066YLN	0.29684
RSN246_MAMMOTH.L_L-BEN270	RSN246_MAMMOTH.L_L-BEN360	1.17215
RSN3289_CHICHI.06_CHY059N	RSN3289_CHICHI.06_CHY059E	1.87265
RSN8158_CCHURCH_LPCCN10W	RSN8158_CCHURCH_LPCCS80W	0.29786
RSN8871_14383980_CIUSCHNN	RSN8871_14383980_CIUSCHNE	3.98589
RSN933_BIGBEAR_SEA000	RSN933_BIGBEAR_SEA090	2.20449
RSN1076_NORTHR_EJS030	RSN1076_NORTHR_EJS120	1.17911
RSN16_NCALIF.AG_A-FRN044	RSN16_NCALIF.AG_A-FRN134	1.66273
RSN1169_KOCAELI_MSK000	RSN1169_KOCAELI_MSK090	3.01971
RSN1377_CHICHI_KAU050-E	RSN1377_CHICHI_KAU050-N	1.95494
RSN4240_NIIGATA_TCG009NS	RSN4240_NIIGATA_TCG009EW	3.33287
RSN3206_CHICHI.05_TCU106N	RSN3206_CHICHI.05_TCU106E	1.77798
RSN5239_CHUETSU_NGNH29NS	RSN5239_CHUETSU_NGNH29EW	1.76756
RSN3830_YOUNTVL_NAP090	RSN3830_YOUNTVL_NAP360	0.7046
RSN4377_UBMARCH.P_I-BCT000	RSN4377_UBMARCH.P_I-BCT090	3.08076
RSN1047_NORTHR_NEW090	RSN1047_NORTHR_NEW180	1.4857
RSN5195_CHUETSU_NGN003NS	RSN5195_CHUETSU_NGN003EW	3.92117
RSN5666_IWATE_MYG007NS	RSN5666_IWATE_MYG007EW	1.35537
RSN1689_NORTH151_PKC090	RSN1689_NORTH151_PKC360	3.7412
RSN1402_CHICHI_NST-E	RSN1402_CHICHI_NST-N	0.51673
RSN4202_NIIGATA_NIG012NS	RSN4202_NIIGATA_NIG012EW	0.72584
RSN8_NCALIF.FH_F-FRN225	RSN8_NCALIF.FH_F-FRN315	1.68757
RSN4218_NIIGATA_NIG028NS	RSN4218_NIIGATA_NIG028EW	0.30169

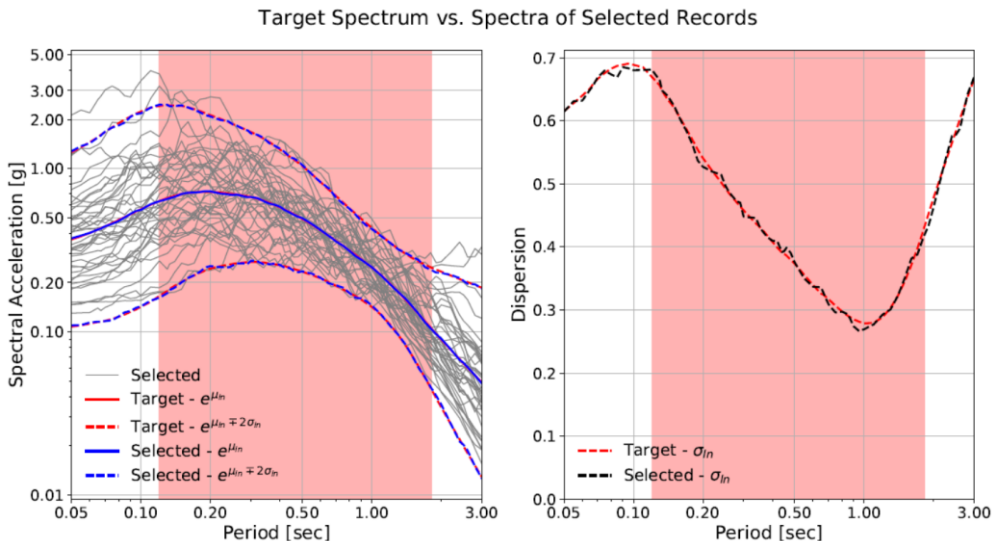
Return period of 224 years



Record Direction 1	Record Direction 2	Scale Factor
RSN258_MAMMOTH.AH_D-CON180	RSN258_MAMMOTH.AH_D-CON270	3.66203
RSN1948_ANZA1_LQB360	RSN1948_ANZA1_LQB090	2.31017
RSN3844_CHICHI.03_CHY004N	RSN3844_CHICHI.03_CHY004W	2.39892
RSN3926_TOTTORI_OKYH08NS	RSN3926_TOTTORI_OKYH08EW	2.29911
RSN4157_NIIGATA_FKS026NS	RSN4157_NIIGATA_FKS026EW	3.29331
RSN625_WHITTINGER.A_A-ING000	RSN625_WHITTINGER.A_A-ING090	1.12034
RSN393_COALINGA_B-CSU000	RSN393_COALINGA_B-CSU090	3.67062
RSN553_CHALFANT.A_A-LVD000	RSN553_CHALFANT.A_A-LVD090	2.15251
RSN448_MORGAN_AND250	RSN448_MORGAN_AND340	0.57182
RSN3959_TOTTORI_TTR002NS	RSN3959_TOTTORI_TTR002EW	2.42488
RSN650_WHITTINGER.A_A-RIM015	RSN650_WHITTINGER.A_A-RIM105	2.85133
RSN3170_CHICHI.05_TCU042N	RSN3170_CHICHI.05_TCU042E	3.12588
RSN3093_CHICHI.05_KAU050N	RSN3093_CHICHI.05_KAU050E	2.7248
RSN6611_NIIGATA_ISK002NS	RSN6611_NIIGATA_ISK002EW	1.67616
RSN4083_PARK2004_36529270	RSN4083_PARK2004_36529360	1.56812

RSN3168_CHICHI.05_TCU039N	RSN3168_CHICHI.05_TCU039E	3.16344
RSN8060_CCHURCH_ASHSN85W	RSN8060_CCHURCH_ASHSS05W	2.2396
RSN1028_NORTHR_LV2000	RSN1028_NORTHR_LV2090	1.90006
RSN493_GREECE_F-DRA-NS	RSN493_GREECE_F-DRA-WE	2.31567
RSN2115_DENALI_PS11-66	RSN2115_DENALI_PS11336	2.0252
RSN1184_CHICHI_CHY010-N	RSN1184_CHICHI_CHY010-W	0.69185
RSN802_LOMAP_STG000	RSN802_LOMAP_STG090	0.36513
RSN367_COALINGA.H_H-PVB045	RSN367_COALINGA.H_H-PVB135	0.42733
RSN2942_CHICHI.05_CHY024N	RSN2942_CHICHI.05_CHY024E	1.97737
RSN2975_CHICHI.05_CHY076N	RSN2975_CHICHI.05_CHY076E	2.97894
RSN4120_PARK2004_PG2090	RSN4120_PARK2004_PG2360	1.52388
RSN972_NORTHR_FEA000	RSN972_NORTHR_FEA090	2.1544
RSN3278_CHICHI.06_CHY041N	RSN3278_CHICHI.06_CHY041E	0.86627
RSN4337_UBMARCHEP_B-CLF000	RSN4337_UBMARCHEP_B-CLF270	0.54385
RSN395_COALINGA_C-ATP270	RSN395_COALINGA_C-ATP360	1.88226
RSN530_PALMSPR_PSA000	RSN530_PALMSPR_PSA090	1.01641
RSN3760_LANDERS_BLC360	RSN3760_LANDERS_BLC270	1.64164
RSN3949_TOTTORI_SMNH03NS	RSN3949_TOTTORI_SMNH03EW	2.48057
RSN3213_CHICHI.05_TCU118N	RSN3213_CHICHI.05_TCU118E	2.11461
RSN188_IMPVAL.H_H-PLS045	RSN188_IMPVAL.H_H-PLS135	3.14368
RSN3568_SMART1.05_05M10EW	RSN3568_SMART1.05_05M10NS	1.67441
RSN1474_CHICHI_TCU025-E	RSN1474_CHICHI_TCU025-N	1.76088
RSN3585_SMART1.25_25I11EW	RSN3585_SMART1.25_25I11NS	3.34096
RSN572_SMART1.45_45EO2EW	RSN572_SMART1.45_45EO2NS	1.07077
RSN4553_L-AQUILA.B_CW119XTE	RSN4553_L-AQUILA.B_CW119YLN	3.83022

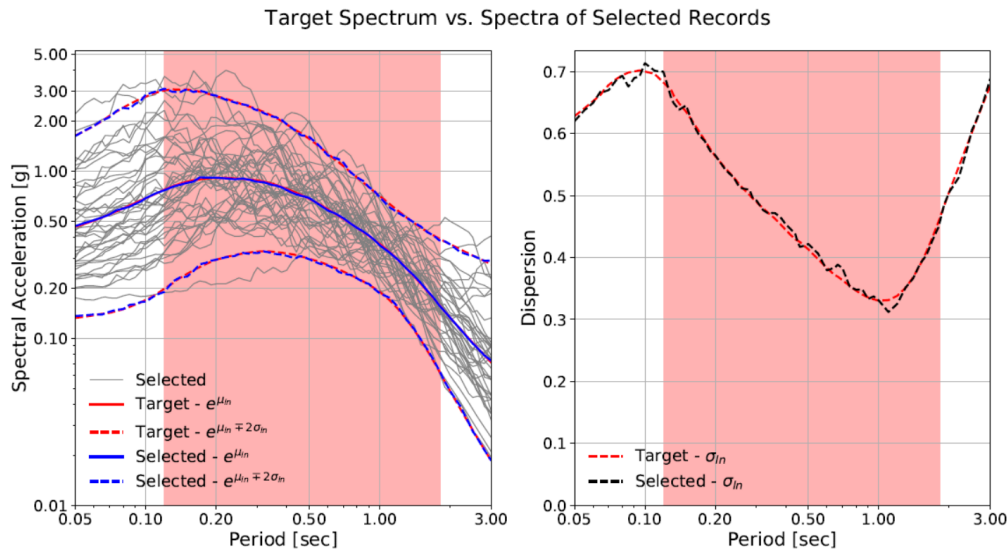
Return period of 475 years



Record Direction 1	Record Direction 2	Scale Factor
RSN1195_CHICHI_CHY026-E	RSN1195_CHICHI_CHY026-N	1.81187
RSN4395_UBMARCHE.P_L-CLC180	RSN4395_UBMARCHE.P_L-CLC270	3.0425
RSN1538_CHICHI_TCU112-E	RSN1538_CHICHI_TCU112-N	1.73397
RSN6960_DARFIELD_RHSCN86W	RSN6960_DARFIELD_RHSCS04W	0.93117
RSN550_CHALFANT.A_A-BPL070	RSN550_CHALFANT.A_A-BPL160	3.20805
RSN1205_CHICHI_CHY041-E	RSN1205_CHICHI_CHY041-N	0.84956
RSN4054_BAM_MOH-L	RSN4054_BAM_MOH-T	2.60441
RSN3215_CHICHI.05_TCU123N	RSN3215_CHICHI.05_TCU123E	2.46185
RSN1007_NORTHR_UNI005	RSN1007_NORTHR_UNI095	1.26371
RSN5495_IWATE_AKTH19NS	RSN5495_IWATE_AKTH19EW	1.36679
RSN1441_CHICHI_TAP066-E	RSN1441_CHICHI_TAP066-N	2.80197
RSN5262_CHUETSU_NIG016NS	RSN5262_CHUETSU_NIG016EW	3.2714
RSN5972_SIERRA.MEX_BRA360	RSN5972_SIERRA.MEX_BRA090	1.78563
RSN1149_KOCAELI_ATK000	RSN1149_KOCAELI_ATK090	1.5011
RSN3190_CHICHI.05_TCU070N	RSN3190_CHICHI.05_TCU070E	3.21264

RSN724_SUPER.B_B-PLS045	RSN724_SUPER.B_B-PLS135	1.25164
RSN5991_SIERRA.MEX_E10320	RSN5991_SIERRA.MEX_E10230	0.50933
RSN464_MORGAN_HD3255	RSN464_MORGAN_HD3345	2.16475
RSN4193_NIIGATA_NGNH29NS	RSN4193_NIIGATA_NGNH29EW	3.41134
RSN1303_CHICHI_HWA058-E	RSN1303_CHICHI_HWA058-N	2.61536
RSN8060_CCHURCH_ASHSN85W	RSN8060_CCHURCH_ASHSS05W	3.61575
RSN4159_NIIGATA_FKS028NS	RSN4159_NIIGATA_FKS028EW	1.76195
RSN671_WHITTIER.A_A-PKC000	RSN671_WHITTIER.A_A-PKC090	2.9615
RSN5268_CHUETSU_NIG022NS	RSN5268_CHUETSU_NIG022EW	1.98703
RSN97_PT MUGU_PHN180	RSN97_PT MUGU_PHN270	2.20842
RSN3757_LANDERS_NPF090	RSN3757_LANDERS_NPF180	1.39558
RSN80_SFERN_PSL180	RSN80_SFERN_PSL270	2.59551
RSN1748_NWCHINA1_JIA000	RSN1748_NWCHINA1_JIA270	2.11255
RSN1157_KOCAELI_CNA000	RSN1157_KOCAELI_CNA090	2.36613
RSN203_IMP VALL.A_A-E05140	RSN203_IMP VALL.A_A-E05230	2.9255
RSN763_LOMAP_GIL067	RSN763_LOMAP_GIL337	0.98063
RSN538_PALMSPR_SN Y225	RSN538_PALMSPR_SN Y315	3.86154
RSN451_MORGAN_CYC195	RSN451_MORGAN_CYC285	0.37214
RSN3857_CHICHI.05_CHY002N	RSN3857_CHICHI.05_CHY002W	3.25228
RSN4390_UBMARCH.E.P_J-NRC000	RSN4390_UBMARCH.E.P_J-NRC270	2.34626
RSN1035_NORTHR_MAN000	RSN1035_NORTHR_MAN090	1.812
RSN5796_IWATE_55203NS	RSN5796_IWATE_55203EW	1.7916
RSN313_CORINTH_COR--L	RSN313_CORINTH_COR--T	0.89484
RSN4134_PARK2004_VYC090	RSN4134_PARK2004_VYC360	1.06351
RSN2622_CHICHI.03_TCU071N	RSN2622_CHICHI.03_TCU071E	2.09631

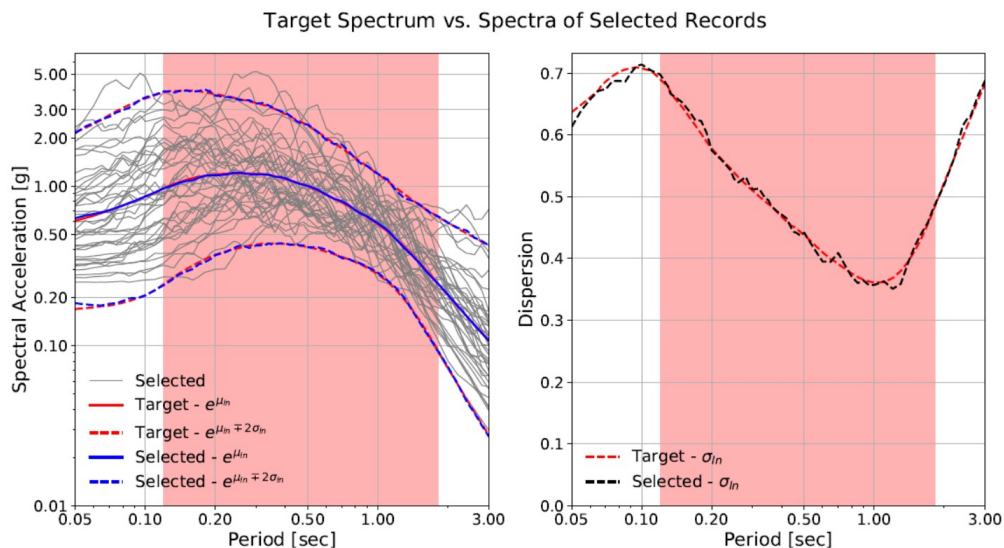
Return period of 975 years



Record Direction 1	Record Direction 2	Scale Factor
RSN4261_ANCONA.P_P-GEN000	RSN4261_ANCONA.P_P-GEN090	3.66109
RSN1536_CHICHI_TCU110-E	RSN1536_CHICHI_TCU110-N	0.9256
RSN974_NORTHR_GLP177	RSN974_NORTHR_GLP267	3.94921
RSN5803_IWATE_55445NS	RSN5803_IWATE_55445EW	2.04135
RSN411_COALINGA_D-PVP270	RSN411_COALINGA_D-PVP360	2.89403
RSN1117_KOBE_TOT000	RSN1117_KOBE_TOT090	3.71819
RSN3512_CHICHI.06_TCU141N	RSN3512_CHICHI.06_TCU141W	2.63453
RSN4226_NIIGATA_NIGH09NS	RSN4226_NIIGATA_NIGH09EW	2.37926
RSN773_LOMAP_HWB220	RSN773_LOMAP_HWB310	2.34379
RSN173_IMPVAL.H_H-E10050	RSN173_IMPVAL.H_H-E10320	1.16032
RSN290_ITALY_A-MER000	RSN290_ITALY_A-MER270	3.07591
RSN4040_BAM_BAM-L	RSN4040_BAM_BAM-T	0.42027
RSN565_GREECE_J-KAL-NS	RSN565_GREECE_J-KAL-WE	2.74125
RSN5787_IWATE_54042NS	RSN5787_IWATE_54042EW	2.3638
RSN4128_PARK2004_SC3090	RSN4128_PARK2004_SC3360	3.28314
RSN5808_IWATE_55463NS	RSN5808_IWATE_55463EW	3.19894

RSN3966_TOTTORI_TTR009NS	RSN3966_TOTTORI_TTR009EW	1.35608
RSN1235_CHICHI_CHY087-E	RSN1235_CHICHI_CHY087-N	2.40878
RSN3286_CHICHI.06_CHY055N	RSN3286_CHICHI.06_CHY055W	3.26787
RSN462_MORGAN_HCH001	RSN462_MORGAN_HCH271	2.76058
RSN3968_TOTTORI_TTRH02NS	RSN3968_TOTTORI_TTRH02EW	0.3653
RSN3267_CHICHI.06_CHY027N	RSN3267_CHICHI.06_CHY027E	3.6254
RSN3954_TOTTORI_SMNH10NS	RSN3954_TOTTORI_SMNH10EW	2.27764
RSN955_NORTHR_FLO020	RSN955_NORTHR_FLO290	3.93229
RSN5836_SIERRA.MEX_EMO360	RSN5836_SIERRA.MEX_EMO270	1.26192
RSN1512_CHICHI_TCU078-E	RSN1512_CHICHI_TCU078-N	0.77573
RSN5478_IWATE_AKT023NS	RSN5478_IWATE_AKT023EW	1.21014
RSN3674_SMART1.45_45M04EW	RSN3674_SMART1.45_45M04NS	1.38564
RSN354_COALINGA.H_H- PG5000	RSN354_COALINGA.H_H- PG5090	3.52866
RSN1703_NORTH392_JEN022	RSN1703_NORTH392_JEN292	2.40159
RSN5829_SIERRA.MEX_RII000	RSN5829_SIERRA.MEX_RII090	0.80756
RSN1012_NORTHR_LA0180	RSN1012_NORTHR_LA0270	1.31708
RSN1120_KOBE_TAK000	RSN1120_KOBE_TAK090	0.27874
RSN585_BAJA_CPE161	RSN585_BAJA_CPE251	0.56525
RSN2734_CHICHI.04_CHY074N	RSN2734_CHICHI.04_CHY074E	0.76241
RSN5657_IWATE_IWTH25NS	RSN5657_IWATE_IWTH25EW	0.39545
RSN162_IMPVAL.H_H-CXO225	RSN162_IMPVAL.H_H-CXO315	1.7003
RSN1499_CHICHI_TCU060-E	RSN1499_CHICHI_TCU060-N	1.76185
RSN1524_CHICHI_TCU095-E	RSN1524_CHICHI_TCU095-N	0.97975
RSN1794_HECTOR_JOS090	RSN1794_HECTOR_JOS360	1.57128

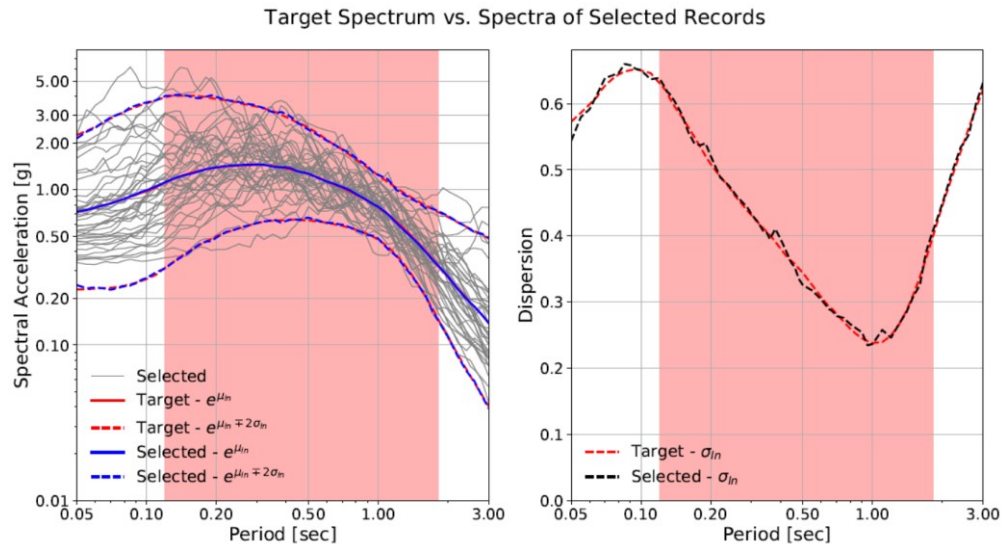
Return period of 2475 years



Record Direction 1	Record Direction 2	Scale Factor
RSN4101_PARK2004_TM3090	RSN4101_PARK2004_TM3360	2.78994
RSN1410_CHICHI_TAP003-N	RSN1410_CHICHI_TAP003-E	2.18378
RSN1728_NORTH392_RRS228	RSN1728_NORTH392_RRS318	2.58438
RSN2509_CHICHI.03_CHY104N	RSN2509_CHICHI.03_CHY104W	3.22099
RSN4133_PARK2004_VC2090	RSN4133_PARK2004_VC2360	3.55422
RSN3505_CHICHI.06_TCU125N	RSN3505_CHICHI.06_TCU125E	3.22706
RSN3311_CHICHI.06_CHY092N	RSN3311_CHICHI.06_CHY092W	3.80772
RSN4891_CHUETSU_70026NS	RSN4891_CHUETSU_70026EW	0.87856
RSN3964_TOTTORI_TTR007NS	RSN3964_TOTTORI_TTR007EW	1.9103
RSN5652_IWATE_IWTH20NS	RSN5652_IWATE_IWTH20EW	3.10163
RSN1186_CHICHI_CHY014-N	RSN1186_CHICHI_CHY014-W	2.63063
RSN2739_CHICHI.04_CHY080N	RSN2739_CHICHI.04_CHY080E	3.73988
RSN1538_CHICHI_TCU112-E	RSN1538_CHICHI_TCU112-N	3.73321
RSN611_WHITTIER.A_A-CAS000	RSN611_WHITTIER.A_A-CAS270	2.36798
RSN3954_TOTTORI_SMNH10NS	RSN3954_TOTTORI_SMNH10E	3.43132
RSN744_LOMAP_BVW220	RSN744_LOMAP_BVW310	2.2802

RSN4145_PARK2004_UP09090	RSN4145_PARK2004_UP09360	2.58589
RSN3512_CHICHI.06_TCU141N	RSN3512_CHICHI.06_TCU141W	3.96898
RSN346_COALINGA.H_H-Z08000	RSN346_COALINGA.H_H-Z08090	2.76836
RSN4210_NIIGATA_NIG020NS	RSN4210_NIIGATA_NIG020EW	1.29742
RSN585_BAJA_CPE161	RSN585_BAJA_CPE251	0.85156
RSN1149_KOCAELI_ATK000	RSN1149_KOCAELI_ATK090	3.23185
RSN5275_CHUETSU_NIGH01NS	RSN5275_CHUETSU_NIGH01EW	3.95871
RSN341_COALINGA.H_H-Z02000	RSN341_COALINGA.H_H-Z02090	2.30287
RSN338_COALINGA.H_H-Z14000	RSN338_COALINGA.H_H-Z14090	1.22684
RSN4878_CHUETSU_65083NS	RSN4878_CHUETSU_65083EW	3.19025
RSN1147_KOCAELI_ATS000	RSN1147_KOCAELI_ATS090	1.4446
RSN415_COALINGA_D-TSM270	RSN415_COALINGA_D-TSM360	1.29511
RSN360_COALINGA.H_H-VC1000	RSN360_COALINGA.H_H-VC1090	3.70117
RSN8099_CCHURCH_KPOCN15E	RSN8099_CCHURCH_KPOCS75E	2.60812
RSN1051_NORTHR_PUL104	RSN1051_NORTHR_PUL194	0.6413
RSN754_LOMAP_CLD195	RSN754_LOMAP_CLD285	2.71702
RSN175_IMPVAL.H_H-E12140	RSN175_IMPVAL.H_H-E12230	3.19538
RSN369_COALINGA.H_H-SCN045	RSN369_COALINGA.H_H-SCN315	2.58839
RSN1044_NORTHR_NWH090	RSN1044_NORTHR_NWH360	0.59663
RSN8119_CCHURCH_PRPCS	RSN8119_CCHURCH_PRPCW	0.74576
RSN8674_40204628_NCCHRHN	RSN8674_40204628_NCCHRHN	3.96725
RSN1087_NORTHR_TAR090	RSN1087_NORTHR_TAR360	0.58937
RSN6893_DARFIELD_DFHSS17E	RSN6893_DARFIELD_DFHSS73W	1.50719
RSN988_NORTHR_CCN090	RSN988_NORTHR_CCN360	1.81989

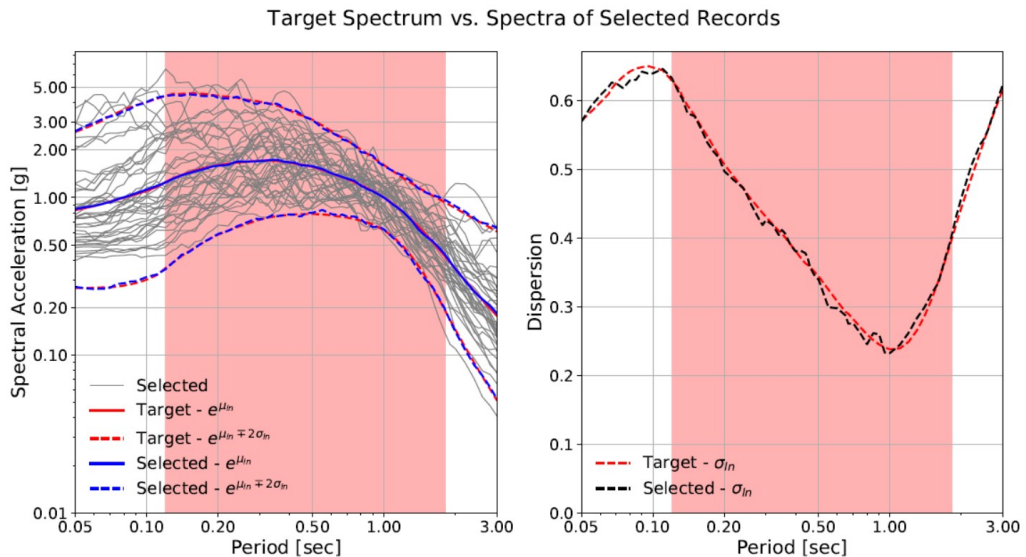
Return period of 4975 years



Record Direction 1	Record Direction 2	Scale Factor
RSN1536_CHICHI_TCU110-E	RSN1536_CHICHI_TCU110-N	1.80287
RSN4143_PARK2004_UP07090	RSN4143_PARK2004_UP07360	3.49598
RSN1238_CHICHI_CHY092-N	RSN1238_CHICHI_CHY092-W	3.5646
RSN341_COALINGA.H_H-Z02000	RSN341_COALINGA.H_H-Z02090	2.97737
RSN4456_MONTENE.GRO_PHO000	RSN4456_MONTENE.GRO_PHO090	1.85342
RSN765_LOMAP_G01000	RSN765_LOMAP_G01090	2.34893
RSN3682_SMART1.45_45O09EW	RSN3682_SMART1.45_45O09NS	3.734
RSN5817_IWATE_48A51NS	RSN5817_IWATE_48A51EW	3.47817
RSN3753_LANDERS_FVR045	RSN3753_LANDERS_FVR135	3.26339
RSN1141_DINAR_DIN090	RSN1141_DINAR_DIN180	1.50227
RSN368_COALINGA.H_H-PVY045	RSN368_COALINGA.H_H-PVY135	1.2143
RSN6960_DARFIELD_RHSCN86W	RSN6960_DARFIELD_RHSCS04W	2.59197
RSN5678_IWATE_MYGH02NS	RSN5678_IWATE_MYGH02EW	3.79096
RSN585_BAJA_CPE161	RSN585_BAJA_CPE251	1.10098
RSN8158_CCHURCH_LPCCN10W	RSN8158_CCHURCH_LPCCS80W	1.80651
RSN367_COALINGA.H_H-PVB045	RSN367_COALINGA.H_H-PVB135	1.9204
RSN619_WHITTIER.A_A-GRV060	RSN619_WHITTIER.A_A-GRV330	3.2494

RSN6_IMPVALLI_I-ELC180	RSN6_IMPVALLI_I-ELC270	2.1176
RSN786_LOMAP_PAE055	RSN786_LOMAP_PAE325	2.38204
RSN963_NORTHR_ORR090	RSN963_NORTHR_ORR360	1.13945
RSN1083_NORTHR_GLE170	RSN1083_NORTHR_GLE260	3.44172
RSN4855_CHUETSU_65024NS	RSN4855_CHUETSU_65024EW	3.48845
RSN769_LOMAP_G06000	RSN769_LOMAP_G06090	3.85302
RSN645_WHITTIER.A_A-OR2010	RSN645_WHITTIER.A_A-OR2280	3.22255
RSN2709_CHICHI.04_CHY035N	RSN2709_CHICHI.04_CHY035E	3.9075
RSN1184_CHICHI_CHY010-N	RSN1184_CHICHI_CHY010-W	3.10917
RSN1147_KOCAELI_ATS000	RSN1147_KOCAELI_ATS090	1.86772
RSN405_COALINGA_D-BNT270	RSN405_COALINGA_D-BNT360	3.82331
RSN3745_CAPEMEND_BVS060	RSN3745_CAPEMEND_BVS330	3.19855
RSN4117_PARK2004_Z15090	RSN4117_PARK2004_Z15360	2.672
RSN8486_PARK2004_NPHOBHNN	RSN8486_PARK2004_NPHOBHNE	2.76091
RSN3756_LANDERS_MVP000	RSN3756_LANDERS_MVP090	2.66896
RSN5859_SIERRA.MEX_WSM360	RSN5859_SIERRA.MEX_WSM090	3.47443
RSN4482_L-AQUILA CU104XTE	RSN4482_L-AQUILA CU104YLN	2.38178
RSN960_NORTHR_LOS000	RSN960_NORTHR_LOS270	1.39471
RSN828_CAPEMEND_PET000	RSN828_CAPEMEND_PET090	1.03884
RSN3307_CHICHI.06_CHY086N	RSN3307_CHICHI.06_CHY086E	3.27
RSN4084_PARK2004_36531-93	RSN4084_PARK2004_36531003	1.70887
RSN5988_SIERRA.MEX_DRE360	RSN5988_SIERRA.MEX_DRE-90	2.42503
RSN1549_CHICHI_TCU129-E	RSN1549_CHICHI_TCU129-N	1.27519

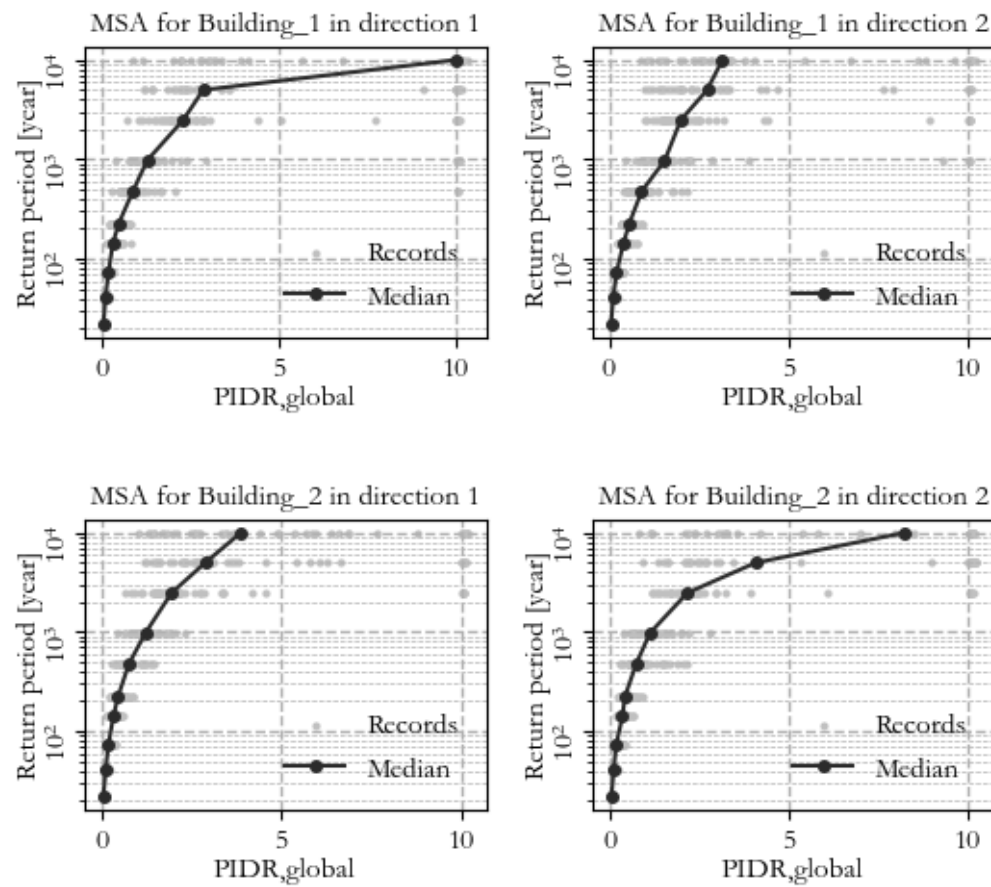
Return period of 9975 years

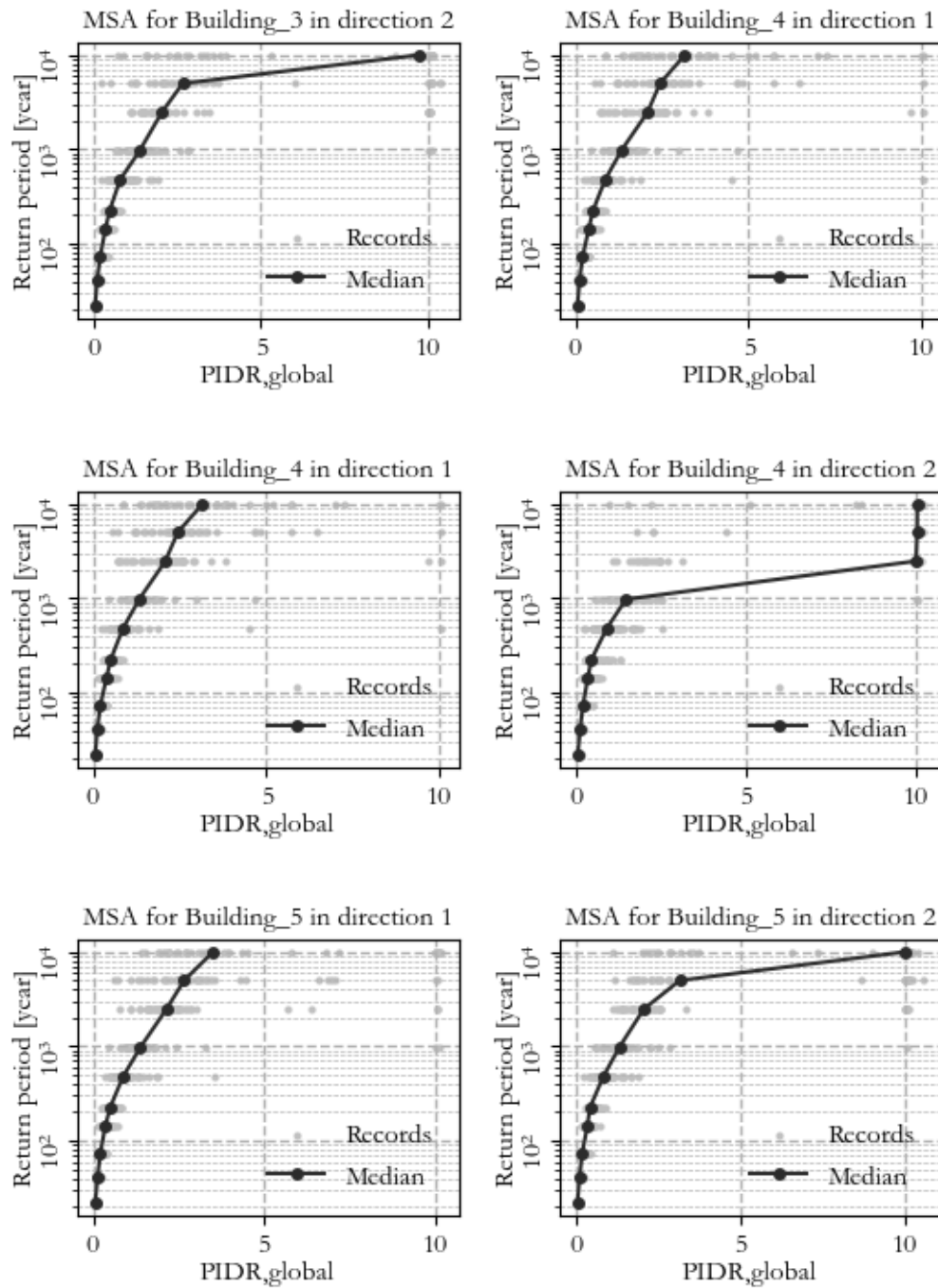


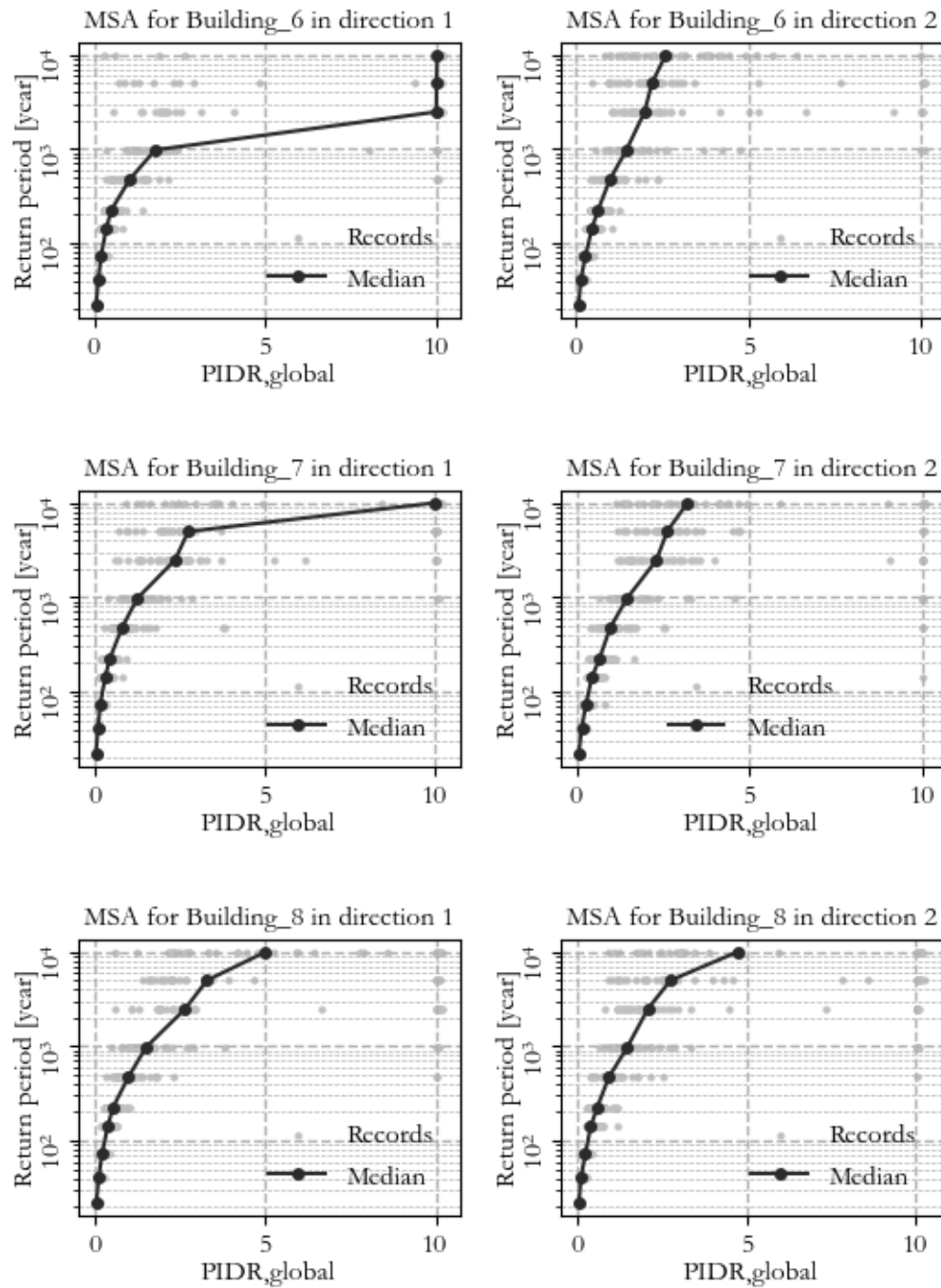
Record Direction 1	Record Direction 2	Scale Factor
RSN4126_PARK2004_SC1090	RSN4126_PARK2004_SC1360	2.8057
RSN727_SUPER.B_B-SUP045	RSN727_SUPER.B_B-SUP135	2.27237
RSN341_COALINGA.H_H-Z02000	RSN341_COALINGA.H_H-Z02090	3.77161
RSN5786_IWATE_54038NS	RSN5786_IWATE_54038EW	2.91325
RSN1119_KOBE_TAZ000	RSN1119_KOBE_TAZ090	0.98809
RSN1080_NORTHR_KAT000	RSN1080_NORTHR_KAT090	1.49997
RSN765_LOMAP_G01000	RSN765_LOMAP_G01090	2.97552
RSN766_LOMAP_G02000	RSN766_LOMAP_G02090	1.86485
RSN4482_L-AQUILA CU104XTE	RSN4482_L-AQUILA CU104YLN	3.01714
RSN4229_NIIGATA_NIGH12NS	RSN4229_NIIGATA_NIGH12EW	3.80664
RSN1794_HECTOR_JOS090	RSN1794_HECTOR_JOS360	3.87691
RSN4117_PARK2004_Z15090	RSN4117_PARK2004_Z15360	3.38477
RSN367_COALINGA.H_H-PVB045	RSN367_COALINGA.H_H-PVB135	2.43268
RSN978_NORTHR_WIL090	RSN978_NORTHR_WIL180	3.10728
RSN953_NORTHR_MUL009	RSN953_NORTHR_MUL279	1.1494
RSN1147_KOCAELI_ATS000	RSN1147_KOCAELI_ATS090	2.36594

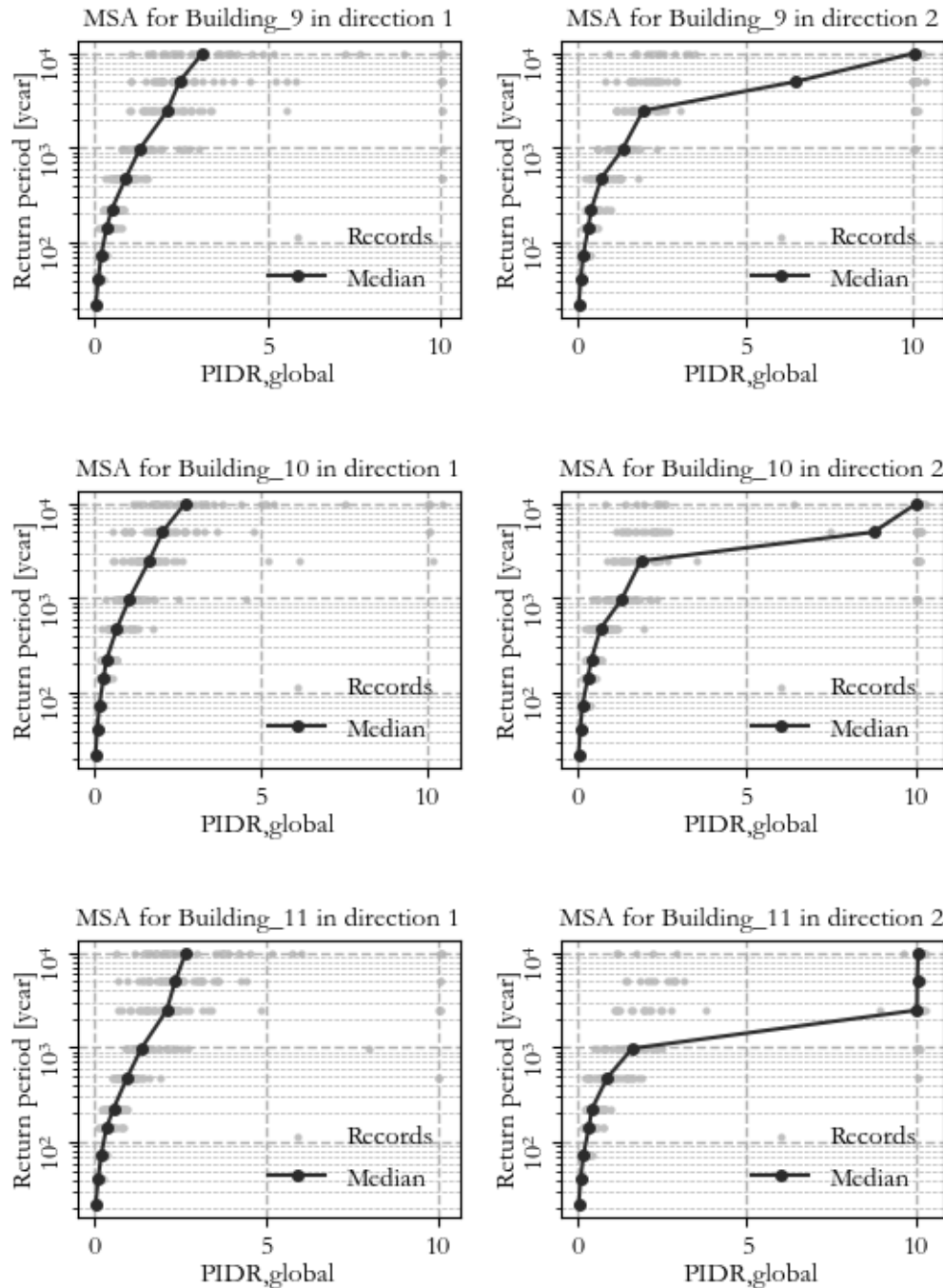
RSN690_WHITTIER.A_A-GRN180	RSN690_WHITTIER.A_A-GRN270	3.95514
RSN1141_DINAR_DIN090	RSN1141_DINAR_DIN180	1.90301
RSN6923_DARFIELD_KPOCN15E	RSN6923_DARFIELD_KPOCS75E	2.69519
RSN3678_SMART1.45_45M10EW	RSN3678_SMART1.45_45M10NS	3.46661
RSN5969_SIERRA.MEX_BCR360	RSN5969_SIERRA.MEX_BCR090	3.72645
RSN564_GREECE_H-KAL-NS	RSN564_GREECE_H-KAL-WE	3.00311
RSN1481_CHICHI_TCU038-E	RSN1481_CHICHI_TCU038-N	3.56145
RSN300_ITALY_B-CTR000	RSN300_ITALY_B-CTR270	3.05657
RSN1082_NORTHR_RO3000	RSN1082_NORTHR_RO3090	2.17918
RSN3966_TOTTORI_TTR009NS	RSN3966_TOTTORI_TTR009EW	3.34595
RSN6971_DARFIELD_SPFSN17E	RSN6971_DARFIELD_SPFSN73W	3.19742
RSN148_COYOTELK_G03050	RSN148_COYOTELK_G03140	3.56165
RSN4097_PARK2004_SCN090	RSN4097_PARK2004_SCN360	2.37551
RSN334_COALINGA.H_H-COW000	RSN334_COALINGA.H_H-COW090	3.52801
RSN4850_CHUETSU_65013NS	RSN4850_CHUETSU_65013EW	1.77264
RSN5264_CHUETSU_NIG018NS	RSN5264_CHUETSU_NIG018EW	1.09075
RSN571_SMART1.45_45EO1EW	RSN571_SMART1.45_45EO1NS	2.9309
RSN1512_CHICHI_TCU078-E	RSN1512_CHICHI_TCU078-N	1.914
RSN778_LOMAP_HDA165	RSN778_LOMAP_HDA255	2.27975
RSN1120_KOBE_TAK000	RSN1120_KOBE_TAK090	0.68775
RSN143_TABAS_TAB-L1	RSN143_TABAS_TAB-T1	0.98697
RSN149_COYOTELK_G04270	RSN149_COYOTELK_G04360	3.32198
RSN1547_CHICHI_TCU123-E	RSN1547_CHICHI_TCU123-N	2.80283
RSN160_IMPVALL.H_H-BCR140	RSN160_IMPVALL.H_H-BCR230	1.53529

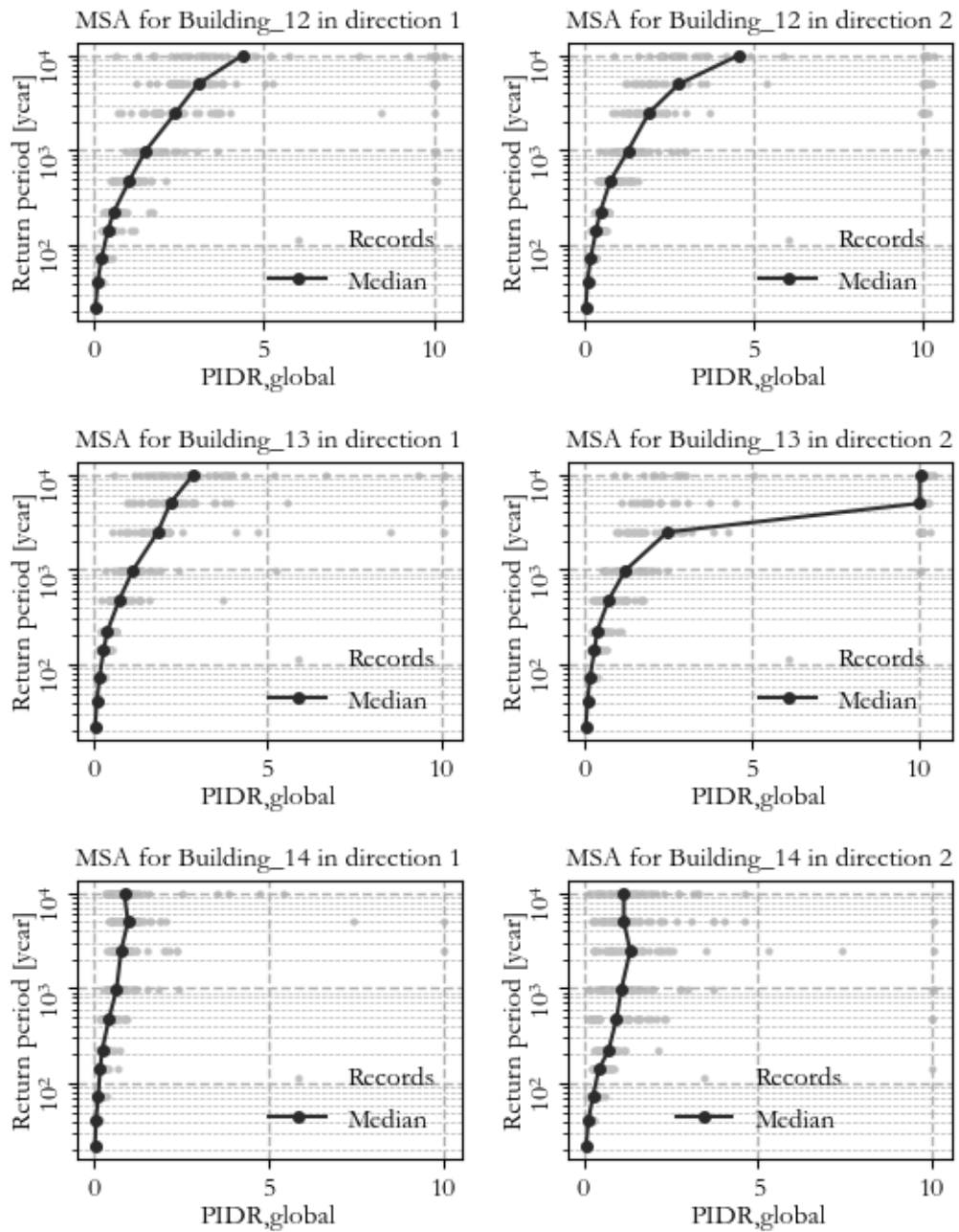
APPENDIX B. RESULTS OF MSA FOR ALL BUILDINGS

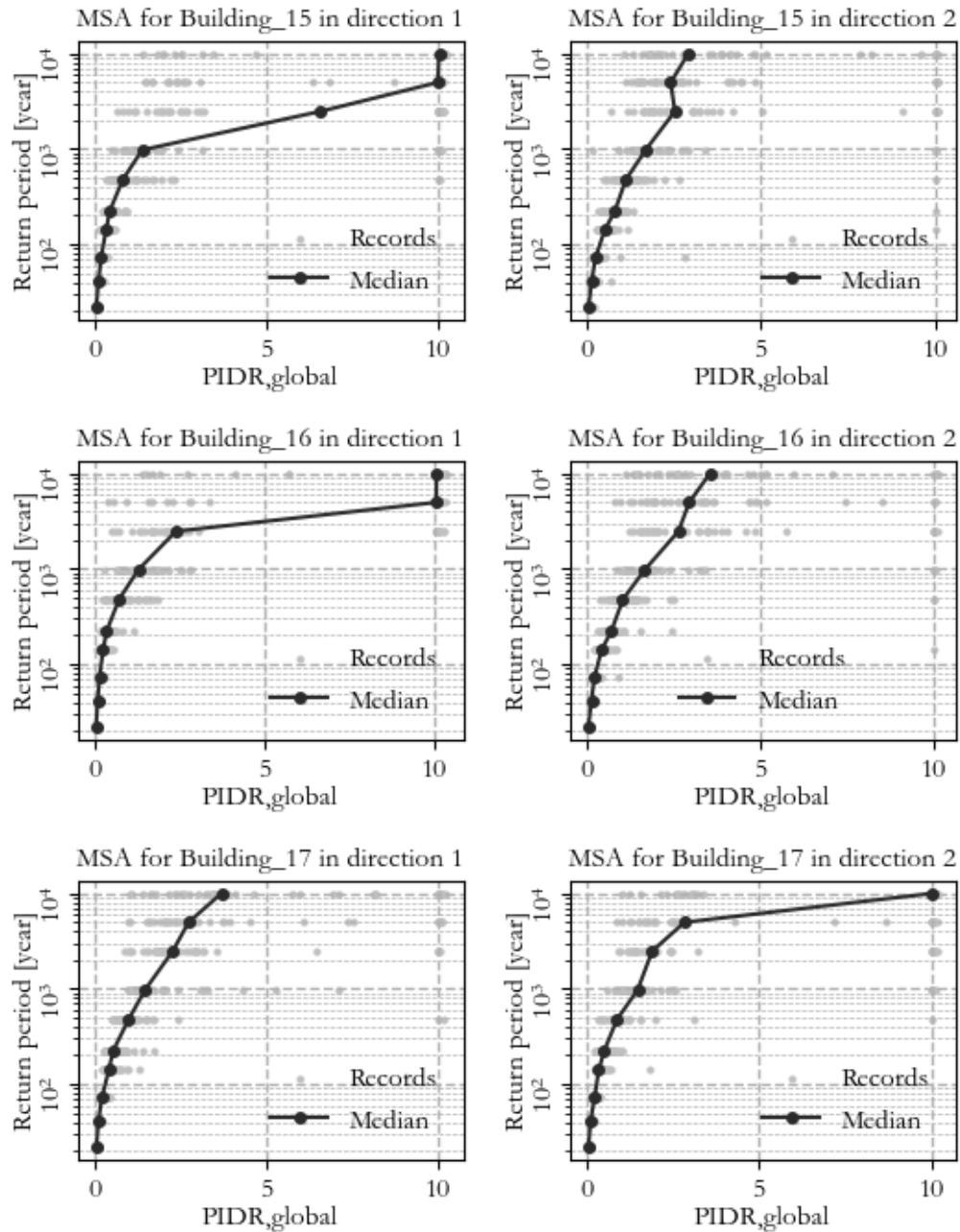


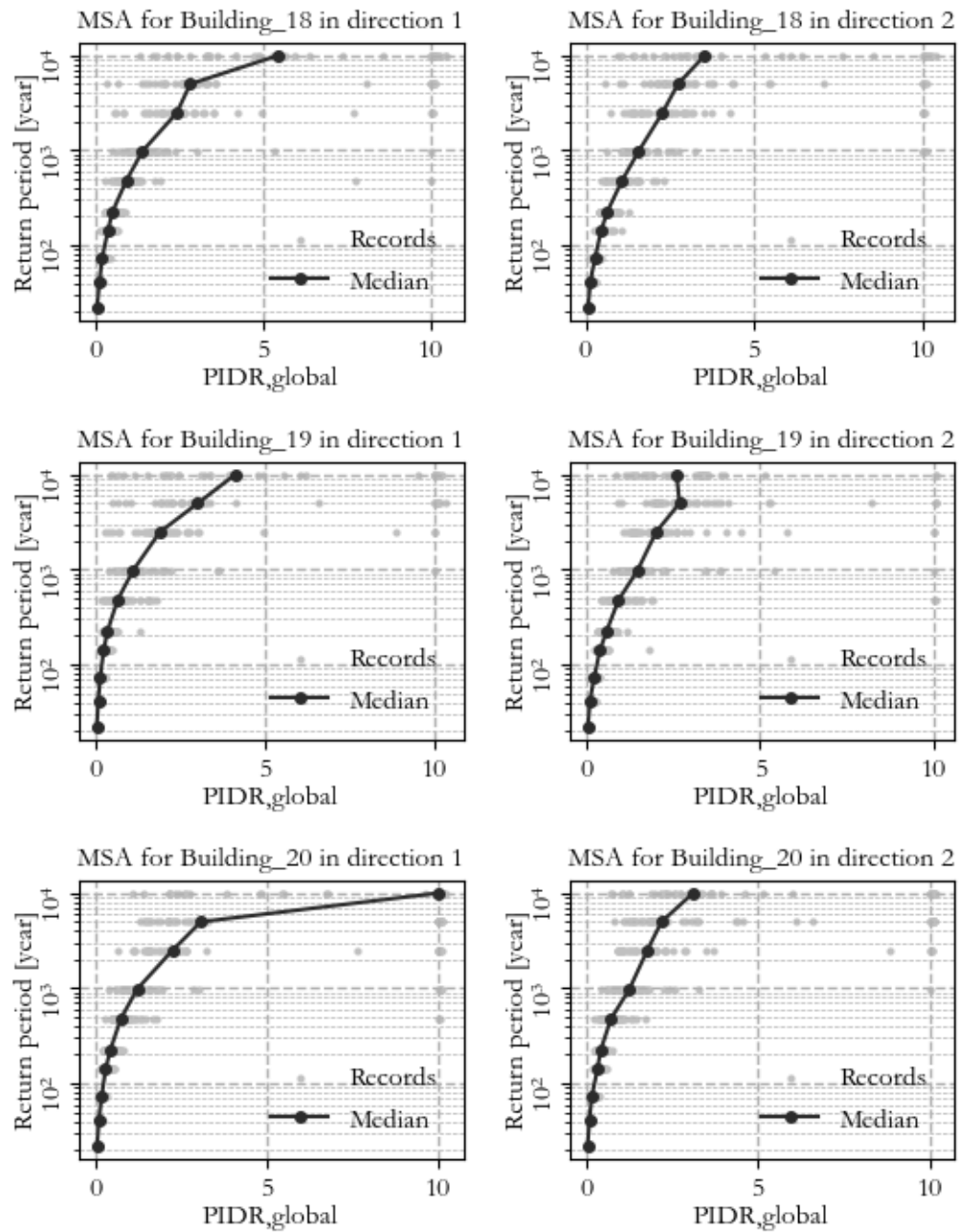


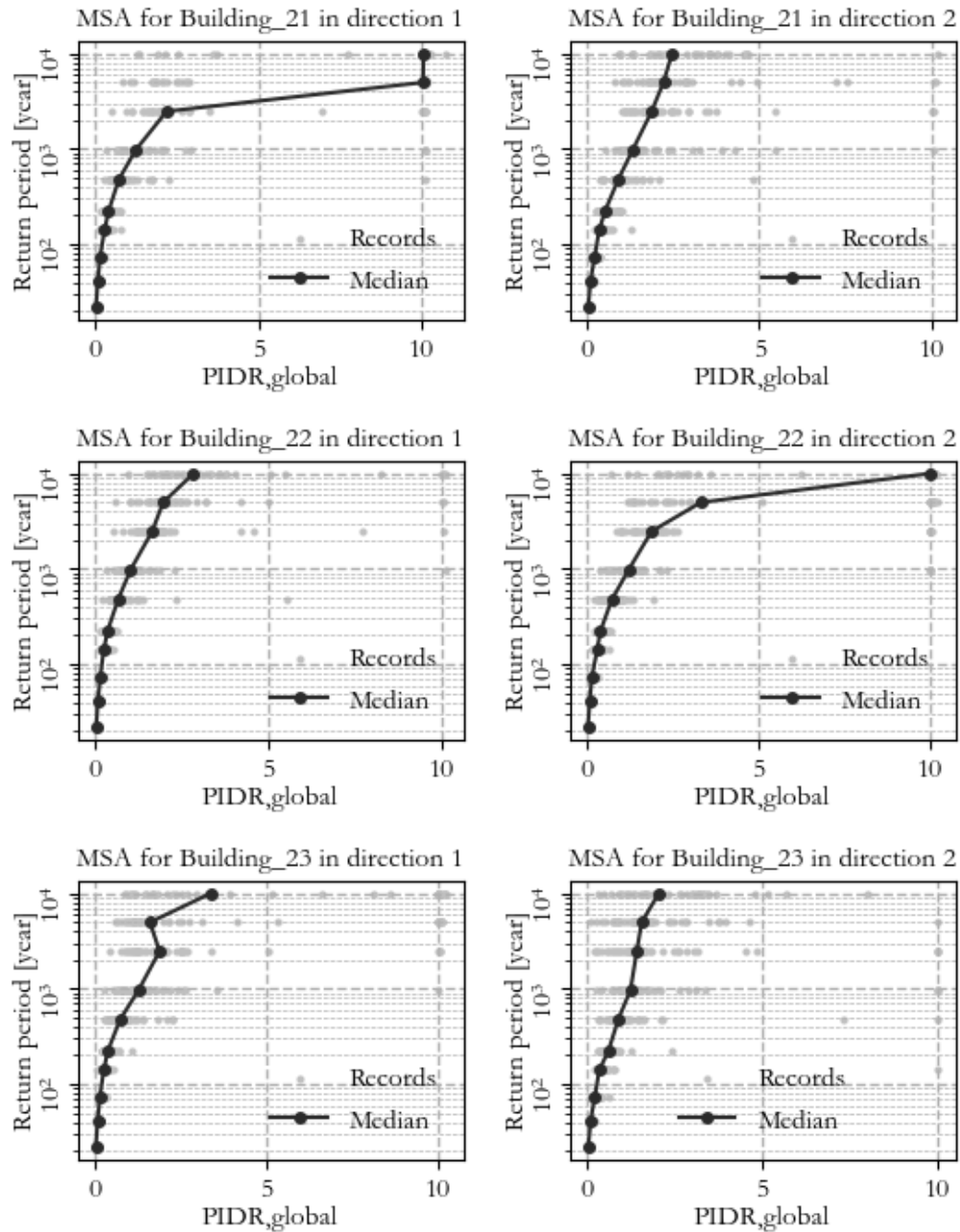


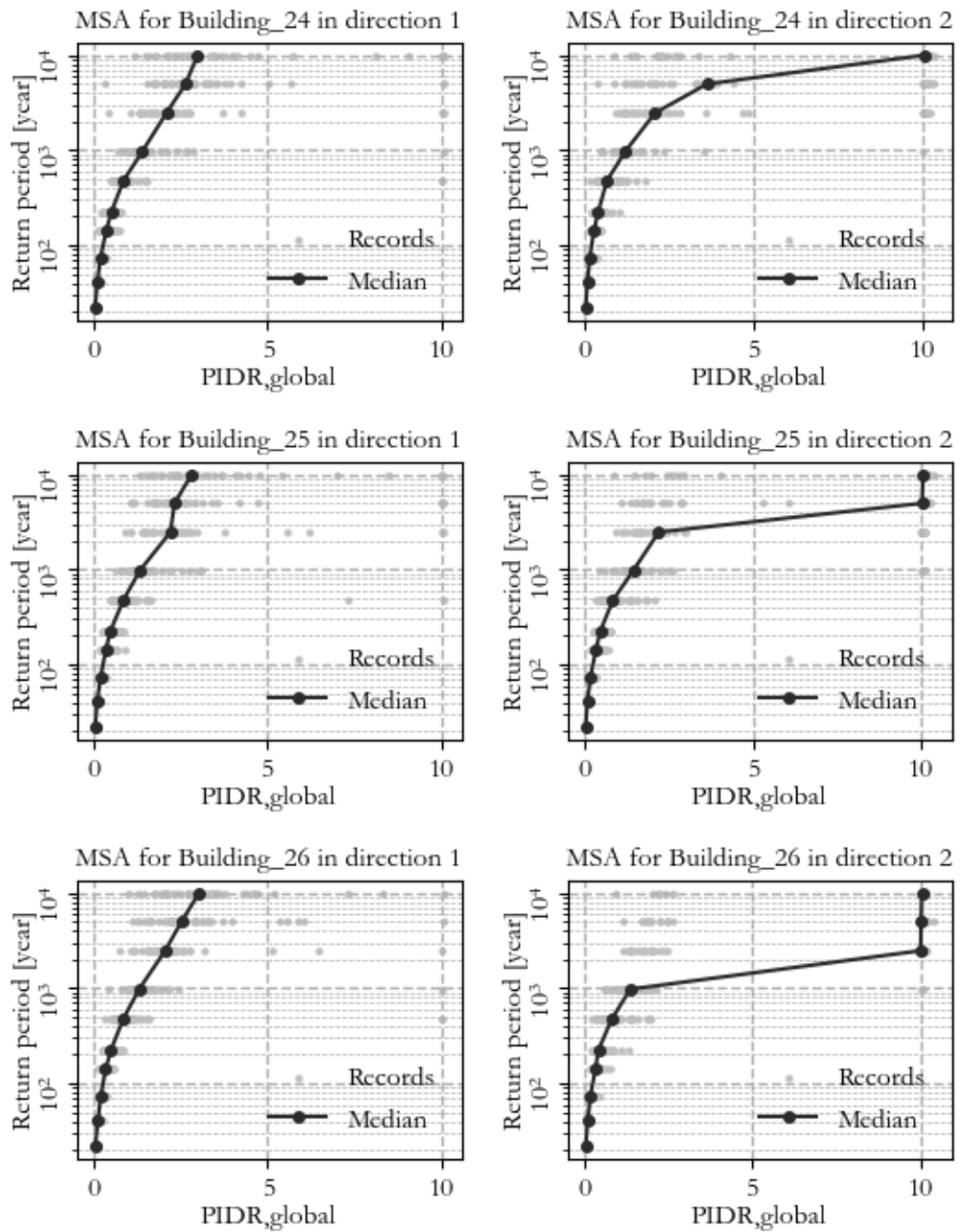


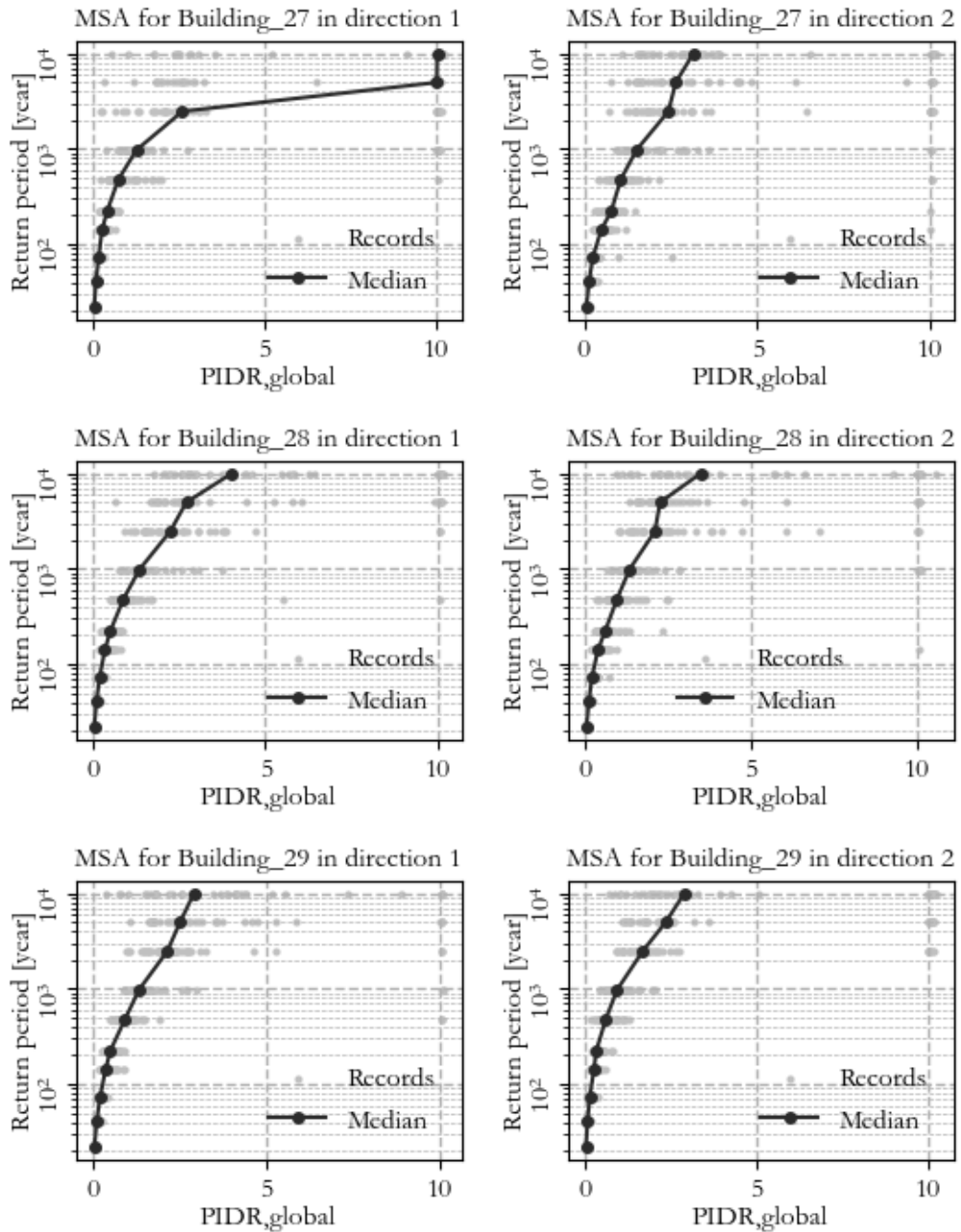


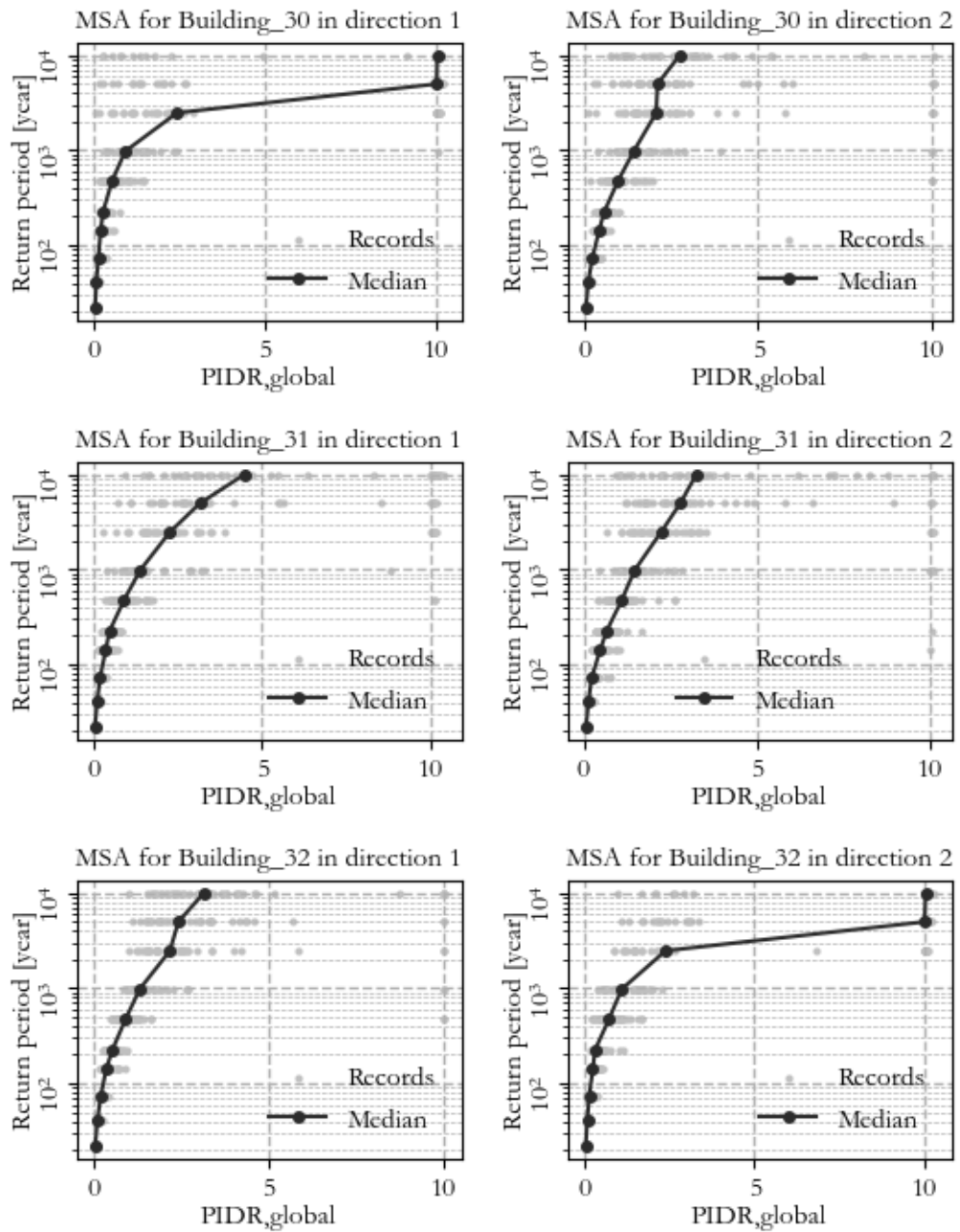


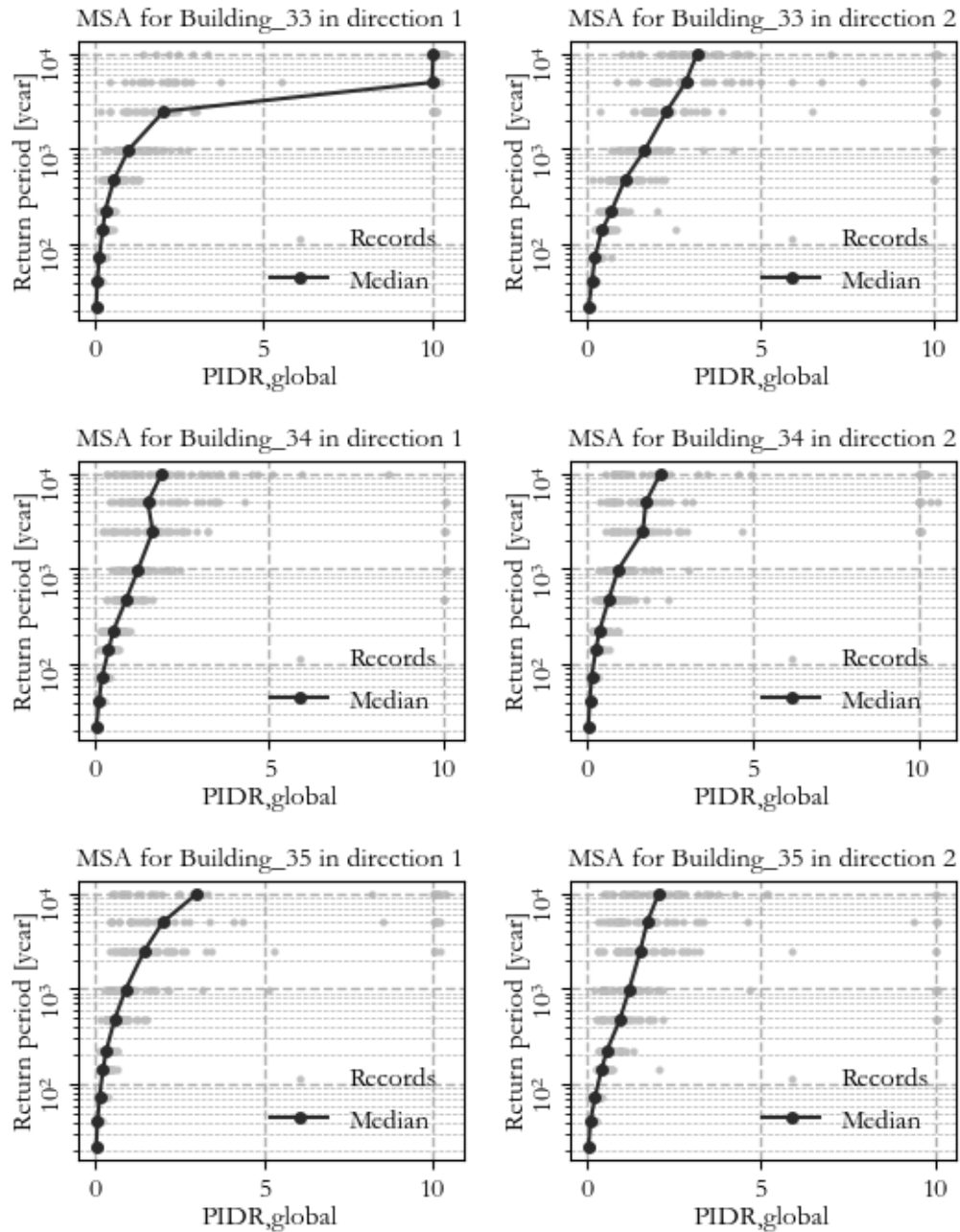


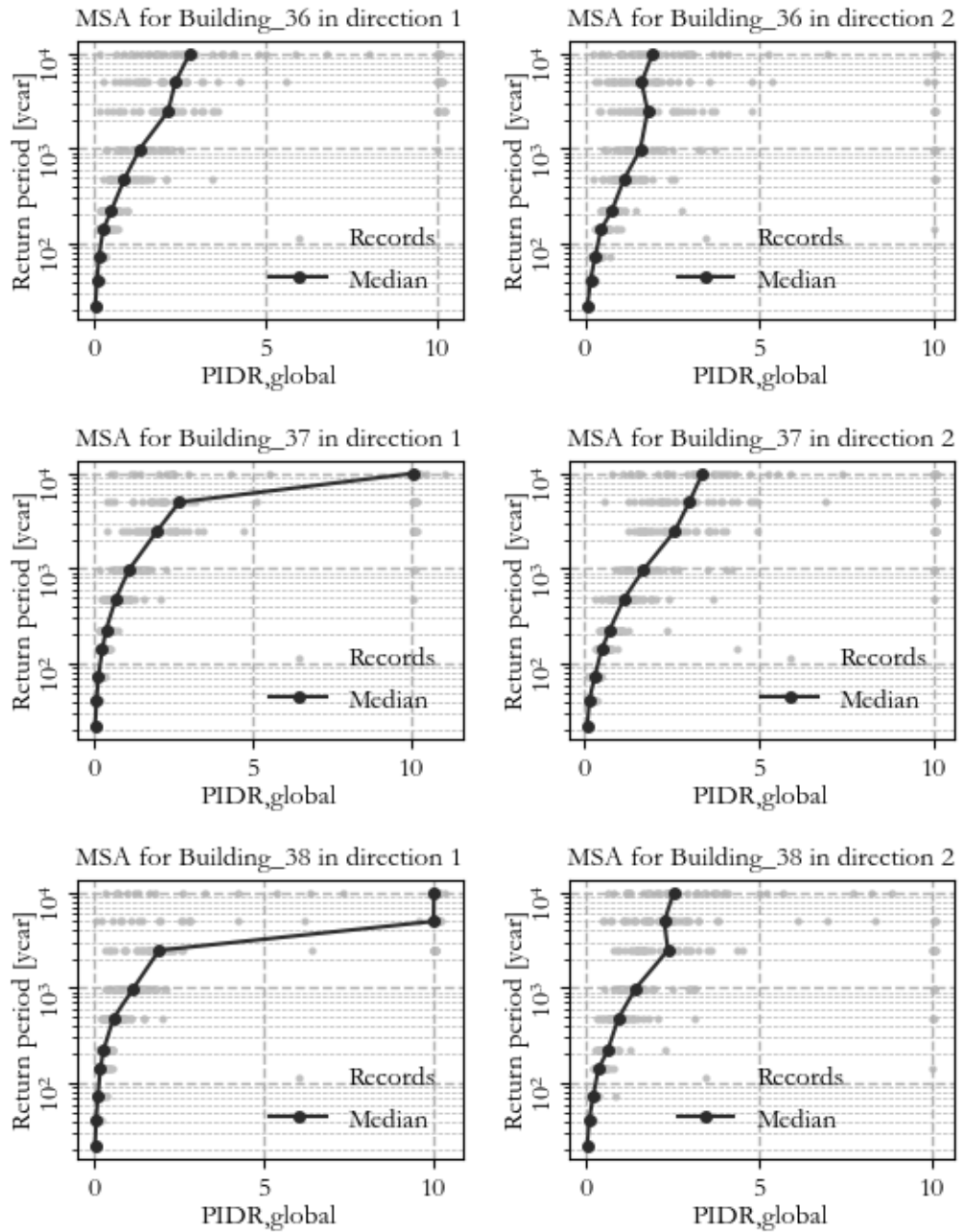


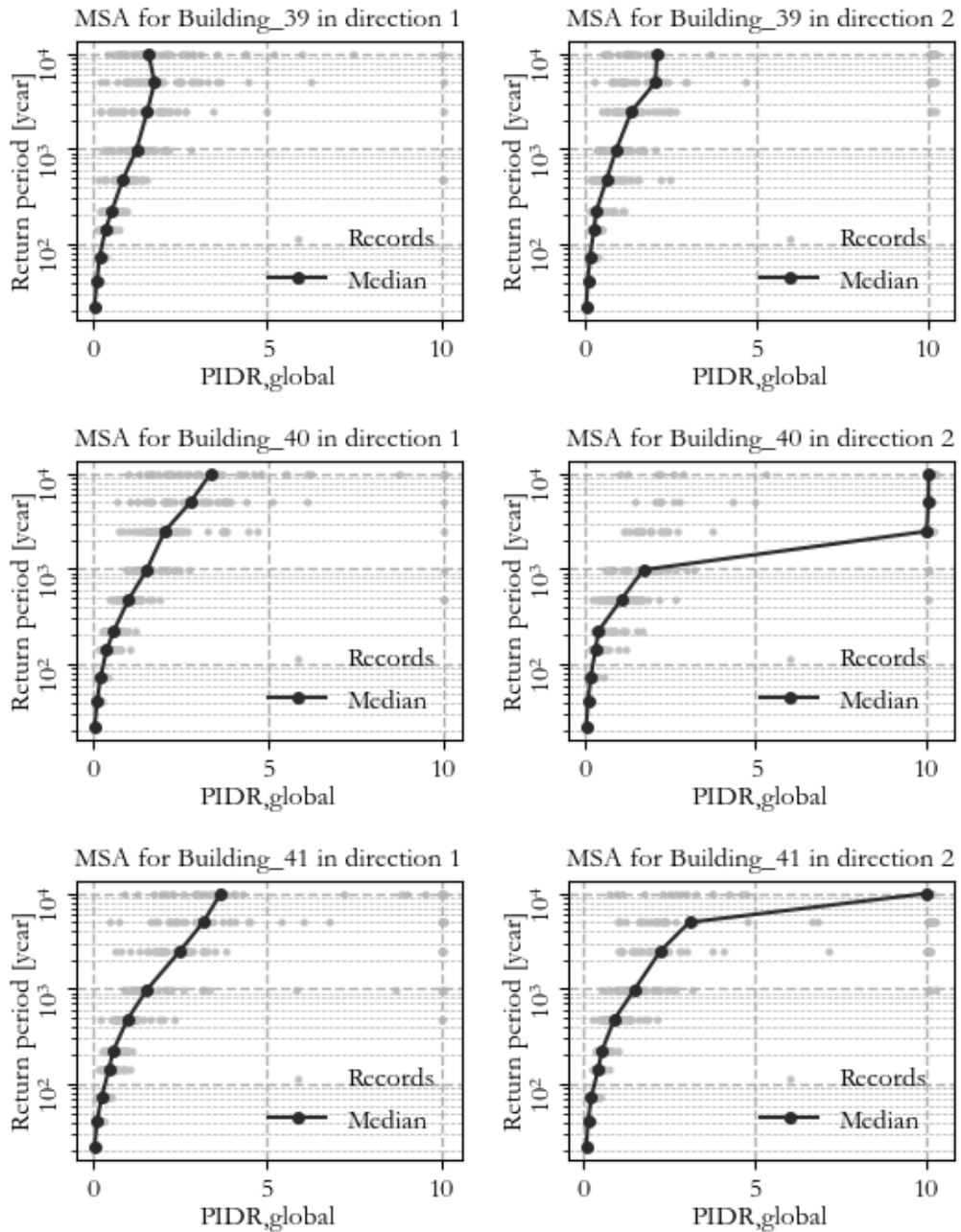


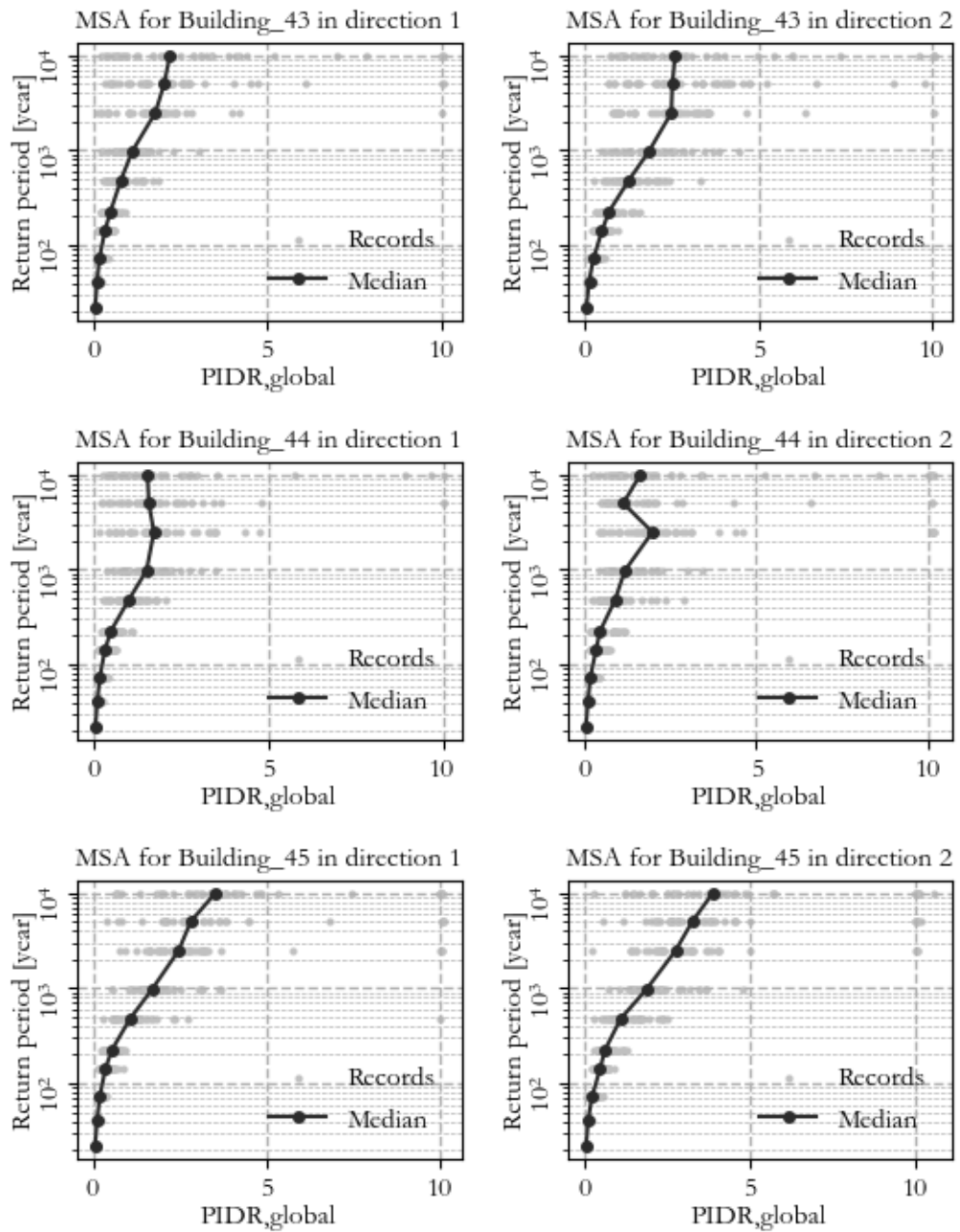


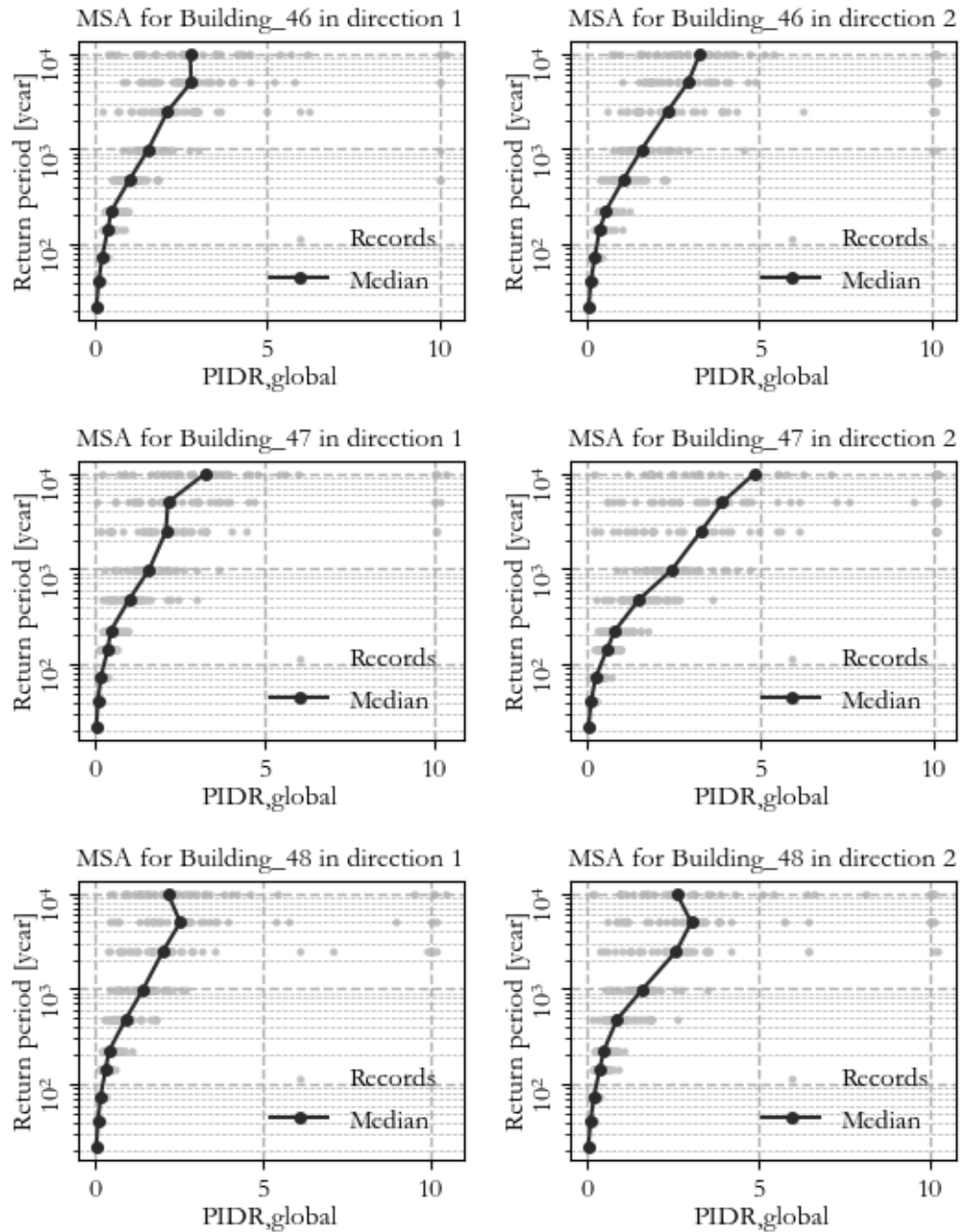


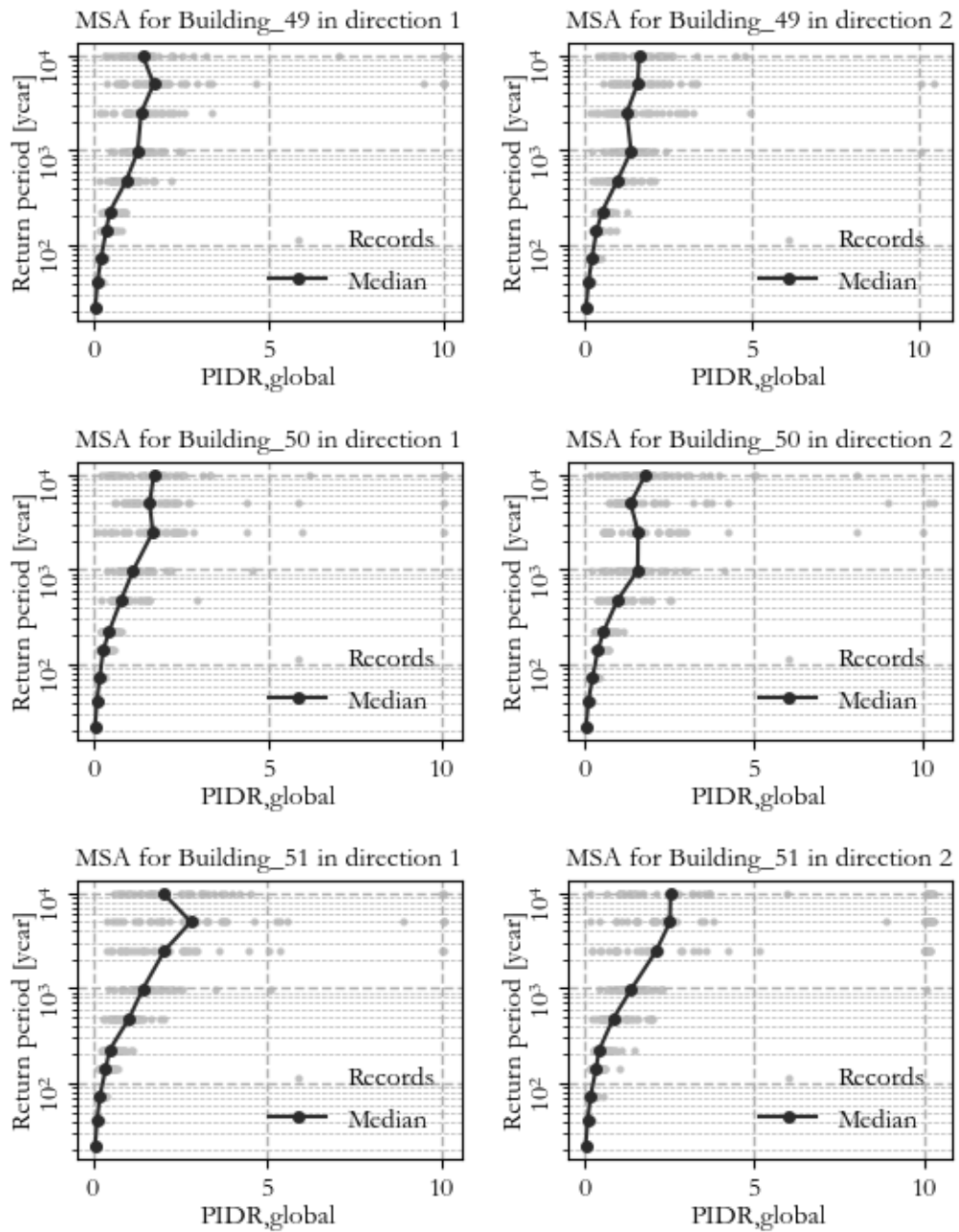


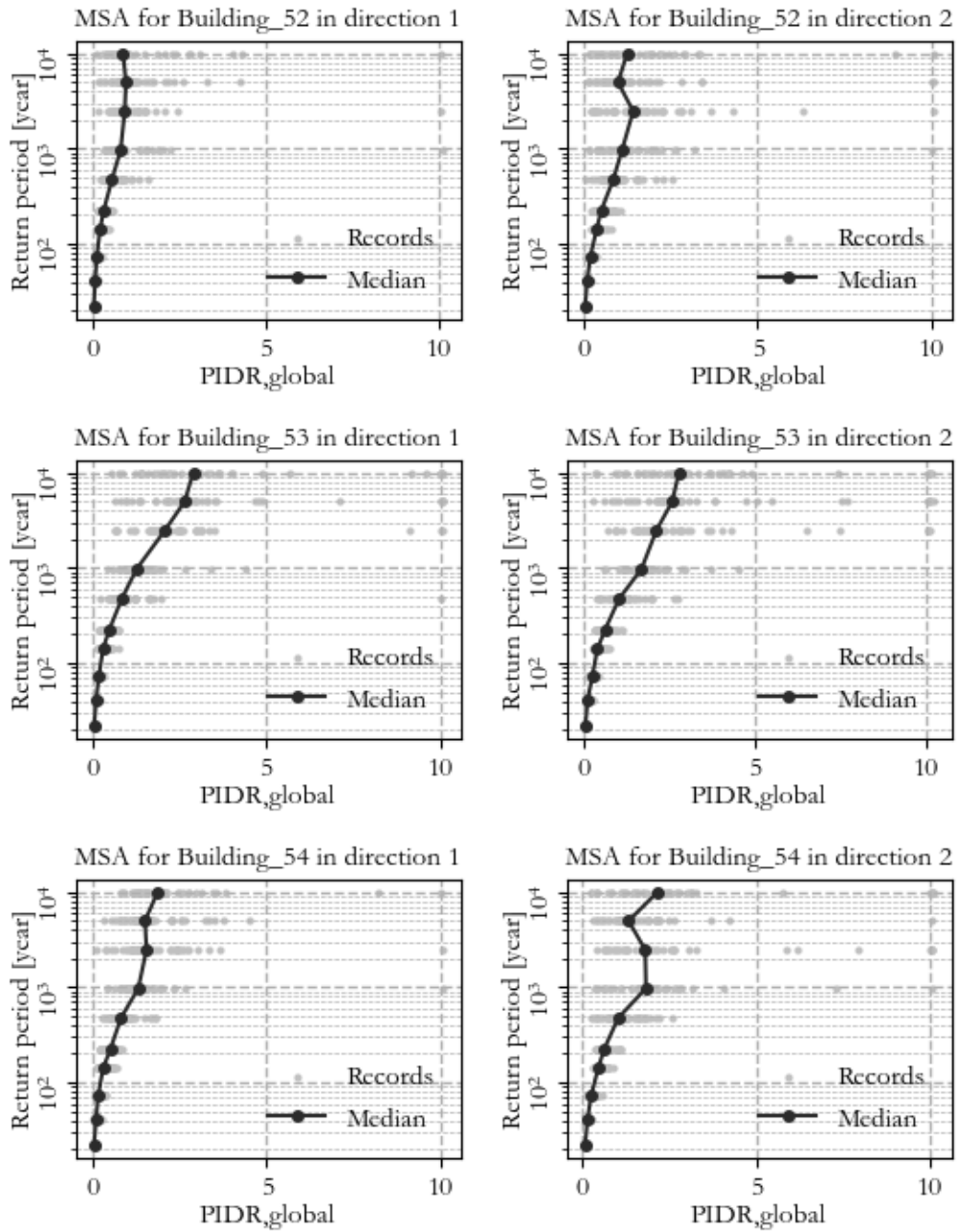


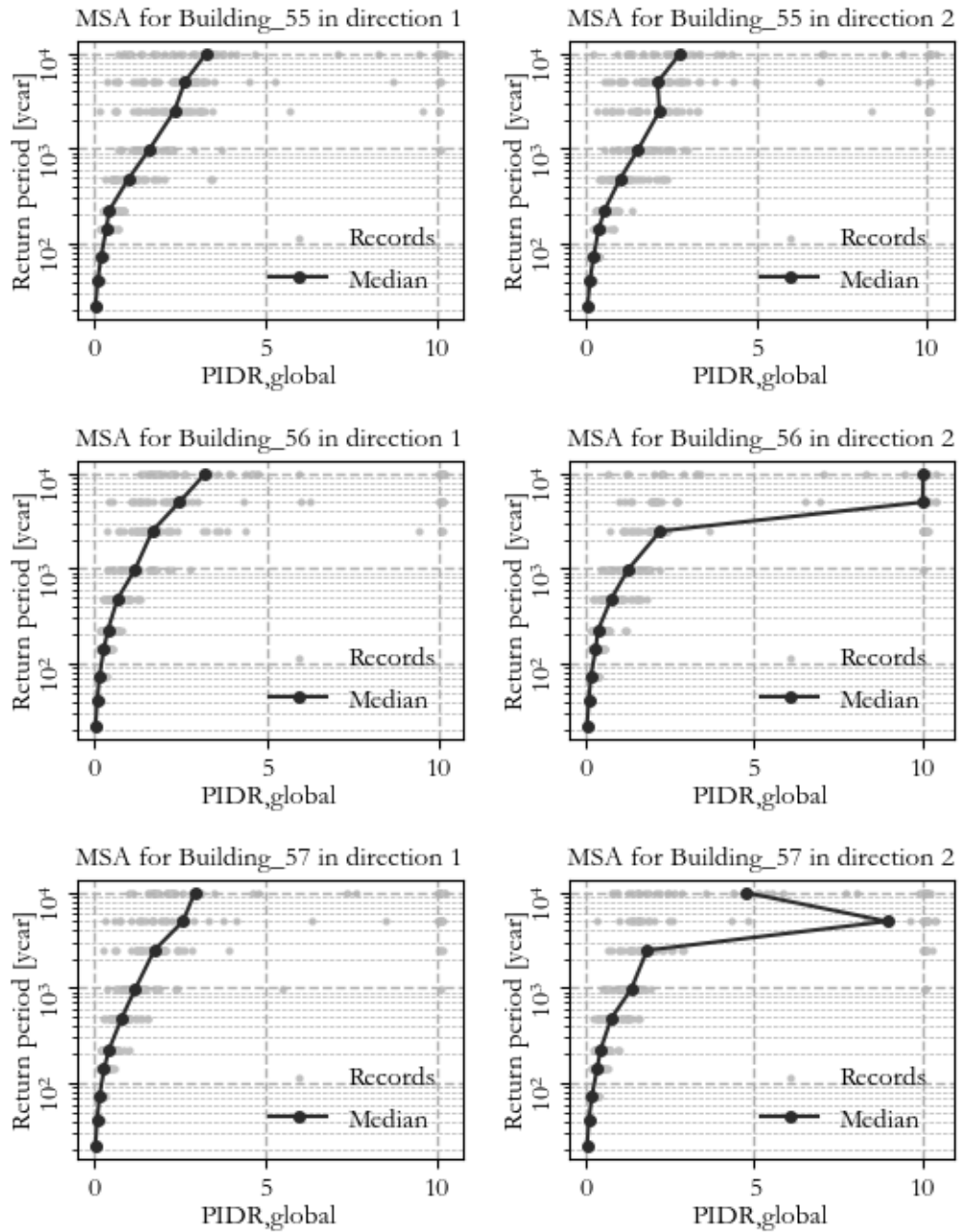


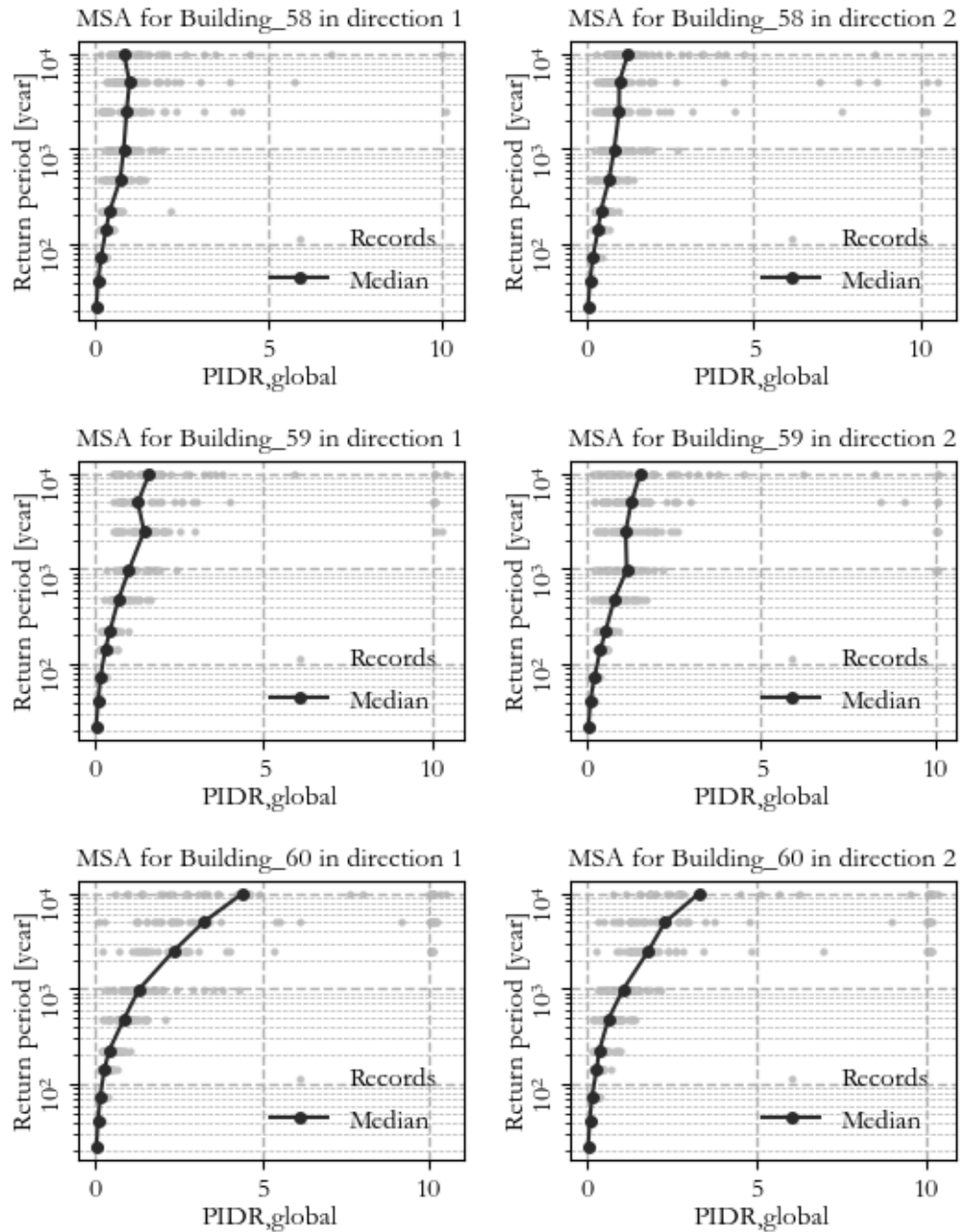


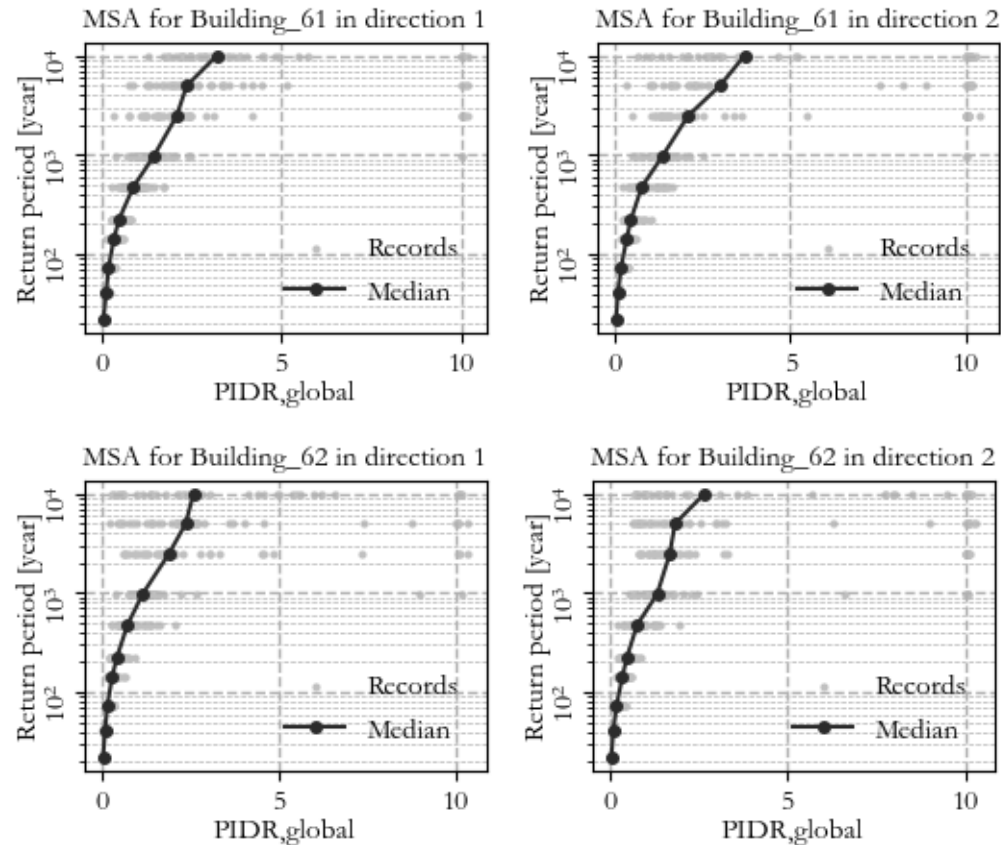












APPENDIX C. RESULTS OF IDA FOR ALL BUILDINGS

